UNIVERSITÀ DEGLI STUDI DI PADOVA

DIPARTIMENTO DI SCIENZE CHIMICHE

SCUOLA DI DOTTORATO DI RICERCA IN SCIENZE MOLECOLARI
INDIRIZZO: SCIENZE CHIMICHE
XXII CICLO

Structural characterization of the STAS domain of the motor protein prestin:

a general template for SLC26/SulP anion transporters

Direttore della Scuola: Ch.mo Prof. Maurizio Casarin
Supervisore: Ch.mo Prof. Roberto Battistutta

Dottoranda: Rosa Aiello

Contents

Abbreviations

ASA	Antisigma factor Antagonist
BLM	Basolateral Membrane
β-OG	Octyl-β-D-Glucopyranoside
CAII	Carbonic Anhydrase isoform II
CD	Circular Dichroism
CF	Cystic Fibrosis
CFTR	Cystic Fibrosis Transmembrane conductance Regulator
CLD	Congenital Chloride Diarrhea
DLS	Dynamic Light Scattering
DRA	Downregulated in Adenomas
DTD	Diastrophic Dysplasia
DTDST	Diastrophic Dysplasia Sulphate Transporter
DTT	Dithiothreitol
ER	Endoplasmic Reticulum
ESI-TOF	Electrospray Ionization Time-Of-Flight
ESRF	European Synchrotron Radiation Facility
HPLC	High Performance Liquid Chromatography
IHCs	Inner Hair Cells
IMAC	Immobilized Metal ion Affinity Chromatography
IPTG	Isopropyl β-D-1-thiogalactopyranoside
LB	Luria Bertani
MES	2-(*N*-morpholino)ethanesulfonic acid
MW	Molecular Weight
NLC	Nonlinear Capacitance
NMR	Nuclear Magnetic Resonance
NTP	Nucleoside Triphosphates
OD	Optical Density
OHCs	Outer Hair Cells
ONC	Overnight Culture
PAGE	PolyAcrylamide Gel Electrophoresis
PCR	Polymerase Chain Reaction
PDB	Protein Data Bank
PDS	Pendred Syndrome
PEG	Polyethylene Glycol
PKA	Protein Kinase A
PM	Plasma Membrane
PPM	Positioning of Protein in Membranes
RPM	Revolutions Per Minute

SAD	Single wavelength Anomalous Dispersion
SDS	Sodium Dodecyl Sulphate
SLC26	Solute Linked Carrier 26
STAS	Sulphate Transporters and Anti-Sigma factor antagonists
SulP	Sulphate Permease
SUMO	Small Ubiquitin-like MOdifier
TEV	Tobacco Etch Virus
TFA	Trifluoroacetic Acid
TRIS	Tris(hydroxymethyl)aminomethane
UV	Ultraviolet

Summary

The subject of this thesis is a small cytoplasmatic domain, the STAS domain, present in the C-terminal portion of the anion SulP transporters. The Sulphate Permease (SulP) family includes more than two hundred proteins, identified in archea, bacteria, fungi, plants and animals, many of which have been functionally characterized as anion exchanger or transporters. In mammals, this family, also known as Solute Linked Carrier 26 (SLC26), includes eleven members with important roles in normal physiology.

The STAS domain is located in the less conserved C-terminal portion of all SulP transporters. STAS is an acronym for Sulphate Transporter and Anti-Sigma factor antagonist. The name derives from a sequence homology between this SulP portion and the bacterial antisigma-factor antagonists (ASAs). Even if the 3D structures of some bacterial ASAs are known, STAS domains are poorly characterized in terms of both their function and structure. However, there are many clues of their involvement in the regulation of transport SulP activity. In fact, mutation in this domain can cause the loss of the transporter function, for instance resulting in serious genetic disease. No three-dimensional structures of the STAS domains are available. Their structural characterization is important to understand their precise role and function.

This work has been focused on production and characterization of STAS domain of two SulP transporters, one from a SLC26 member, the motor protein prestin, and the other from *Arabidopsis Thaliana* Sultr1.2. Because it is difficult to identify the exact boundaries of the STAS domains in the C-terminal SulP transporters, various constructs of the two selected STAS domains have been produced and characterized. The 3D structure of a chimeras prestin variant has been determined through X-ray crystallography at 1.57 Å resolution. The structure revealed a common global fold with the ASA protein but there are significant differences compared to the ASA STAS particularly at the N-terminus. Unexpectedly, our data reveal that the prestin STAS domain starts immediately after the last transmembrane segment and lies just beneath the lipid bilayer. A structure-function analysis suggests that our model can be a general template for most SLC26 and SulP anion

transporters and supports the notion that the STAS domain is involved in functionally important inter- and intra-molecular interactions.

Riassunto

Oggetto di questo lavoro di tesi è stato il dominio STAS, presente nella porzione C-terminale di proteine transmembrana della famiglia SulP (*Sulphate Permease*). Tale famiglia include oltre 200 trasportatori o scambiatori di anioni inorganici appartenenti a batteri, funghi, piante e animali. Nei mammiferi questa famiglia è anche conosciuta con il nome di Solute Linked carrier 26 (SLC26)I trasportatori SulP sono caratterizzati da una comune organizzazione strutturale: un *core* centrale idrofobico transmenbrana ed due porzioni N- e C- terminali citoplasmatiche, la seconda delle quali contiene lo STAS *domain*.

Con dominio STAS (*Sulphate Transporter and AntiSigma factor antagonist*) si indica un piccolo dominio citoplasmatico dei trasportatoti SulP che mostra omologia di sequenza con gli antagonisti batterici al fattore anti-sigma (o proteine ASA).

Al contrario degli ASA batterici, di cui è nota la struttura, il dominio STAS dei trasportatori di anioni è poco caratterizzato sia in termini di funzione che di struttura. Esistono, però, diversi indizi sul coinvolgimento di tale dominio nella regolazione dell'attività di trasporto delle proteine SulP. Nei mammiferi, mutazioni nello STAS possono causare la perdita dell'attività di trasporto, portando anche all'insorgenza di gravi patologie genetiche. Al momento non sono note strutture 3D di domini STAS e la loro caratterizzazione sarebbe fondamentale per comprendere il loro ruolo e la funzione all'interno della famiglia SulP.

Questa tesi è stata incentrata sulla produzione e caratterizzazione del dominio STAS della proteina di mammifero prestina e del trasportatore Sultr1.2 di *Arabidopsis thaliana*. Poiché le esatte estremità dello STAS all'interno del C-terminale dei trasportatori SulP sono difficili da identificare, sono stati disegnati diversi costrutti delle due proteine selezionate.

La struttura 3D di una variante dello STAS di prestina è stata risolta tramite cristallografia ai raggi X ad una risoluzione di 1.57 Å rivelando un *fold* comune tra lo STAS di prestina e le proteine ASA batteriche ma notevoli differenze particolarmente all' N-terminale. I nostri dati hanno mostato inaspettatamente che il domino STAS inizia

subito dopo l'ultimo segmento transmembrana, situato giusto al di sotto del doppio strato fosfolipidico. Inoltre, un' attenta analisi struttura-funzione ha suggerito che la nostra struttura può essere considerato un modello generale per molti trasportatori di anioni SulP e SLC26 e conferma l'ipotesi che il dominio STAS è coinvolto in interazioni inter- intra-molecolari.

1

INTRODUCTION

1.1 THE SULPHATE PERMEASE FAMILY

The Sulphate Permease (SulP) family is a large and diverse family of anion transporters, with members identified by sequence homology in prokaryotes and eukaryotes (Saier *et al.*, 1999b). Many bacteria and eukaryotes possess multiple SulP family paralogues. A few of these proteins are functionally characterized, and all are inorganic anion uptake transporters or anion/anion exchange transporters. Some transport their substrates with high affinities, while others transport them with relatively low affinities. Some catalyze SO_4^{2-}/H^+ symport, but SO_4^{2-}/HCO_3^-, or more generally, anion/anion antiport, has been reported for others.

PROKARYOTIC SulP TRANSPORTERS

Little functional data on bacterial SulP proteins are available. Sulphur is a key element in bacterial metabolism. Rapidly growing numbers of anaerobic, sulphate-reducing chemolithoauxotrophic species have been identified in samples from deep-sea hydrothermal vents (Rosenberg *et al*., 2006). Genes involved in sulphur metabolism have been implicated as virulence determinants in mammalian pathogens.

The overexpression of the Rv1739c transporter (which is a SulP member) from the Gram-positive *Mycobacterium tuberculosis* is able to increase sulphate transport in *E. coli* (Zolotarev *et al*., 2008). The increase sulphate uptake occurs by a mechanism requiring the cytoplasmatic CysA subunit of the ABC sulphate permease.

Members of the SulP family, carrying additional non-transporter domains, have been described in some prokaryotes (figure 1). One SulP subfamily includes transporters fused to homologues of carbonic anhydrase, suggesting that these chimeric proteins function in bicarbonate or carbonate transport. In another subfamily, a SulP protein is joined to the rhodanese catalytic domain, indicating that this carrier may also be involved in sulfur metabolism (Felce & Saier, 2004). Some SulP proteins possess putative Na^+/H^+ antiporter or Na^+/bicarbonate symporter domains (Price *et al.*, 2004)

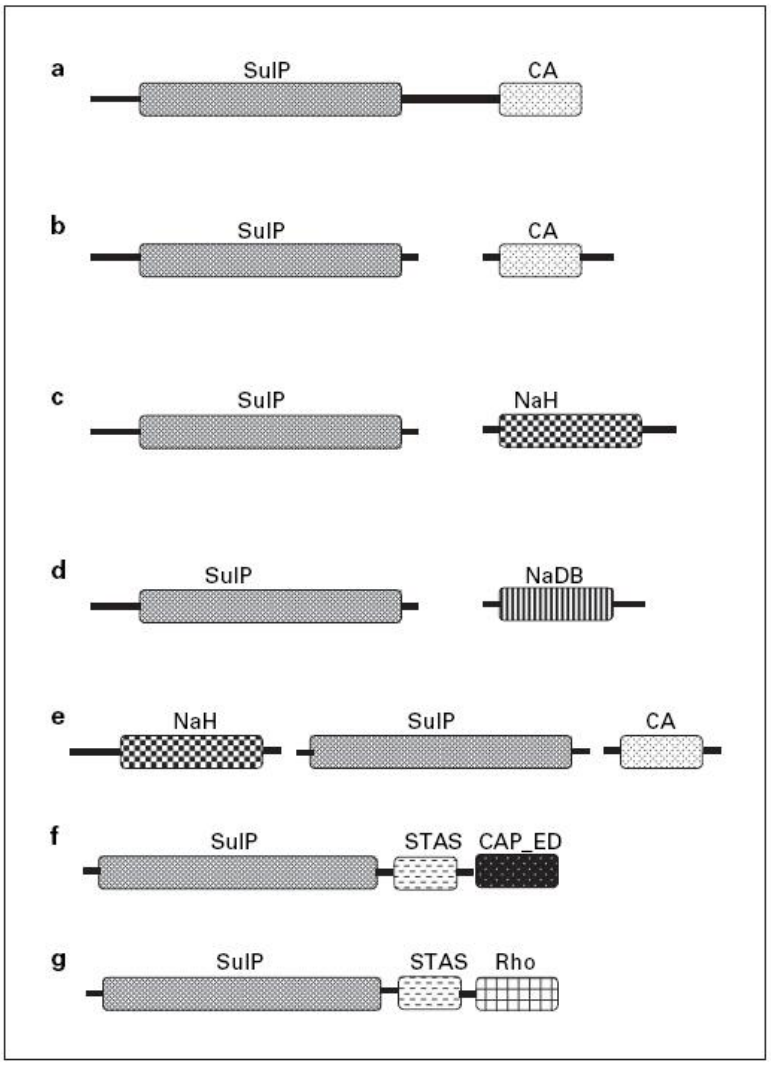

Figure 1: Schematic depiction of the gene arrangements observed for close homologues of the putative bicarbonate permease of the SulP family. **a**) A SulP homologue fused to a carbonic anhydrase (CA) homologue. **b**) Two adjacent genes encoding the SulP homologue and the carbonic anhydrase homologues. **c**) A SulP homologue with an adjacent gene encoding a Na^+/H^+ antiporter homologue of the NhaD family. **d**) A SulP homologue with an adjacent gene encoding a putative Na + bicarbonate symporter of the SBT family. **e**) A SulP homologue with adjacent genes encoding both a Na^+/H^+ antiporter homologue of the NhaD family and a carbonic anhydrase. **f**) A SulP homologue with fused STAS and a CAP_ED cyclic AMP-binding domain. **g**) A SulP homologue with fused STAS and rhodanese domains (Felce & Saier, 2004).

EUKARYOTIC SulP TRANSPORTERS

While the role of the SulP transporters in prokaryotes is not clear, most eukaryotic members of this family have actually been shown to be involved in sulfate uptake (Sandal

& Marcker, 1994; Smith *et al*., 1995). These proteins are inorganic anion transporters or anion/anion exchangers. Many of them have been well characterized functionally. They differ in their affinities to substrates. Some may function as sulphate/H^+ or sulphate/bicarbonate symporter, but generally anion/anion antiport has been reported for several SulP homologues in vertebrates.

Investigations on sulphate transport in fungi have so far been limited to a few species (Cherest *et al*., 2007; van de Kamp *et al.*, 1999). In plants, SulP members have been subdivided into five groups, depending on their properties, localization and substrate affinity (Hawkesford, 2003). All of them are induced transcriptionally by sulphur availability.

In mammals, the SulP family, also known as Solute Linked Carrier 26 (SLC26) family of anion transporters, shows broader anion specificity and more complex functions.

THE SLC26 FAMILY

The human SLC26 transporter family comprises 11 members, with SLC26A10 likely being a pseudogene (table 1). This family is relatively new and many structural and functional features of all members of the family are still not well understood.

The family members have varied tissue distributions, some being expressed in most organs and others with more restricted tissue expression patterns (table 1). The SLC26A proteins function as anion exchangers or anion channels in the luminal membrane of epithelial cells, transport solutes, including oxalate, SO_4^-, I^-, Cl^-, HCO_3^-, NO_3^-, SCN^-, OH^-, and thus are important in a number of physiological processes (Dorwart *et al.*, 2008b; Mount & Romero, 2004; Ohana *et al.*, 2009).

THE TRANSPORT FUNCTION OF THE SLC26 TRANSPORTER

On the basis of the known functional similarities, members of the SLC26A family can be grouped into three general categories (figure 2): the SO_4^{2-} transporters SLC26A1 and SLC26A2; the Cl^-/HCO_3^- exchangers SLC26A3, SLC26A4 and SLC26A6; and the ion channels SLC26A7 and SLC26A9 (Dorwart *et al.*, 2008b; Ohana *et al.*, 2009). SLC26A5 does not appear to function as anion transporter in mammals (Detro-Dassen *et*

al., 2008; Oliver *et al.*, 2001) and the current knowledge of the transport properties of SLC26A8 and SLC26A11 is deficient and not sufficient to place them in one the classified groups.

Table 1: SLC26-The multifunctional anion exchanger family

Human Gene Name	Aliases	Reported substrates	Tissue distribution	Disease association (s)
SLC26A1	Sat-1	SO_4^{2-}, oxalate,	kidney, liver, brain skeletal muscle, testis	unknown
SLC26A2	DTDST	SO_4^{2-}, Cl^-,	rib cartilage, small intestine	Diastrophic dysplasia, achondrogenesis Type IB, atelosteogenesis Type II, autosomal recessive multiple epiphyseal dysplasia
SLC26A3	DRA,	Cl^-, HCO_3^-, NO_3^-, SCN^-	intestine, pancreas, prostate, sweat gland	congenital chloride diarrhea
SLC26A4	pendrin	I^-, Cl^-, HCO_3^-, OH^-, formate, fructose, mannose	kidney, inner ear, thyroid, salivary gland	Pendred syndrome, DFNB4
SLC26A5	prestin	Cl^-, HCO_3^-, fructose, mannose	inner ear	non-syndromic hearing loss
SLC26A6	CFEX, PAT-1	Cl^-, HCO_3^-, NO_3^-, SCN^-, oxalate, formate	kidney, pancreas intestine, liver, stomach, heart	unknown
SLC26A7	none	Cl^-	endothelial venules, kidney, stomach, nasal epithelium, epididymal ducts	unknown
SLC26A8	Tat1	Cl^-, I^-, oxalate, SO_4^{2-},	brain, testis	male infertility?
SLC26A9	none	Cl^-, HCO_3^-, Na^+, OH^-, SO_4^{2-}, oxalate	lung, stomach, pancreas, prostate	unknown
SLC26A10P	none	pseudogene		unknown
SLC26A11	none	SO_4^{2-}	kidney, placenta, brain	unknown

Abbreviations: CFEX: chloride/formate exchange; DRA: Downregulated in Adenomas; DTDST: Diastrophic Dysplasia Sulphate Transporter; PAT-1: putative anion transporter-1; Sat-1: Sulphate anion transporter-1; Tat-1: testis anion transporter-1.

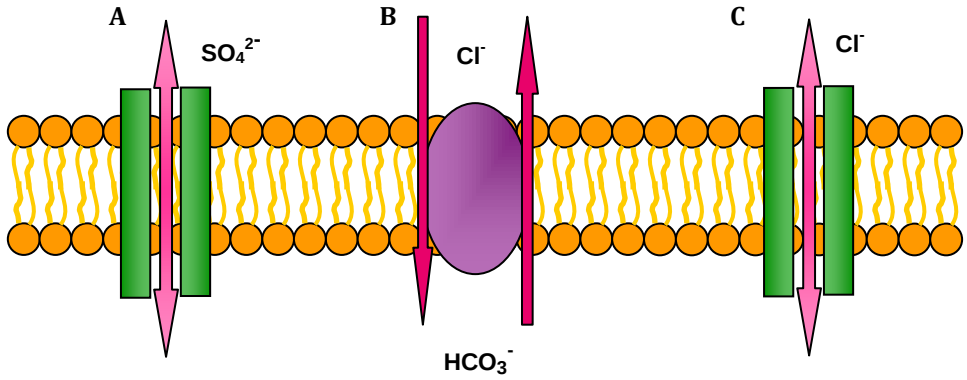

Figure 2: Transport modes of the SCL26A family members. **A**) SLC26A1 and SLC26A2 are SO_4^{2-} transporter. **B**) SLC26A3, SLC26A4 and SLC26A6 function as Cl^-/HCO_3^- exchanger. **C**) SLC26A7 and SLC26A9 are selective Cl^- channel.

Actually, this is a very narrow classification. In fact, the SLC26 proteins can also transport other anions of physiological relevance. For example, SLC26A4 has a relatively high affinity for I^- and prefer I^- over Cl^- and HCO_3^- (Shcheynikov *et al.*, 2008) and Pendred syndrome is associated with goitre as a result of impaired I^- organification in the thyroid (Everett & Green, 1999; Taylor *et al.*, 2002).

Moreover, many SLC26 members show different transport mode. SLC26A3 and SLC26A6 are Cl^-/HCO_3^- exchangers but also Cl^- channel (Ohana *et al.*, 2009; Shcheynikov *et al.*, 2006). SLC26A9 is a widely expressed SLC26 paralogue, particularly abundant in lung and stomach where CFTR, SLC26A3 and SLC26A6 are also present. Recently, Chang and colleagues showed the SLC26A9 moves *in vitro* inorganic ions by three distinct modes: (a) electrogenic nCl^-/HCO_3^- exchange, (b) electrogenic Na^+/nAnion cotransport, and (c) anion channel (figure 3). Chang assumed that the three SLC26A9 transport modes are unlikely simultaneously functionally and he speculated that kinases/phosphatases, binding proteins, and domain structures may dictate the Slc26a9 physiology in specific tissues, e.g., channel (figure 3 B) vs. transporter (figure 3 A and C) (Chang *et al.*, 2009b).

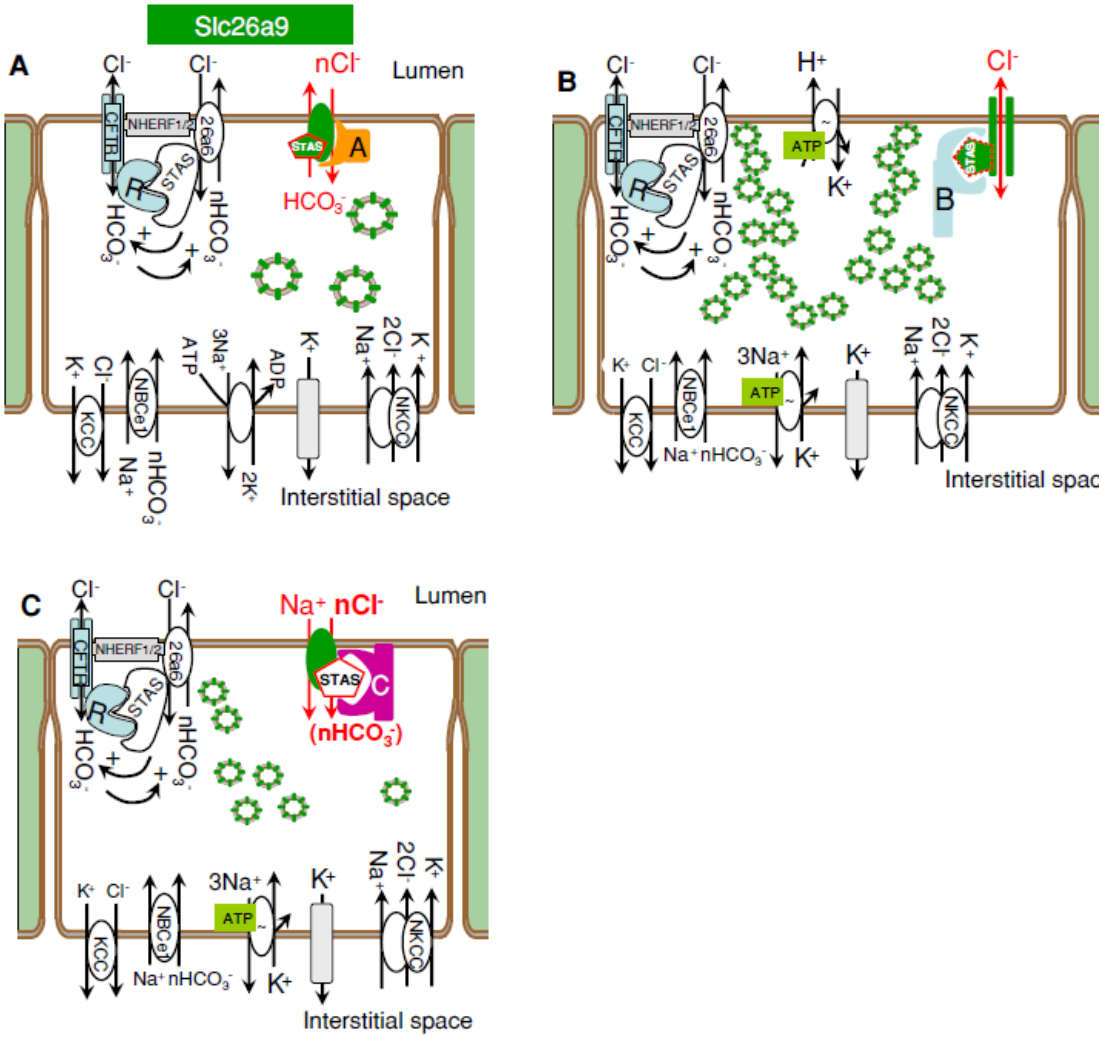

Figure 3: Model of SLC269 function in stomach and lung. **A**) An epithelial cell which is both absorbing Cl^- and secreting HCO_3^-. SCL26A9 is also indicated in intracellular vesicles. These vesicles could be recruited to the plasma membrane as a mechanism for controlling the amount of SLC26A9 plasma membrane function. **B**) One potential model of H^+ in the gastric parietal cell. While the parietal cell model shows SLC26A9 as Cl^- channel, it is possible to accomplish H^+ secretion with SLC26A9 as an electrogenic Cl^-/HCO_3^- exchanger. **C**) An epithelial cell in which SLC26A9 plays the role of a Na^+/ $nAnion^-$ cotransporter. These panel also depict putative interacting proteins (**A, B** and **C**) that would "switch" the physiological mode of SLC26A9 (Chang *et al.*, 2009b).

THE SLC26 FAMILY AND GENETIC DISEASES

Numerous mutations in four SLC26 genes have been shown to lead to human disorders (table 1). These disorders highlighted the important roles of these transporters in human physiology.

SLC26A2 was discovered by positional cloning of the gene responsible for diastrophic dysplasia (DTD)), a rare form of dwarfism, (Hastbacka *et al.*, 1994). Early

studies showed that primary skin fibroblasts from DTD patients had a greatly diminished sulphate uptake (Hastbacka *et al*., 1994). when compared to normal individuals, suggesting that the wild-type SLC26A2 gene may encode a functional sulphate transporter whose transport activity is abolished when mutated in DTD patients. This sulphate transporter linked to DTD became known as the diastrophic dysplasia sulphate transporter (DTDST).

More than 30 different disease-associated mutations have been identified in the SLC26A2 gene (Dawson & Markovich, 2005), of which the vast majority are private mutations found in single families of various ethnic origins. In all SLC26A2-related clinical conditions, the common biochemical defect has been demonstrated to be a reduced sulphate transport leading to undersulfation of cartilage proteoglycans, suggesting that a defect in sulphated proteoglycan biosynthesis occur in patient with the more severe chondrodysplasias (Hastbacka *et al*., 1994; Rossi *et al.*, 1996)

In 1993 Schweinfest and colleagues isolated a human cDNA from colon tissues, whose expression was downregulated in adenomas (DRA) and adenocarciromas. (Schweinfest *et al*., 1993). Mutations in the human DRA gene (*SLC26A3*) cause a genetic disorder congenital chloride diarrhea (CLD), (Moseley *et al.*, 1999) a rare autosomal disease characterized by watery diarrhea, containing elevated Cl^- concentrations, which can prove fatal, if left untreated. Currently, 30 mutations in SLC26A3 have been linked to CLD (Dawson & Markovich, 2005) and four of these are missense, deletion or insertion mutations that reside in the C-terminal portion of the transporter, probably resulting in misfolding and mistrafficking of SLC36A3 (Dorwart *et al.*, 2008a).

Pendred syndrome (PDS) is an autosomal-recessive disorder It was first described in 1896 as the combination of deafness and goiter (Pendred, 1896) but the precise phenotype has been detailed in recent year (Blons *et al.*, 2004; Campbell *et al.*, 2001) and involved two organ systems: the ear and the thyroid gland. PDS is caused by mutations of the SLC26A4 gene encoding pendrin, a transmembrane exchanger, which is expressed in inner ear and in the thyroid (Everett & Green, 1999). In addition to Pendred syndrome, mutations in SLC26A4 cause DFNB4, a type of nonsyndromic autosomal recessive deafness associated with enlargement of the vestibular aqueduct (Scott *et al.*, 2000). To date, more than 150 different variations have been reported. Several variations have been identified, including splice site mutations, missense mutations, insertions or deletions that lead to a stop codon (Yoon *et al.*, 2008).

SLC26A5 (or prestin) was identified by searching for the gene responsible for the electromotility of outer hair cells in the cochlea (Zheng *et al.*, 2000) and was subsequently linked to a form of no-syndromic hearing loss, confirming the physiological role of prestin in human auditory processing (Liu *et al.*, 2003).

STRUCTURAL FEATURES OF THE SulP FAMILY

The bacterial proteins vary in size from 434 residues to 573 residues with only a few exceptions. The eukaryotic proteins vary in size from 611 residues to about 1000 residues with a few exceptions. Thus, the eukaryotic proteins are usually larger than the prokaryotic homologues.

Although the level of amino acid identity between all members of the SulP family is low, at around 25%, hydropathy plot analysis of SulP family members are clearly similar and suggest that they contain 10-14 transmembrane helices with intracellular N- and C-termini. (Saier, 1999a; Smith *et al.*, 1995). SulP transporters also contain a C-terminal domain, the STAS domain in C-terminal cytosolic portion (see cap. 1.2) (Aravind & Koonin, 2000).

Much of the homology between SulP exchangers is found within the hydrophobic core of transmembrane domain. The first two putative transmembrane α-helices show a significantly higher level of conservation than that observed for the entire protein. This region includes one of the two "sulphate transporter motifs" that have been used to define the SulP family (Saier *et al.*, 1999b). The first *consensus* signature extends across putative helix 2 and comprises 22 amino acids (Prosite, PS01130; figure 2).

Although not all members of the family conform to the exact *consensus* sequence, this region contains several invariant residues that are presumably critical for anion transport. Moreover, an alignment of eukaryotic family members shows that there are also positions in helix 1 with high levels of conservation. In addition to conservation of the residue at each position, the spacing between them, including a short loop between the first two helices, is maintained throughout the eukaryotic members of the family (Leves *et al.*, 2008). Mutagenesis studies on these residues were performed on a plant sulphate transporter, SHST1, from the tropical legume *Stylosanthes hamata* (Leves *et al.*, 2008;

Loughlin *et al.*, 2002; Shelden *et al.*, 2001) and prestin (SLC26A5) (Rajagopalan *et al.*, 2006). These studies confirm the predicted importance of conserved residues in helices 1 and 2.

The second cluster of invariant residues defined by Saier and colleagues extends across putative helix 9 (figure 4; Saier *et al.*, 1999). Two mutations of conserved amino acids in this region affect the function of the plant sulphate/proton symporter, SHST1 (Khurana *et al.*, 2000). Moreover, mutations in the correspondent residues in SLC26A2 result in serious diseases (Hästbacka *et al.*, 1996). These result indicate that conserved residue between distinct members of the family may share essential roles in structure or function.

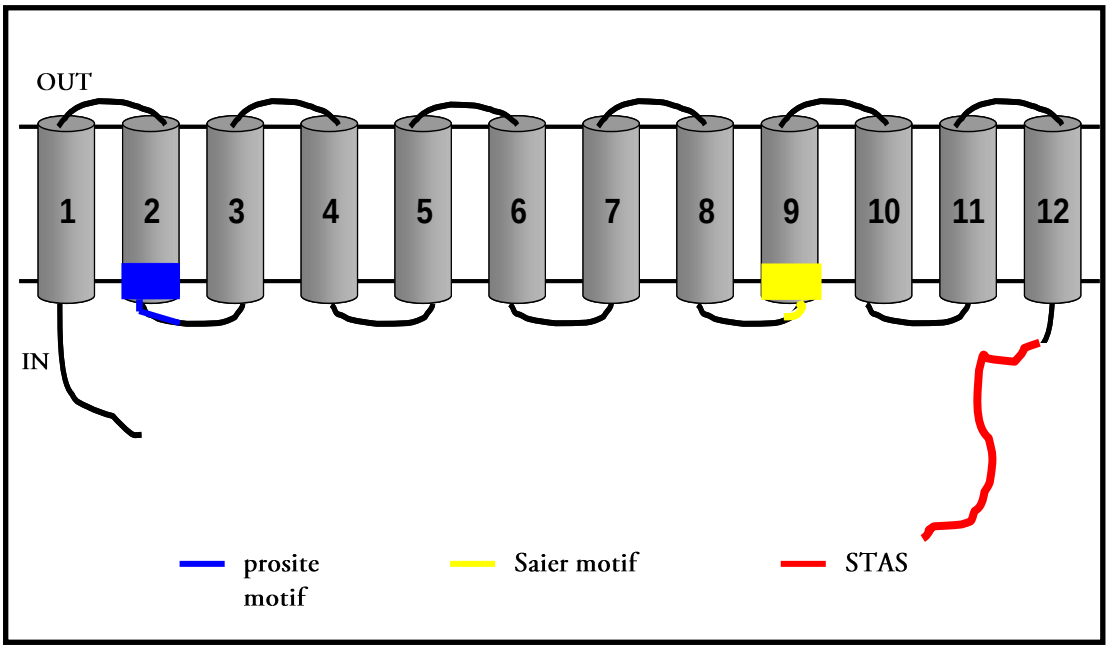

Figure 4: One predicted topology model of the SulP proteins. The position of various conserved motifs and domains is depicted. The number of transmembrane helices can vary from 10 to 14.

Concerning with the quaternary structure, SulPs appear to be assembled as dimers composed of two identical subunits. Detro-Dassen and colleagues studied the subunit stoichiometry of various SLC26 homologs from humans, rat, zebrafish, and *Pseudomonas aeruginosa* and they demonstrated that all tested isoforms exhibited a dimeric subunit stoichiometry. (Detro-Dassen *et al.*, 2008).

These transporters are not characterized in the 3D structure yet.

1.2 THE STAS DOMAIN

The less conserved C-terminal portion of all SulP transporters extends into the cytoplasm of the cell and includes a so called STAS (Sulphate Transporter and Antisigma-factor antagonist) domain. The name derives from a statistically significant similarity between this SulP portion (that can vary in length from 115 to around 250 amino acids) and the bacterial antisigma-factor antagonists (ASAs), typified by *Bacillus subtilis* SpoIIAA (117 residues long) (Aravind & Koonin, 2000).

Even if the 3D structures of some bacterial ASA are known (Campbell *et al.*, 2002; Etezady-Esfarjani *et al.*, 2006; Kovacs *et al.*, 1998; Lee *et al.*, 2004; Masuda *et al.*, 2004; Seavers *et al.*, 2001), STAS domains are poorly characterized in terms of both their function and structure.

THE ASA PROTEINS

The protein SpoIIAA participates, via phosphorylation and dephosphorylation, in the four-component system that regulates the sporulation sigma factor σ^F. Sporulation is a response of Gram-positive bacteria to nutrient deprivation. Instead of continuing normal vegetative cell division, the bacterium divides asymmetrically, and the resulting two chambers sporangium enters a pathway of differential gene expression that leads to the formation of a dormant cell type called the endospore (Errigton, 1996). Differential gene expression depends on specialized transcription factors called sigma factors that direct the RNA polymerase to transcribe specific genes in one or other of the two chambers at various stages of sporulation. Early in sporulation, SpoIIAA is in the phosphorylated state (SpoIIAA-P) (Feucht *et al.*, 1996), as a result of the activity of the ATP-dependent protein kinase SpoIIAB. SpoIIAA-P has very low affinity for SpoIIAB. About 80 min after the

initiation of sporulation a specific phosphatase, SpoIIE (Feucht *et al.*, 1996), begins to hydrolyse SpoIIAA-P, and the resulting SpoIIAA again becomes a substrate for SpoIIAB. SpoIIAB is also an anti-sigma factor that in its free form inhibits σ^F by binding to it. Competition by SpoIIAA (the anti-anti-sigma factor) for binding to SpoIIAB releases σ^F activity (Alper *et al.*, 1994).

SpoIIAA from *Bacillus subtilis* is a single domain globular protein with a largely compact structure (figure 5). The molecule contains four β strands (β_1–β_4) and four α helices (α_1–α_4) in the order $\beta_1\beta_2\alpha_1\beta_3\alpha_2\beta_4\alpha_3\alpha_4$. The central element of the SpoIIAA structure is a β-pleated sheet formed by four prominent β-strands, surrounded by four α-helices. The β-sheet in association with hydrophobic surface of α-helices, forms a hydrophobic core that is not readily accessible to the external medium. In contrast, the peripheral exposed surface of α-helices and loops are available for interactions with molecules in the environment.

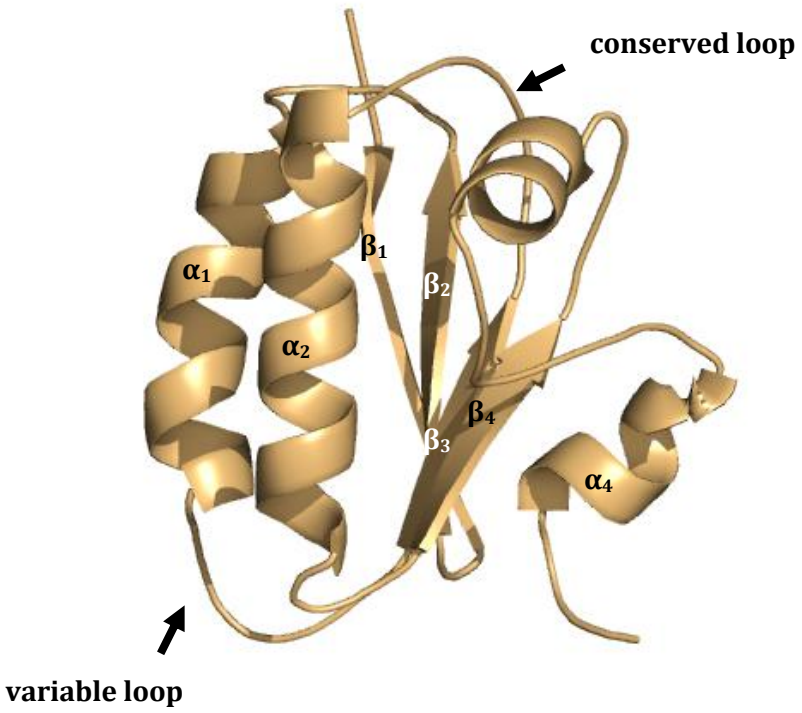

Figure 5: Global fold of SpoIIAA from *Bacillus subtilis* (Kovacs *et al.*, 1998) (PDB: 1AUZ). α-helices and β-strands are numbered sequentially. The position of two relevant loops in anion transporters, the variable and the conserved one, are indicated by arrows.

A phosphorylatable serine (Ser^{57} in *Bacillus subtilis*) in SpoIIAA is situated at N-terminus of helix α_2 in the conserved loop (figure 5). Its side chain is oriented away from

the main body of the molecule and into the solvent and phosphorylation does not perturb the gross structure of SpoIIAA (Seavers *et al.*, 2001).

THE SulP STAS DOMAIN

The SLC26 transporter C-terminal STAS domains were found to be homologous with the ASA proteins (Aravind & Koonin, 2000). However, the SulP STAS domain shows low overall sequence identity with SpoIIAA (about 15-20%). The conservation is traced largely to the four strands that form the scaffold of the STAS domain. There is also a highly conserved loop between the strand β3 and helix α2 (figures 5 and 6). This loop and the β-pleated sheet were proposed to play a role in nucleotide binding and hydrolysis, by extension from the known biochemistry of the ASA proteins (Aravind & Koonin, 2000). It has been shown that SpoIIAA binds GTP and ATP (Najafi *et al*., 1996; Seavers *et al.*, 2001) and possesses a weak NTPase activity that is abolished by phosphorylation or by mutation of the phosphorylable serine in the conserved loop (Najafi *et al*., 1996). The strong conservation of this loop in the STAS domains suggests that it could possess general NTP-binding activity. The presence of a predicted NTP-binding domain in the cytoplasmic portions of anion transporters indicates that anion transport could be regulated by intracellular concentrations of GTP and/or ATP.

Most of the variability between SulP STAS domains and ASA proteins is in the loop between helix α1 and strand β3 (figures 5 and 6), with inserts of considerable size in some of the anion transporters, of as much as 150 amino acids in the case of SLC26A8. This is evident from sequence alignment of all the anion transporters STAS domains and their structural homologues, the SpoIIAA proteins (figure 6). In the STAS domain of the bacterial transporters the loop is absent, in the plant transporter, Sultr1.2, it comprises around 10 residues, while for the mammalian transporters this loop is invariably longer. Secondary structure predictions algorithms suggest that this region is largely unstructured (Dorwart *et al.*, 2008b).

Moreover, in the SulP transporters, a variable extension at the C-terminal end of the domain is present and the secondary structure predictions of the extreme N- and C-termini do not correlate with that found in the bacterial ASAs.

Taking into account these differences in lengths as well as the low amino acid conservation observed, most probably the 3D structure of the anion transporters STAS domains significantly deviates from that of the bacterial ASAs, in a way not predictable solely on the basis of the sequence alignment. This is conceivable given the completely different biological roles and functions.

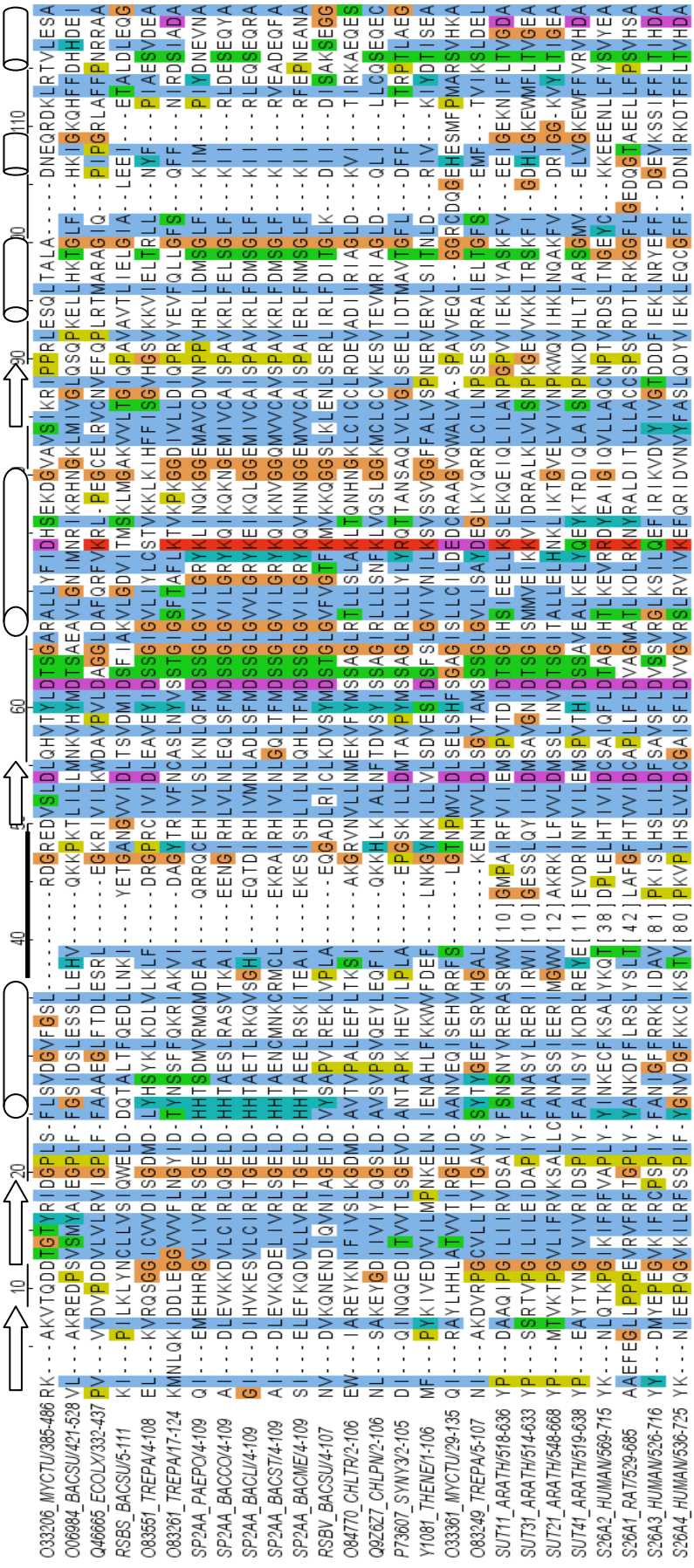

Figure 6: Multiple alignment of a selected set of STAS domains from antisigma-factor antagonist and anion transporters. Proteins are named according to their UniProtKB/TrEMBL accession number followed by the species abbreviation and the corresponding amino acids sequence. The secondary structure elements are derived from the structure of SPOIIAA and they are indicated above the alignment; cylinders represent α-helices and arrows represent β-strands. The thick line corresponds to the conserved loop. The sequence in the square brackets corresponds to the number of amino acids of the variable loop. The species abbreviations are: MYCTU: *Mycobacterium tuberculosis*; BACSU: *Bacillus subtilis*; ECOLX: *Escherichia coli*; TREPA: *Treponema pallidum*; PAEPO: *Paenibacillus polymyxa*; BACCO: *Bacillus coagulans*; BACLI: *Bacillus licheniformis*; BACST: *Bacillus stearothermophilus*; BACME: *Bacillus megaterium*; CHLTR: *Chlamydia trachomatis*; CHLPN: *Chlamydia pneumoniae*; SYNY3: *Synechocystis sp.*; THENE: *Thermotoga neapolitana*; ARATH: *Arabidopsis thaliana*. Sequence alignment was visualized using Jalview (Waterhouse *et al.*, 2009), using the Clustal X colour matrix.

THE STAS DOMAIN AND GENETIC DISEASES

The functional role of the STAS domain with respect to SulP family is largely unknown but the STAS importance is underlined by the fact that mutations that alter this domain in the SLC26 family can cause loss of function, resulting in serious diseases, like diastrophic dysplasia, Pendred syndrome, and congenital chloride diarrhea (Dawson & Markovich, 2005).

A715V, C653S, G678V and H665P are four disease-causing single amino acid mutations known, found in the 30-cytoplasmic putative STAS domain of DTDST (SLC26A2) (Rossi & Superti-Furga, 2001). Karniski tested three of these mutations and found that A715V and C653S are partial-function mutations, whereas G678V has no measurable sulfate transport activity in mammalian cells. The loss of function of the G678V mutation in mammalian cells is probably due to its inability to be properly targeted to the plasma membrane (Karniski, 2004).

Four of SLC26A3 mutations linked to CLD are missense, deletion or insertion mutations that reside in STAS domain (Chernova *et al.*, 2003; Dorwart *et al.*, 2008a; Ko *et al.*, 2002 and 2004). These mutations cause disease by two distinct molecular mechanisms: misfolding and mistrafficking, both ultimately leading to loss of functional protein at plasma membrane (Dorwart *et al.*, 2008a).

Currently, over 40 mutations in C-terminal domain of SLC26A4 are associated to Pendred syndrome (www.healthcare.uiowa.edu/labs/pendredandbor/slcMutations.htm). The majority of these mutant proteins has improper plasma membrane targeting and reduction or loss of transport function (Dossena *et al.*, 2009). For example, H723R-pendrin, the most common mutation in East Asians, is mostly expressed in endoplasmic reticulum (ER), and it causes defects in protein processing and ion transporting activities (Yoon *et al.*, 2008).

THE ROLE OF THE STAS DOMAIN IN THE SulP FAMILY

As already mentioned, the involvement of the STAS domain in the function/regulation of SLC26 transporter is underlined by mutations in this domain that cause acute diseases.

There are other lines of evidence confirming that the presence, folding and structure of the STAS domain are important in the SLC26 (or more generally SulP) transporter.

THE STAS DOMAIN AND THE SulP ANIONS TRANSPORT

It is not clear whether or not the STAS domain is directly involved in the anions transport of the SulP transporters.

In SLC26-related SulP polypeptide Rv1739c of *Mycobacterium tuberulosis*, the STAS domain is dispensable for Rv1729c-associated enhancement of sulphate uptake (Zolotarev *et al.*, 2008).

SLC26A9 can function as both an electrogenic nCl^-/HCO_3^- exchanger and a Cl^- channel (Chang *et al.*, 2009b). Deletion of the STAS domain does not generate a "dead" transport/channel but it produces different effects on two transport activities. After the STAS deletion, the SLC26A9 channel activity is drastically reduced (<80%) but STAS domain appears to be less crucial for the SLC26A9 electrogenic nCl^-/HCO_3^- exchange because a9-ΔSTAS maintains one-third of this exchange activity (Chang *et al.*, 2009a). It appears that the STAS domain of SLC26A9 can change the magnitude of these two SLC26A9 functions or perhaps enable SLC26A9 to favour one functional mode over the other.

In SLC26A3, removal of the STAS domain completely abolishes anion activity (Chernova *et al.*, 2003).

Studies on the sulphate transporter from *Arabidopsis thaliana* Sultr1.2 examined the effect of deleting or modifying the STAS domain. Deleting the last 4, 7, 8 or 12 amino acids of the Sultr1.2 C-terminal extension resulted in a corresponding 20, 50, 70 or 100% reduction in the ability of protein to transport sulphate (figure 7). The eighth and ninth from the end of the transporter are two cysteine residues. The mutation of the two cysteines revealed that their importance for the optimum sulphate uptake by Sultr1.2, even

though neither the single nor the double cysteine substitutions completely abolished the transport ability (Rouached *et al.*, 2005).

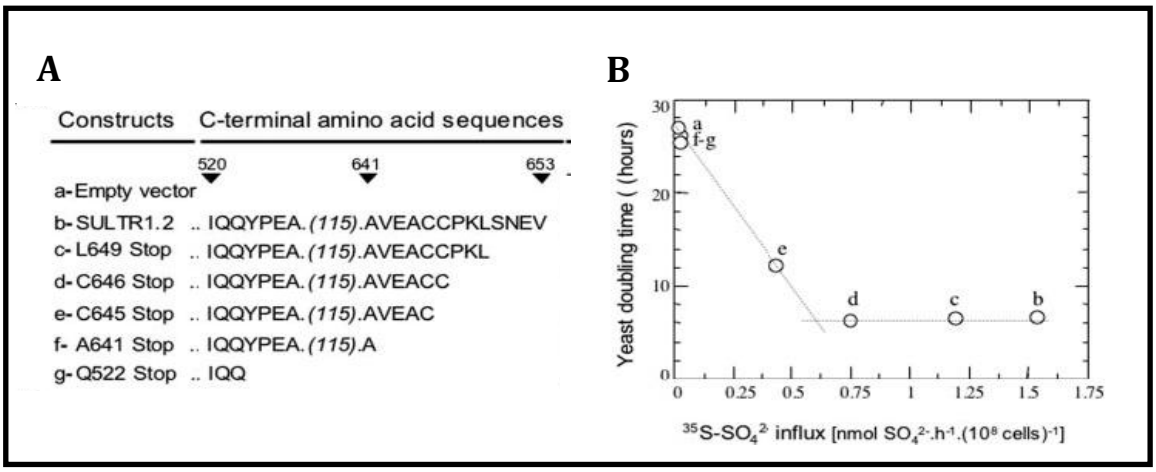

Figure 7: Growth phenotype and sulfate uptake capacity of theyeast YSD1 mutant expressing Sultr1.2 constructs displaying C-terminal deletions. **A**) pYES2 vectors empty (*a*) or containing serial deletions (*b–g*) of the C-terminal region of Sultr1.2 (as specified) were used to transform the yeast YSD1 mutant defective in its sulfate transport capacity. Numbers above the sequence relate to the position of the corresponding amino acids in the Sultr1.2 sequence. **B**) Relationship between [^{35}S] sulfate short term influx measurements and the doubling time of the corresponding YSD1 yeast mutant transformed with the constructs (*a–g*) described in panel A. Dotted lines correspond to a least square adjustment. (Adapted from Rouached *et al.,* 2005).

A theoretical model for the STAS domain of Sultr1.2 has been derived on the basis of the available NMR structure of *B. subtilis* SpoIIAA and the crystal structure of *B. sphaericus* SpoIIAA (figure 8) (Rouached *et al.*, 2005; Shibagaki & Grossman, 2006). Mutations in the N-termini of the first α-helices and in the loop adjacent to α_1 (Y542C, F543Y, N545I, A540S, V549I and I608S in figure 8) of Sultr1.2 STAS showed a number of amino acids critical for the function of the protein; mutations in these regions still allow protein accumulation in the plasma membrane, but the protein is no longer capable of efficiently transporting sulphate into cells (Shibagaki & Grossman, 2006).

The Q522K and the Y523H substitutions at N-terminus of β_1 (figure 8) result in the accumulation of non functional Sultr1.2 in the plasmamembrane (Shibagaki & Grossman, 2006) and a T587A substitution (potentially a phosphorylation site) is shown to eliminate Sultr1.2 activity (Rouached *et al.*, 2005). It very interesting to note that these last three residues are located on the same STAS surface (figure 8). Shibagaki & Grossman assumed that this surface is a probable interaction site because this is the same face that forms the SpoIIAA-SpoIIAB dimer interface (Shibagaki & Grossman, 2006).

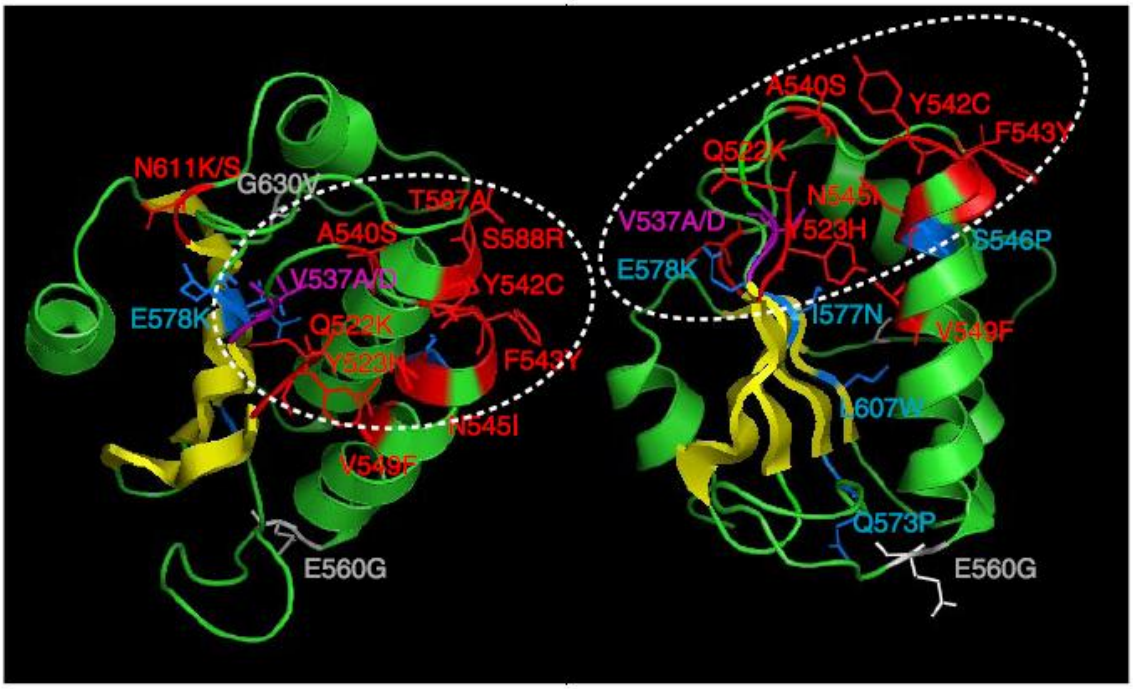

Figure 8: Two different view of three-dimensional theoretical model of the STAS domain of Sultr1;2, with mutations that affect its function **(**Rouached *et al.*, 2005). β-Strands are colored yellow and helices in green. The structures show side chains of the original residues substituted in mutant Sultr1;2 polypeptides. Coloring of the residues indicates the consequences of the substitution. E560G and G630V (substitutions in *gray*) cause decreased accumulation of the Sultr1;2 polypeptide, but the remaining protein exhibits some activity (suggesting that Glu-560 and Gly-630 are important in Sultr1;2 biogenesis). Mutations that allow Sultr1;2 protein accumulation but diminish its function are mostly clustered on the STAS surface, which is delimited in both STAS domain orientations shown by *dotted lines*. This surface includes Ala-540, Tyr-542, Phe-543, and Asn-545, which are in or contiguous to the N terminus of α1, Thr-587 and Ser-588 in the N-terminal end of α2, Gln-522 and Tyr-523 in the N-terminal end of β1, and Val-537 in the C-terminal end of β2 (Shibagaki & Grossman, 2006).

THE STAS DOMAIN AND THE MEMBRANE TARGETING OF SulP TRANSPORTERS

The most frequent result of STAS mutations is the ER retention and the loss of a functional protein in plasma membrane. This is a common disease-causing mechanism in the SLC26A protein family as a number of mutations in SLC26A2, SLC26A3 and SLC26A4 have shown ER retention when monitored by immunofluorescence (Dorwart *et al.*, 2008a; Karniski, 2004; Rotman-Pikielny *et al.*, 2002; Taylor *et al.*, 2002).

SLC26A1 (or sat-1) is expressed on basolateral membrane (BLM) of the kidney proximal tubule where it function as a sulphate/oxalate exchanger (Karniski *et al.*, 1998). The STAS domain of sat-1 includes a dileucine motif at position 677/678 which is an important sorting determinants for trafficking to BLM of ephitelia cells. Deletion of these residues resulted in the loss of BLM sorting (Regeer & Markovich, 2004).

Studies on Sultr1.2 suggest that the STAS domain is essential not only for the sulphate transport but also for facilitating localization of the transporter to the plasma membrane (Shibagaki & Grossman, 2004 and 2006). An experiment of random mutagenesis in the STAS domain of Sultr1.2 identified domain lesions that altered the transporter biogenesis (Shibagaki & Grossman, 2006). A number of mutations in the β-sheet that forms the core of the STAS domain prevent plasma membrane accumulation of Sultr1.2. So the β-sheet seems to serve as a core structure of the STAS domain and lesions within this structure may disrupt proper STAS folding, which could destabilize the entire transporter.

THE INTERACTION BETWEEN STAS DOMAIN AND OTHER PROTEINS

A most interesting example of the STAS role in the regulation of membrane transport through interaction with other proteins comes from the SLC26A6 transporter. The SLC26A6 STAS domain interacts with the carbonic anhydrase isoform II (CAII) (Alvarez *et al.*, 2005).

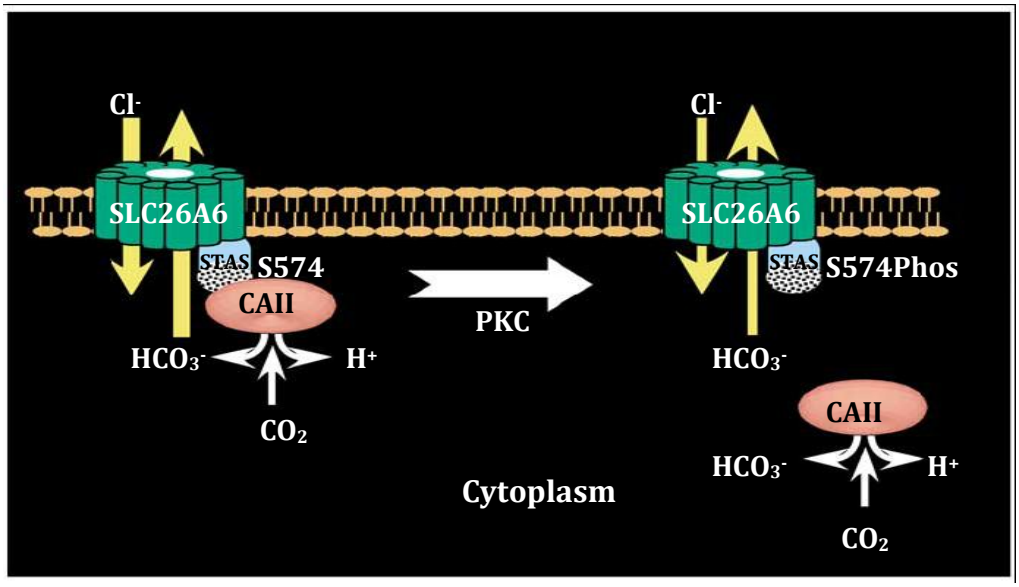

Figure 9: Regulation of SLC26A6 bicarbonate transport. CAII binds the STAS domain of SLC26A6. Interaction with the CAII maximizes the local HCO_3^- concentration at the SLC26 transport side, thereby maximizing transport rate. PKC phosphorylates SLC26A6 at S574, which displaces CAII. Isolation of CAII from the surface of SLC26A6 reduces the local concentration of HCO_3^-, reducing the transport rate. Arrows on the SLC26A6 image represent the movement of Cl^- and HCO_3^-, where the arrow width indicates the relative rate in each case (Adapted from Alvarez *et al.*, 2005).

Mutations in the CAII-binding site significantly reduces SLC26 transport activity, probably because the CAII/transporter association maximize the HCO_3^- transport flux. Moreover, in the SLC26A6-expressing cells, PKC activation resulted in (1) phosphorylation of S574 in the SLC26A6 STAS domain, (2) reduction of SLC26A6 transport activity and (3) displacement of CAII from the cytosolic surface of the plasma membrane (figure 9) (Alvarez *et al.*, 2005). The CAII-binding site (568D-F571) and the S574 PKC site are in a position corresponding to the beginning of the variable loop, suggesting a role of the loop in the transport regulation.

Another important physiological interaction is between several SLC26 members and the cystic fibrosis transmembrane conductance regulator (CFTR).

The STAS domain and CFTR

Chloride absorption and bicarbonate secretion are tightly associated process vital to the function of all epithelia. Their critical importance is reflected in cystic fibrosis (CF), in which the primary defect is a problem with the inability of mutant forms of CFTR to activate chloride-bicarbonate exchange (Choi *et al.*, 2001).

Cystic fibrosis transmembrane conductance regulator (CFTR) is a member of the ABC family of membrane transporters. CFTR functions as cAMP-regulated channel that is regulated by PKA phosphorylation and is expressed mainly in the apical membrane of the epithelial tissues, where it has a crucial role in regulating fluid secretion (Sheppard & Welsh, 1999).

CFTR is a poor transporter for HCO_3^- but it is able to regulate the activity of SLC26 chloride-bicarbonate exchangers, A3 and A6 (Ko *et al.*, 2002 and 2004; Shcheynikov *et al.*, 2008). There is a mutual activation between CFTR and SLC26 transporters. In fact, SLC26 anion exchange activity is enhanced when CFTR is activated by phosphorylation and also the PKA-stimulated CTFR channel activity is six fold higher in HEK cells co-expressing either SLC26 exchanger with CFTR, compared with CFTR alone (Ko *et al.*, 2004).

The interaction between CFTR and SLC26 members is mediated by binding of the phosphorylated regulatory (R) domain of CFTR to the STAS domain of SLC26 and is modulated by PDZ scaffold proteins (CAP70, EBP50 or NHERF) that tether the two transporters into a multimeric complex (figure 7) (Ko *et al.*, 2004; Lohi *et al.*, 2003; Rossman *et al.*, 2005). The formation of this complex is a crucial point to explain the

interaction between CFTR and SLC26 members. The chloride-bicarbonate exchangers SLC26A4, which is coexpressed with SLC26A6 and CFTR in parotid duct, is not regulated *in vivo* by CFTR, whereas SLC26A6 is, probably because SLC26A6, but non SLC26A4, has a C-terminus PDZ ligand (Shcheynikov *et al.*, 2008). In this respect, when PDZ ligands of CFTR and SLC26A6 are deleted, the activation of SLC26A6 by CFTR is attenuated and can be rescue by over-expression of these mutants (Ko *et al.*, 2004).

CFTR channel activity requires an intact R domain of CFTR and the STAS domain of the SLC26 transporters, and the purified STAS domain alone was sufficient to induce the activation (Ko *et al.*, 2004).

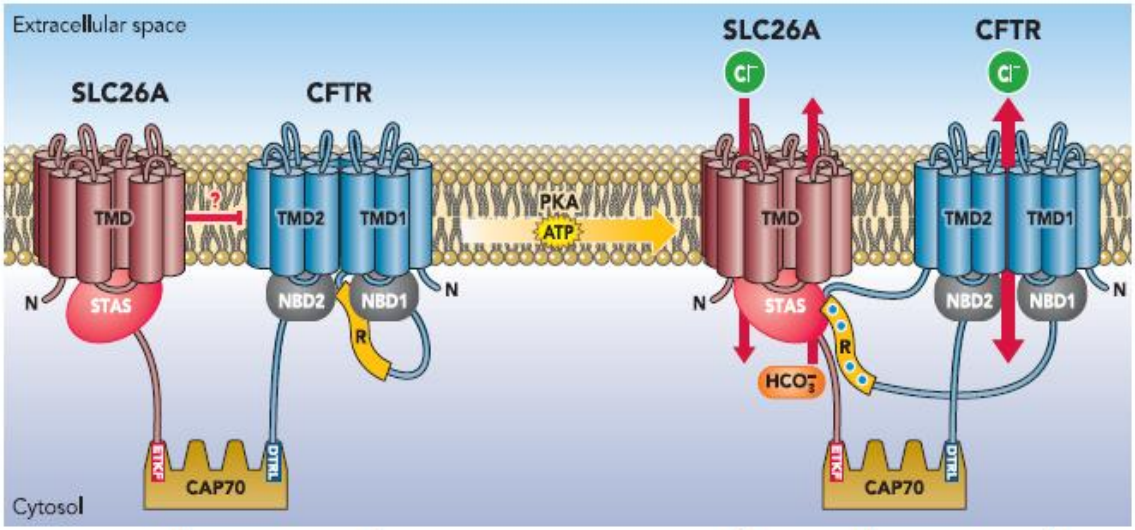

Figure 7: The regulatory interaction between SLC26 transporter and CFTR. A PDZ domain-containing scaffolding protein assembles membrane complexes of CFTR and the SLC26 transporters. To avoid unnecessary secretion in resting state, the nonphosphorylated R-domain interacts with NBD1 to prevent interaction with NBD2 and activation of CFTR Cl^- channel activity. Activation of PKA phosphorylates the R-domain to alter its binding to NBD1 and the same time enhances its binding to the STAS domain. This results in the mutual activation of CFTR and the SLC26 transporter and in the activation of fluid and electrolyte secretion (Dorwart *et al.*, 2008b).

Loss-of–function mutations in the STAS domain of the SLC26A3 that give rise to the CLD, prevent activation of CFTR, suggesting a possible role for the CFTR in pathogenesis of this disease, and mutants of CFTR associated with CF, modify activation of SLC26A3 (Ko *et al.*, 2002 and 2004).

Also SLC26A9 is able to bind CFTR in the R-region (Chang *et al.*, 2009a). However, unlike previously reported data, the binding interaction inhibits SLC26A9 ion transport activity. Chang and colleagues assumed that different structural interactions may

exist between specific STAS domains and the R-domain of CFTR or alternatively, if the CFTR R-region interaction with different STAS domains is identical, differing structural response must.

1.3 THE PRESTIN PROTEIN

Prestin is the fifth member (A5) of the SLC26 family of anion exchangers. It is highly and almost exclusively expressed in the Outer Hair Cells (OHCs) of the organ of Corti in the inner ear of mammals. Although the basic function of SLC26A members is to transport anions (Mount & Romero, 2004), this is not prestin principal role. Unlike the other members of the SLC26 family, mammalian prestin has the unique property of the voltage-dependent conformational changes and it is considered the key player in the OHC somatic electromotility (Zheng *et al.*, 2000). Since its discovery, it was clear that prestin is fundamentally different from other biological force generators. Its particular mechanism of action makes it the most interesting subject among SLC26A family members, as shown by the increasing number of publications within recent years.

THE OHCs AND PRESTIN

The mammalian cochlea of the inner ear is a fluid-filled duct. It is coiled into a compartment within the temporal bone on either side of the head. Sound is funnelled through outer ear and transmitted through the middle ear to the cochlear fluids where the final effect is to stimulate, appropriately, the sensory hair cells of the cochlea. The mammalian cochlea contains two classes of hair cells arranged in rows along the organ of Corti. Inner hair cells (IHCs) are innervated by dendrites of the auditory nerve and are considered to be the primary sensory hair cells of the cochlea. Outer hair cells (OHCs) receive dominant efferent innervations and are responsible for the sensitivity. It is assumed that OHCs are the amplifiers and that the IHCs are passive detectors of the amplified vibratory signal (Dallos, 1992). In 1985, the distinctive properties of OHCs were first discovered by William Brownell, who showed that these cells can convert electrical signals into motion, a phenomenon called electromotility. (Brownell *et al.*, 1985) In the absence of the OHCs hearing sensitivity is severely degraded (Ryan & Dallos, 1975).

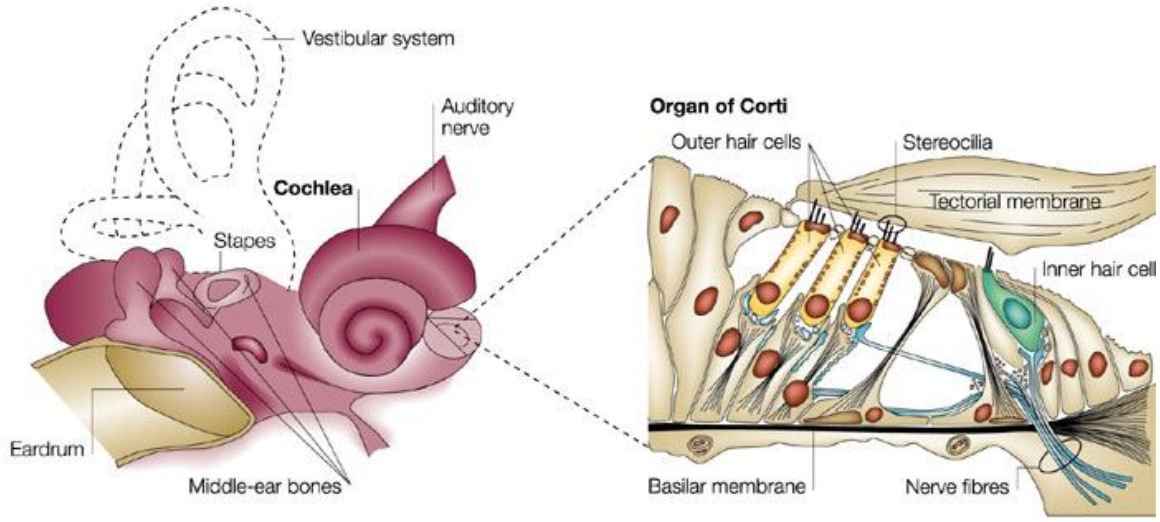

Figure 8: A cross section of the cochlea illustrating the organ of Corti, the sensory epithelium of the inner ear. A single row of inner hair cells and three rows of outer hair cells are located on the basilar membrane. The tectorial membrane overlies the epithelium and normally contacts the stereocilia of the outer hair cells (Dallos & Fakler, 2002).

The OHC is a cylindrically shaped cell whose length varies from short (~10–20 μm) to long (>80 μm) along the length of the basilar membrane. OHCs contract with depolarization and elongate with hyperpolarization (Ashmore, 1990; Santos-Sacchi & Dilger 1988). The salient features of the OHCs electromotility include the following: first, electromotility takes place without hydrolysis of high-energy phosphates such as ATP and energy is supplied by the changing membrane potential of the cell; second, whereas internal Ca^{2+} levels modulate motility, Ca^{2+} ions are not required for the expression of this response; third, the electromotile response occurs at microseconds rates and works in cycle-by-cycle mode up to a frequency at least 70 kiloHertz (Dallos & Fakler, 2002).

About a decade ago Peter Dallos and co-workers discovered a membrane protein, unique to OHCs, that can respond to electrical signals (Zheng *et al.*, 2000). The Dallos group coined the name "prestin" for this protein in an analogy with the musical term "presto" (quickly) due to its rapid response to electrical signals. When prestin was heterologously expressed in several cell lines, the transfected cells exhibited behaviors that are normally observed only in OHCs: voltage-dependent NLC (nonlinear capacitance, the capacitance the arise from the movement of charge that is driven by changes in the transmembrane potential), and shape changes (Zheng *et al.*, 2000); charge transfer across the membrane (Dong & Iwasa, 2004); temperature sensitivity (Meltzer & Santos-Sacchi,

2001). In addition, the electromotile responses in prestin transfected kidney cells can be inhibited by salicylate, an inhibitor of somatic electromotility in OHCs (Oliver *et al.*, 2001; Zheng *et al.*, 2001). OHCs from prestin-null mice lack somatic electromotility, and those mice also lose 40– 60 dB of hearing sensitivity (Liberman *et al.*, 2002) and lack frequency selectivity (Cheatham *et al.*, 2004). A splicing mutation in prestin gene causes non-syndromic deafness (Liu *et al*., 2003).

PRESTIN AND DEAFNESS

The restricted expression of prestin in OHCs and its proposed function as a mechanical amplifier make it a strong candidate for an association with human deafness. However, the role and the extent of the *prestin* gene defects in human non-syndromic hearing impairment are still poorly understood.

The human *prestin* gene contains 21 exons and is localized on the long arm of chromosome 7 (7q22.1). A single nucleotide change in the *prestin* gene was reported to be associated with hearing loss (Liu *et al.*, 2003). The DNA sequence variation, IVS2-2A>G, is an A to G transition in the splice acceptor site for exon 3. It was suggested that this mutation leads to aberrant mRNA splicing and results in non-syndromic moderate-to-profound sensorineural hearing impairment. In addition, a relatively high frequency of heterozygosity for this sequence change was observed in affected subjects, suggesting the possibility of a semi-dominant influence of the mutation. By contrast, further studies demonstrated that the IVS2-2A>G variant may not occur more frequently in hearing impaired patients than in controls, and heterozygosity for this transition may not be sufficient to cause hearing loss (Tang *et al.*, 2005; Teek *et al.*, 2009).

In addition, a heterozygous missense mutation (R150Q) in the sixth coding exon of the *prestin* gene was reported to potentially cause mild to moderate non-syndromic hearing loss (Toth *et al.*, 2007). This is the first genetic and electrophysiological analysis of a human mutation in a coding exon of the *prestin* gene, although the pathogenic role of the R150Q mutation is not unambiguous.

These two changes are, so far, the only ones reported with potential clinical importance. Further studies are needed to clarify the pathogenic role, if any, of these

nucleotide substitutions, as well as of other *prestin* changes, in the etiology of hearing loss.

MECHANISM OF ACTION

Prestin is a new type of biological motor. It is entirely different from the conventional enzymatic-activity-based motor proteins, in that it does not need ATP to function, but it is a direct voltage-to-force converter. In this case the energy is supplied by the changing membrane potential of the cell and this is probably unique in the animal kingdom (Dallos *et al.*, 2006). The action of prestin is also orders of magnitude faster than that of any other cellular motor protein, as it functions at microsecond rates. In fact, OHC motility works at frequencies up to at least 70 kHz (Frank *et al.*, 1999).

In addition, prestin, like other transducers, exhibits piezoelectrical properties: it generates mechanical force upon electrical stimulation and may also change its electrical properties upon mechanical stimulation (Ludwig *et al.*, 2001; Santos-Sacchi *et al.*, 2001). It was estimated that a single prestin molecular assembly produces a force in the OHC axial direction of about 2.4 picoNewtons and a conformational displacement of around 1 nm (Zheng *et al.*, 2000).

How the membrane potential change of OHCs results in structural changes in prestin, corresponding to the motor function, is not understood yet. Conceptually, prestin should comprise at least two essential functional domains: the voltage sensor that detects changes in the transmembrane potential of the cell, and the actuator that undergoes a conformational change and thereby facilitates cell contraction or elongation in response to depolarization and hyperpolarization, respectively (Dallos & Fakler, 2002).

The NLC associated with prestin was found to depend upon intracellular chloride (Oliver *et al.*, 2001). As for other member of SLC26 family, prestin is likely to have at least one Cl^- binding or interaction site and chloride ions have a powerful effect on prestin (Oliver *et al.*, 2001; Rybalchenko & Santos-Sacchi, 2003; Song *et al.*, 2005). Like other member of SLC26 family, prestin can bind a broad range of substrates (Rybalchenko & Santos-Sacchi, 2003; Song *et al.*, 2005). Two different transport modes have been proposed to explain the prestin function.

INCOMPLETE TRANSPORTER

Initially it was assumed that the voltage sensor of prestin is made up of a charged residue non-conserved between prestin and the other SLC26A member, which produces no motility. Oliver and colleagues altered each charged, non-conserved amino acid in the putative membrane-interacting region of prestin, individually or in groups Surprisingly, no combination of mutations eliminated NLC or altered its gain. These results led to the suggestion that the voltage sensor may not be an intrinsic component of the protein, but an extrinsic ion. Using inside-out and outside-out membrane patches, it was demonstrated that intracellular Cl^- functions as the extrinsic voltage sensor. After binding to a site with millimolar affinity, this anion is translocated across the membrane, without being released in the extracellular space, by the transmembrane voltage: toward the extracellular surface upon hyperpolarization, toward the cytoplasmic side in response to depolarization. Subsequently, this translocation triggers conformational changes of the protein that finally changes its surface area in the plane of the plasma membrane, shifting from an expanded to a contracted state (figure 9A) (Oliver *et al.*, 2001).

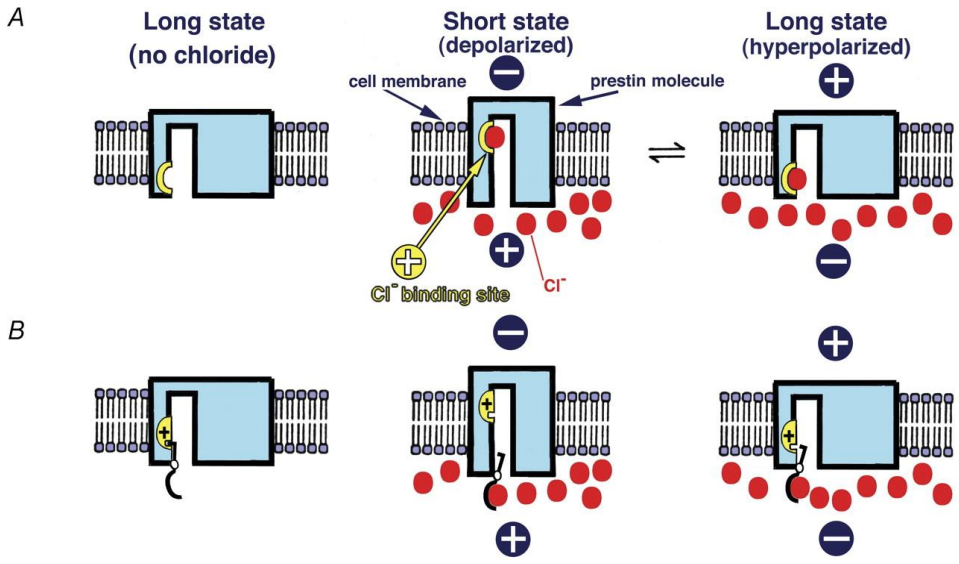

Figure 9: Two models of prestin gating by voltage, in which the presence of intracellular chloride is an essential factor in both, but the gating mechanisms are different The long (or extended) state of the molecule corresponds to hyperpolarization of the cell; the short (or compact) state to depolarization. The no-chloride case is arbitrarily modelled as long. **A**) Cl^- is assumed to associate with a positive binding site and the combination is translocated across the membrane. **B**) chloride binding enables a positive gating particle to unlock and be translocated (Oliver *et al.*, 2001).

Subsequent investigations showed that as intracellular Cl^- concentration decreases, the amount of charge transferred also decreases and voltage sensitivity shifts in the depolarizing direction (Rybalchenko & Santos-Sacchi, 2003; Santos-Sacchi *et al.*, 2006). The direction of shift implies that the net charge moved across the membrane is positive. Thus, two alternatives exist to the idea that Cl^- is the voltage sensor. It is possible that monovalent anions need to attach to a binding site and their combination, with net positivity, is translocated across the membrane. Alternatively, chloride binding could enable an allosteric change, thereby allowing a positive gating charge to be moved (figure 9) (Rybalchenko & Santos-Sacchi, 2003). In this case, all charge movement is provided by the translocation of the intrinsic positively charged sensor.

ANION ANTIPORTER

Recent theoretical work suggests that many experimental data could be better explained if one assumes that prestin acts as an electrogenic anion exchanger, exchanging one Cl^- ion for one divalent or two monovalent anions According to this model, the charge movement arises as a result of both a Cl^- ion and intrinsic charged residues moving across the membrane. Thus net positive charge is moved across the membrane as the Cl^- ion is moved towards the extracellular surface. This model is independent of the nature of the Cl^- replacing anion, which could be mono- or divalent as long as it guarantees that the reorientation of the intrinsic charged residues is electroneutral (figure10) (Muallem & Ashmore, 2006).

This is the transport mode (with a 1:1 stoichiometry) shown for two nonmammalian orthologs of prestin, from zebrafish and chicken (Schaechinger & Oliver, 2007). The zebrafish prestin ortholog, zprestin, shares around 50% amino acid identity with mammalian prestin. Like its mammalian ortholog, zprestin is expressed in hair cells of the ear and confers NLC to the membranes of transfected cells, similar to the characteristic electrogenic charge movement that accompanies the prestin-mediated somatic electromotility of mammalian OHCs (Albert *et al.*, 2007). The localization of chicken prestin is not clear. Mammalian and nonmammalian isoforms share a substial degree of sequence conservation, especially in hydrophobic core region (Okoruwa *et al.*, 2008).

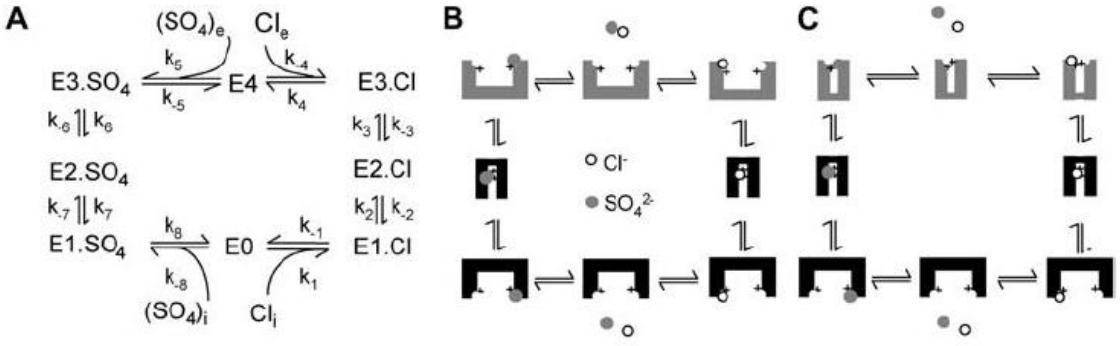

Figure 10: **A**) The reaction scheme for a Cl^-/SO_4^{2-} exchanger model. Prestin exchanges one Cl^- ion for one SO_4^{2-} ion via an alternating-access mechanism, in which prestin can only change between inward and outward facing states with an anion bound. **B**) and **C**) Two alternative representations of the reaction scheme: both assignments ensure that the critical voltage-dependent transition, E1.Cl↔E2.Cl, is associated with a conformational change of prestin into a compact state and symmetry is maintained (Muallem & Ashmore, 2006).

The unusually high density of prestin in OHCs compared with other transporters suggest its primary function is to drive electromotility, and it is unlikely that is also plays the critical role in regulating intracellular chloride (Muallem & Ashmore, 2006).

PRESTIN TOPOLOGY

Prestin is a transmembrane glycoprotein of 744 residues, with a molecular weight of about 81 kDa (Zheng *et al.*, 2000). It contains about 50% of non-polar residues and it shares the overall structure and specific protein domains of the SLC26 family, such as a highly conserved central core of hydrophobic amino acids (~400 a.a.) and a cytoplasmatic N- (~100 a.a.) and C-termini (~240 a.a.) (figure 11). Prestin is a highly conserved protein with 92.7% of amino acids being identical among four different mammalian species: human, mouse, rat and gerbil (He *et al.*, 2006). Such a high degree of conservation is not common among other SLC26A members Significant changes in prestin primary sequence occurred after the split between mammalian and avian lines, suggesting that prestin evolved in order to fit special mammalian needs (Dallos *et al.*, 2006).

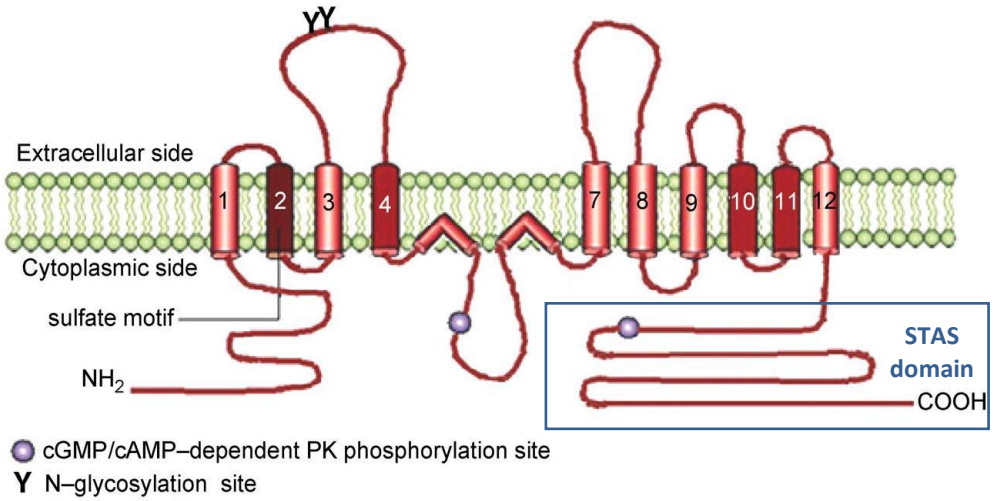

Figure 11: A membrane topology model of prestin, with 12 membrane helixes, N- and C-terminal cytoplasmic domains. On the basis of the existence of a phosphorylation site at the level of the third loop, helices 5 and 6 are inserted into the membrane, but do not cross it, forming re-entrant loops. The conserved "SulP transporter motif" is present in the second transmembrane domain while a STAS motif is located in the C-terminal region. The two potential N-glycosilation sites Y (Asn163 and Asn166) are labelled on the extracellular surface of the protein (Adapted from Deak *et al.*, 2005).

The number of the membrane helixes is still disputed as topology prediction programs produce ambiguous results: 10 or 12 transmembrane helixes can be hypothesized (Deak *et al.*, 2005; Navaratnam *et al.*, 2005; Oliver *et al.*, 2001; Zheng *et al.*, 2001). The 12 transmembrane domains model is supported by more experimental evidence and it is, in part, based on placing two potential N-glycosilation sites (Asn163 and Asn166) on the extracellular surface of the protein (Matsuda *et al.*, 2004). In figure 11, prestin is represented with 12 membrane helixes: on the basis of the existence of a phosphorylation site (cGMP/cAMP-dependent protein kinase phosporylation site) at the level of the third loop, helices 5 and 6 are inserted into the membrane, but do not cross it, forming re-entrant loops (Deak *et al.*, 2005).

The conserved "SulP transporter motif" is present in the second transmembrane domain, while the C-terminal cytoplasmic region includes the Sulphate Transporter and Anti-Sigma factor antagonist (STAS) domain. Two distinctive charged segments are located in the C-terminal region: a positive-charge cluster is located at residues 557-580; adjacent to this there is a negative-charge cluster at residues 596-613.

OLIGOMERIZATION PROPERTIES

The examination of OHC lateral membrane (where prestin is located) by freeze-fracture reveals densely packed 11 nm diameter particles (Forge, 1991; Kalinec *et al.*, 1992). How prestin forms oligomers and what part of the molecule is involved in their formation is not completely clear yet, although the involvement of both the N- and the C-terminal domains has been suggested (Navaratnam *et al.*, 2005; Zheng *et al.*, 2005).

The first evidence for prestin multimerization came from fluorescence resonance energy transfer experiments that showed that homodimerization of prestin depends on an intact N-terminus (Greeson *et al.*, 2006; Navaratnam *et al.*, 2005).

The issue of the number of subunits necessary to form a functional motor protein was first addressed by Zheng and colleagues. In their study, native and recombinant prestin, obtained from different expression systems, including yeast and mammalian cell lines, are seen resistant to dissociation by lithium dodecyl sulphate and behaves as a stable oligomer. Chemical cross-linking and perfluoro-octanoate-electrophoresis (PFO-PAGE) combined with immunoblotting and affinity purification suggest a tetrameric subunit stoichiometry of prestin. Moreover sodium dodecyl sulphate (SDS) dissociates the tetramer into dimers that can be converted to monomers by hydrophobic reducing agents, but not by the hydrophilic ones. These data suggest that prestin is composed by dimmers covalently linked by disulfide bonds located in the hydrophobic membrane core and that these dimers associate via hydrophobic interactions to form a tetramer. They proposed that the stable covalent dimer may act as the building block for producing the higher order oligomers that form the 11 nm particles in the OHC lateral membrane (Zheng *et al.*, 2006).

By contrast, the experiments of Detro-Dassen, while acknowledging dimers as the functional form, deny that these are formed by covalent bonds. They studied the subunit stoichiometry of rat, zebrafish prestin and of other SulP proteins, SLC26A3 and the bacterial paralog from *Pseudomonas aeruginosa* (PASulP), expressed in *Xenopus laevis* oocytes or in mammalian cells. According to blue native PAGE and chemical cross-linking experiments, prestin and the other SulP proteins form dimers as predominant oligomeric state. Oligomers dissociate entirely into monomers under non-reducing conditions in the presence of low concentrations of SDS. So they concluded that dimers

are held together by non-covalent forces rather than by covalent disulfide bonds (Detro-Dassen *et al.*, 2008).

A preliminary indication of prestin shape was provided by Mio and colleagues who expressed prestin in baculovirus-infected Sf9 cells and purified it. They observed the negatively stained molecules using electron microscopy, and reconstructed the 3D structure of prestin at 2 nm resolution by single particle analysis. Their result is consistent with prestin being a tetramer, having a large cytoplasmic domain and assuming a "bullet shape", with a fourfold symmetry (figure 12) (Mio *et al.*, 2008).

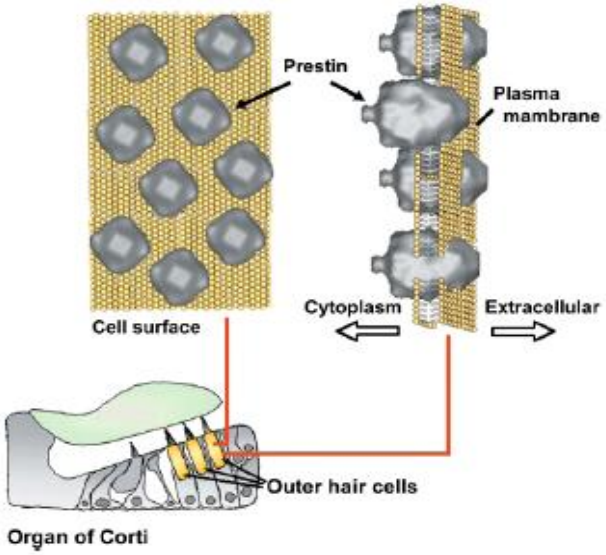

Figure 12: Representation of prestin particles embedded in the plasma membrane of the OHCs, viewed from outside the cell (*left*) and across the membrane (*right*) (Adapted from Mio *et al.*, 2008).

THE PRESTIN STAS DOMAIN

The intracellular C-terminus of prestin includes a STAS domain. It has only 25-35% homology with its other SLC26A relatives. Since it is the least conserved region of the protein among SLC26A family, it was assumed that STAS is responsible for the protein specific function (Zheng *et al.*, 2005).

Intracellular chloride was found to play a key role in influencing NLC in OHCs and prestin-transfected cells (Oliver *et al.*, 2001; Rybalchenko & Santos-Sacchi, 2003) and removal of intracellular chloride by substitution with other anions alter NLC (Rybalchenko & Santos-Sacchi, 2003; Song *et al.*, 2005). For this reason, charged residues

within prestin may interact with intracellular anions or influence interaction with other protein (Bai *et al.*, 2006).

Different experiments showed that changing charged amino acids in the C-terminus to either the opposite charge (R, K > D; E, D > K) or a neutral amino acid (Q) is not able to abolish NLC and does not disrupt plasma membrane (PM) targeting of prestin (Oliver *et al.*, 2001; Bai *et al.*, 2006). However, Bai and colleagues reported clear effects on voltage sensing following mutations of cluster a and b (figure 13).

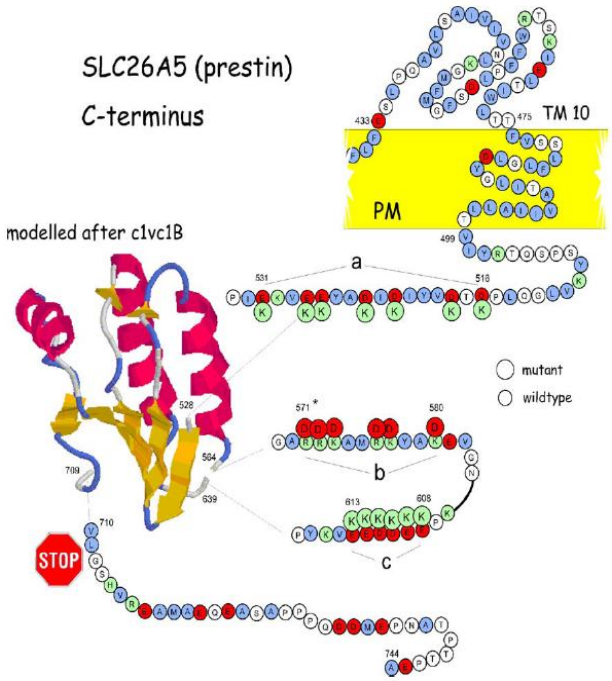

Figure 13: C-terminal cartoon of gerbil prestin. Indicated are the charged clusters (a–c) which were mutated to residues of opposite polarity (large circles). The final transmembrane domain is shown along with the intracellular residues that were not captured in the model based on 3D structure of the sequence of c1vc1B, the putative anti-sigma factor antagonist tm1442. (Bai *et al.*, 2006).

The authors assumed that anions might interact with this C-terminal charge clusters, namely via allosteric means (Bai *et al.*, 2006).

Truncations at residues more proximal to 710 (indicated with a stop in figure 13) produced non-functional motors despite proper membrane targeting and the deletion of the full C-terminus (stop498) led to a non functional and intracellulary confined protein (Navaratnam *et al.*, 2005).

The role of the C-terminus of prestin was investigated in some detail by Dallos and his group with a series of deletion, point and chimeric mutants. The function and cellular expression of mutants were examined in a heterologous expression system (mammalian

cell lines) by measurement of NLC and confocal immunofluorescence. The subcellular localization of mutant proteins was analyzed by co-localization experiments of prestin with other subcellular component markers. The following set of C-terminal truncation mutants was examined in this study: Del516, Del525, Del590, Del630, Del709 and Del719 (Zheng *et al.*, 2005) (figure 15).

Del719 was the only deletion mutant that retained NLC function and proper PM targeting. The mutants Del516, Del525 and Del590 all lost NLC and showed prestin localization consistent with retention of the protein in the endoplasmic reticulum (ER) and in the Golgi apparatus of the cells. Del630, Del709, aside from ER and Golgi retention, displayed widespread cytoplasmic membranous distribution, without apparent PM localization. A comparison of Del590 and Del630 is also particularly revealing. The subcellular localization results suggest that the region of prestin between amino acids 590 and 630 is necessary for prestin to exit from the ER/Golgi into cytoplasmic vesicles.

Deletion of more than 35 C-terminal amino acids results in impaired delivery of prestin to the PM and consequent complete removal of NLC function. This indicates that amino acids between 709 and 719 are required for proper PM targeting and NLC function (Navaratnam *et al.*, 2005).

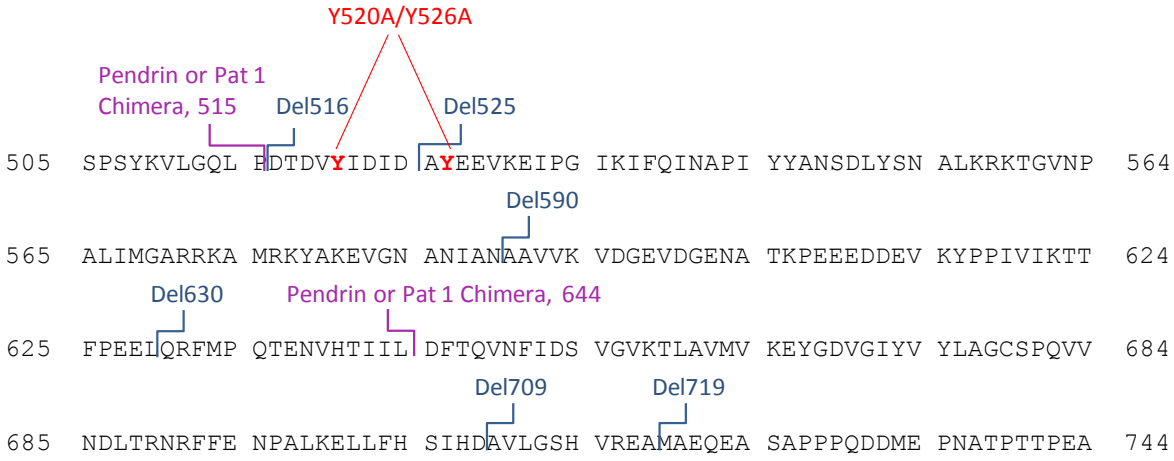

Figure 14: Primary sequence [505-744] of prestin C-terminus from gerbil. The locations of the mutations created and examined in the study are indicated (Zheng *et al.*, 2005). These include deletion mutants (in blue), chimera junction points (in violet) and double point mutations (in red).

In attempt to restore PM targeting, a set of chimeric prestin constructs were created in which the analogous C-terminus portions of PAT1 (SLC26A6) or Pendrin (SLC26A4), the two most closely related proteins to prestin, were exchanged for the prestin C-terminus

at sites 515 and 644. The “515” chimera replaced almost the entire C-terminus of prestin with either pendrin or Pat1, while the “644” chimera replaced part of the STAS domain (figure 14). All chimeric proteins lacked NLC, and had altered cellular distribution, with ER and Golgi retention as well as cytoplasmic membranous distribution.

Since the chimera mutants (Prestin/Pendrin and Prestin/PAT1) could not restore prestin PM targeting, the capacity for prestin to insert into the PM of cultured epithelial cells may be dependent on prestin specific C-terminal amino acid residues.

The mutant Y520A/Y526A abolished two of the prestin seven potential tyrosine-containing motifs that could direct the transport of newly synthesized membrane protein from the trans-Golgi network to the lateral membrane (Keller & Simons, 1997). It resulted in lost of NLC function and in intracellular accumulation of prestin, indicating that specific sequences within the C-terminus are essential for the NLC function in addition to its role in membrane targeting.

The mutant double mutant V499G/Y501H produced a protein that was efficiently delivered to the PM, but which completely lacked NLC.

A recent study on variants of prestin STAS domain, isolated from the rest of the molecule, showed that the C-terminal domain has an intrinsic tendency to form oligomers whose nature is highly dependent on the chemical composition of the environment (Pasqualetto *et al.*, 2008). These properties *in vitro* show many analogies with those of the full-length protein *in vivo* that forms oligomers in living cells, that are supposed to be essential for the motor function (Zheng *et al.*, 2006). The authors suggested that the aggregation properties of prestin C-terminus may play a role in the regulation of the full-length prestin function.

1.4 AIM OF THE PROJECT

Despite the increasing interest in the SLC26 genes and, in general, in the SulP members, very little is known about the structural organization of these proteins and no three-dimensional structures of domains or full-length sequences are available for any mammalian SLC26A anion transporter or for other members of the SulP family, of any species. The structural characterization is fundamental for the comprehension of the mode of action of a protein and it is an essential step for the understanding of the functional consequences of the mutations responsible for related pathologies. The structural characterization of the functionally important C-terminal STAS domain of a SLC26 member would represent an important step in the structure-function analysis of these transporters.

The work described in this thesis is focused on the production of STAS domains of two SulP transporters and on their biophysical and structural characterization, with the final aim to get the first 3D structure of such a domain by X-ray crystallography The selected SulP transporters are the intriguing motor protein, prestin, or SLC26A5, and a well functional characterized protein of *Arabidopsis thaliana*, Sultr1.2. The structural characterization of these two evolutionary distant STAS domains may shed light on the evolution mechanisms of this domain and in the different roles played in the various transporters.

In order to identify a sequence corresponding to a compact single domain, several types of analyses and predictions are performed on the C-terminal part of SulP protein, such as multiple sequence analyses, secondary structure predictions, predictions of intrinsic disordered regions and homology modeling outputs. The accurate selection of the N- and C-termini is more critical for domains that are part of a larger protein, as it is the case of the SulP STAS domains, whose boundaries are not clearly defined by sequence alignments. For this reason constructs of different length will be selected.

The main difference between mammalian and non-mammalian STAS domain is found in a long insertion (70-80 amino acids long in prestin), called variable loop. The evolutionary and functional role of this insertion is unknown; secondary structure

predictions suggest it is largely unstructured. To investigate the role of the variable loop, we intend to produced prestin STAS constructs with and without this region.

The derived structural information and 3D model will help in a better understanding of the role played by the STAS domain in the activity of the transporters and allow the interpretation of functional data on mutations and deletions available in literature.

2
EXPERIMENTAL PART

2.1 OVERVIEW

To characterize a protein from a structural point of view, it is necessary to produce it in amounts of the order of milligrams. Due to the low abundance in natural sources, the unavoidable choice is the production of recombinant material. The adopted strategy includes amplification of the selected genes, starting from the cDNA of the related proteins, cloning into appropriate bacterial expression plasmids, expression in *E. coli* and purification through chromatographic methods. All the used expression vectors produce a recombinant protein linked to another protein or a short peptide with well-known properties (called tags). These fusion tags allow performing affinity chromatography as first step in the purification of the protein of interest. Subsequently, the recombinant protein is excided from the tag by an appropriate proteolytic enzyme and further purified. For the structural and biophysical characterization, several complementary techniques were used, such as circular dichroism (CD), dynamic light scattering (DLS), Thermofluor, and, if possible, X-ray crystallography for the characterization at atomic level.

Since the size of the STAS domain is suitable, it is characterized also by solution NMR spectroscopy, by Prof. Stefano Mammi and Dr. Massimo Bellanda from the Department of Chemical Sciences of the University of Padua. The joint crystallographic and NMR efforts may provide a complete structural characterization of the STAS domains, giving complementary information. Crystallography can reveal the high resolution structural details of the STAS domains and their binding properties to tightly bound small molecules and ions. NMR can complete the structural characterization by providing information about the flexibility and dynamics of the domain in solution and the binding properties to medium or low affinity species.

2.2 MATERIALS AND METHODS

DESIGN OF STAS DOMAIN CONSTRUCT

Seven STAS domain variants of prestin from *Rattus norvegicus*, five of which are chimera constructs devoid of the variable loop, and one from Sultr1.2 from *Arabidopsis thaliana* were cloned (table 2). To design the selected constructs we took into consideration various elements.

The design of prestin variant named $STAS_L$ (table 2) came from the degradation study of a prestin STAS construct, [529-744], which was characterized previously (Pasqualetto *et al.*, 2008). This construct underwent a slow proteolytic degradation at room temperature; N-terminal sequencing showed the formation of the $STAS_L$ construct. The $STAS_S$ variant was designed in order to have a construct of length similar to the ASA proteins, with the help of secondary structure predictions.

.

Table 2: Survey of the selected STAS domain

Construct	Sequence
Prestin form *Rattus norvegicus*	
$STAS_L$	[623-727]
$STAS_S$	[583-727]
Chim1	[505-563]GS[637-727]
Chim2	[522-563]GS[637-727]
Chim3	S[529-563]GS[637-727]
Chim1del	[505-563]GS[637-718]
Chim3del	S[529-563]GS[637-718]
Sultr1.2 from *Arabidopsis thaliana*	
	[517-653]

Numbering is relative to the entire sequence of prestin and Sultr1.2. The prefix Chim indicates the prestin chimera STAS variants devoid of the variable loop. In red the amino acids introduced during the cloning.

Most of the variability between SulP STAS domains and ASA proteins is the presence of a loop, named variable loop. This loop is ~70 residues long in prestin, around

10 in Sultr1.2 from *Arabidopsis thaliana* (figures 5, 6, 15). This loop is predicted mostly disordered. Because previously studied constructs of the prestin C-terminal domain showed a strong tendency to aggregate (Pasqualetto *et al.*, 2008), in search for proteins more amenable for crystallographic, new chimera constructs without the variable loop were designed (table 2). The variable loop was deleted between position 564 and 636, where a GlySer dipeptide was introduced to connect the two halves (in particular the predicted helix α1 and strand β3) mimicking the bacterial ASAs. Moreover, given the uncertainty in the N- and C-terminal ends, we designed different chimera of STAS domains

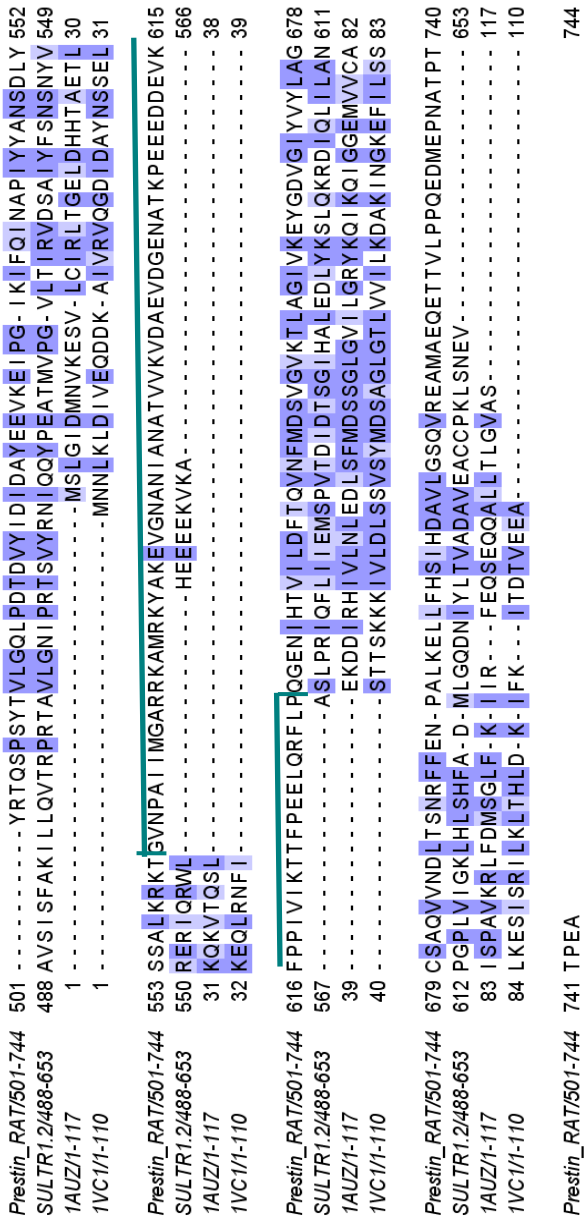

Figure 15: Multiple sequence alignment of C-terminal portions, comprising the STAS domain of two selected anion transporter: prestin from *Rattus norvegicus* and Sultr1.2 from *Arabidopsis thaliana*. For comparison, the sequences of the ASA from *Bacillus subtilis*, PDB code: 1AUZ, and from *Thermotoga maritime*, PDB code: 1VC1, are reported. The blue navy lines indicate the boundaries of the variable loop. The alignment is visualized with the program Jalview using a matrix Blosum62 for coloring.

According to literature functional data (Rouached *et al.*, 2005) and secondary structure predictions, a Sultr1.2 C-terminal variant, including the STAS domain, was designed (table 2). This construct extends to the extreme C-terminus of Sultr1.2 because the last residues are fundamental for the sulphate transport activity of the transporter (figure 7) (Rouached *et al.*, 2005).

PLASMIDS CONSTRUCTION

For all constructs, the nucleotide sequences were generated by PCR, using the forward and reverse primers shown in table 3 and the amplified fragments were inserted into the selected expression vectors, pET151D-TOPO® (Invitrogen) for $STAS_L$ and $STAS_S$ and pET SUMO (Invitrogen) for all the others.

The cloning of the prestin STAS domain variant, Chim1 (which was used as template for chimera cloning) followed the scheme reported in figure 16.

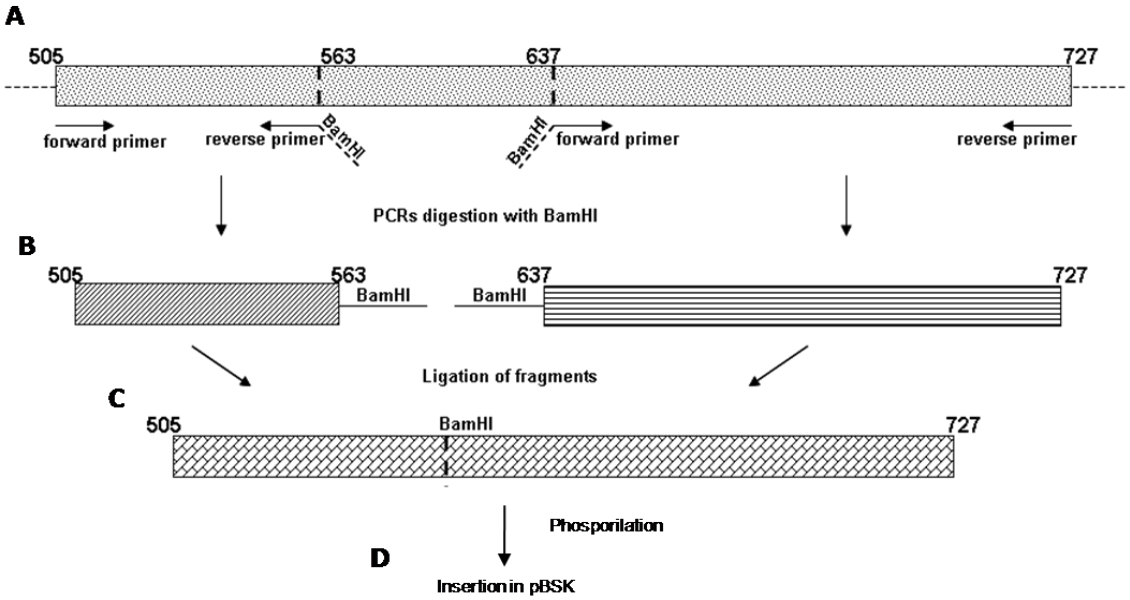

Figure 16: Scheme of the steps for the construction of a chimera prestin STAS domain devoid of the variable loop. **A**) The DNA fragments corresponding to the amino acids 505-567 and 637-727 were amplified using appropriate primers in order to insert a BamHI site. **B**) The two resulting fragments were digested with BamHI and **C**) ligated using a T4 DNA Ligase. Subsequently, **D**) the resulting fragments was phosphorylated and insert in the pBSK vactor.

The fragments 505-563 and 637-727 were amplified using the primer sets indicated in table 4 in order to insert a BamHI site as shown in figure 16 A. After ligation with T4 DNA ligase (New England BioLabs), since the BamHI restriction site encodes for the amino acids GS, the DNA sequence corresponds to the protein sequence [505-563]GS[637-718]. This fragment was phosphorylated using T4 Polynucleotide Kinase (New England BioLabs) and inserted into pBluescript II SK (+/–) vector (Stratagene), previously digested to create blunt ends by EcoRV restriction enzyme. Chim1-pBSK was used as template for the subsequent cloning of prestin chimera STAS variants.

Table 3: Oligonucleotide primers used for the indicated constructs

Construct	Primer	Sequence
Prestin from *Rattus norvegicus*		
$STAS_L$	5′	caccggaaatgccaacatagctaa
	3′	ctattacagaaccgtggtttcttgc
$STAS_S$	5′	cacccaacatttcctgaagagctg
	3′	ctattacagaaccgtggtttcttgc
Chim1	5′	agtccgagctacacagtcc
	3′	ctattacagaaccgtggtttc
Chim2	5′	gacattgatgcctatgaggag
	3′	ctattacagaaccgtggtttc
Chim3	5′	tccgtgaaagaaattcctggaata
	3′	ctattacagaaccgtggtttc
Chim1del	5′	agtccgagctacacagtcc
	3′	ctattacgcctcacggacttgg
Chim3del	5′	tccgtgaaagaaattcctggaata
	3′	ctattacgcctcacggacttgg
Sultr1.2 from *Arabidopsis thaliana*		
	5′	tacagaaatattcaacagtatcc
	3′	ttatcagacctcgttggagag

The DNA template of the prestin chimera constructs was the Chim1-pBSK vector.

Table 4: Oligonucleotide primers used for the Chim1-pBSK vector

Construct	Primer	Sequence
Prestin from *Rattus norvegicus*		
[505-563]	5′	agtccgagctacacagtcctg
	3′	atggatccgttcacgccagtctttc
[637-727]	5′	atggatccgaaaatatccacactgtca
	3′	ctattacagaaccgtggtttcttgc

The Bam H1 restriction site is underlined.

To increment the efficiency of SUMO protease, we introduced a Serine residue at the N-terminal of chim3 and chim3del constructs.

All the resulting vectors were transformed into the TOP10 or Mach1-T1 *E. coli* strain (Invitrogen) for the amplification. The correctness of the sequences was verified by sequencing methods.

PROTEINS EXPRESSION

For the heterologous expression, the pET- vectors were transformed into the BL21(DE3) *E. coli* strain (Invitrogen). All the expression vectors produced a recombinant protein with a N-terminal cleavable poly(His)-tag: a $(His)_6$-protein with the pET151D-TOPO® vector and a $(His)_6$-Small Ubiquitin-like MOdifier (SUMO)-protein using pET SUMO vector.

For protein expression, single colonies were grown, for about 16 h in LB medium (10 g/l tryptone, 5 g/l yeast extract, and 10 g/l NaCl), containing 100 µg/ml ampicillin for pET151D-TOPO® vector or 50 µg/ml kanamicin for pET SUMO plasmid; this is called overnight culture (ONC). LB medium was inoculated with the ONC (ratio 1:50) grown at 37 °C, in a suitable shaker. Protein expression was induced when OD_{600} of the culture reached 0.5-0.6, by adding IPTG to a final concentration of 1 mM. After induction the bacteria were grown at 30 °C for 4 h. At the end, cells were harvested after centrifugation at 8500 g for 15'.

In order to obtain the Se-Met derivative of Chim1del, bacteria were grown in minimal medium M9 supplemented with 2% (w/v) glucose, salts and all the amino acids except Met, substituted by Se-Met. About 5 minutes before induction with 1 mM IPTG, a further solution of Se-Met plus Leu, Ile, Val, Phe, Lys and Thr was added to the medium to inhibit the *E. coli* methionine pathway and to force the incorporation of Se-Met. The Se-Met derivative was purified as the native protein.

PURIFICATION AND PROTEOLYTIC CLEAVAGE OF FUSION PROTEINS

The harvested cells were resuspended in a solubilization buffer supplemented with protease inhibitors (Roche) and lysed with a French press (Thermo Spectronic) at high pressure. The lysate was centrifuged to remove cell debris at 27000 g for 30' and loaded onto an IMAC affinity column (HIS-Select Cartridge, Sigma-Aldrich or His-Trap, GE Healthcare) equilibrated with the solubilization buffer. The fusion proteins were eluted from the affinity column with solubilization buffer containing high concentration of imidazole.

Fractions containing the proteins were pooled, concentrated by ultrafiltration and at the same time the buffer was replaced to ensure the optimal protease activity (TEV for pET151D-TOPO® vector or SUMO protease for pET SUMO). The sample was incubated with the protease overnight at 4 °C for the proteolytic cleavage of the $(His)_6$-tag. The resulting hydrolyzed material was applied onto the IMAC affinity column and immediately recovered to separate the purified protein from the $(His)_6$ -tag, the uncleaved fusion protein and from the protease, which were all retained in the column.

The eluate was further purified by size exclusion chromatography performed on an Äkta FPLC chromatographic system (GE Healthcare).

ANALYTICAL REVERSE PHASE CHROMATOGRAPHY AND MASS SPECTROMETRY

Analytical reverse phase HPLC was performed using a Jupiter C5 column (0.46 x 25 cm, Phenomenex) and the following solvents: A (100% H_2O, 0.08% TFA) and B (90% CH_3CN, 0.08% TFA). The elution of the protein was obtained through a concentration gradient from 45% to 65% of B in 20 min, at a flow rate of 1 ml/min. Mass spectrometry was performed on an ESI-TOF mass spectrometer.

CIRCULAR DICHROISM (CD) SPECTROSCOPY

CD data were recorded on a J-715 Spectra were determined as an average of 10 scans. The protein concentration was 1 mg/ml in 50 mM Na_2HPO_4, 150 mM NaCl, pH 7.5. The data were recorded and analyzed with Spectra Manager Software (JASCO).

THERMOFLUOR ASSAY

To monitor thermal protein unfolding, the fluorescent dye Sypro orange (Sigma-Aldrich) was used. Thermofluor assay was conducted on a Mini Opticon Real-Time PCR detection system (Bio-Rad). Solution of 1 µl of 10 mg/ml protein, 1 µl of SyproOrange 100x and 18 µl of test compound were added to the 48-well low-profile plates (Bio-Rad). The plates were spun and heated from 20 to 90 °C, with a heating rate of 0.5 °C/min. The data were recorded and analyzed with the CFX Manager Software (Bio-Rad).

ANALYTICAL GEL PERMEATION CHROMATOGRAPHY

Analytical gel permeation chromatography was performed on a Superdex 200 5/150 column (GE Healthcare) equilibrated with 20 mM TRIS, 150 mM NaCl, 5 mM DTT, pH 7.5, at a flow rate of 0.3 ml/min using an Äkta FPLC chromatographic system (GE Healthcare).

DYNAMIC LIGHT SCATTERING (DLS)

DLS data were recorded on a Zetasizer Nano S instrument (Malvern) at 20 °C, using a quartz cuvette and 20 µl of sample. Protein solutions were filtered with centrifugal filters

with a membrane pore of 0.22 μm. The data were recorded and analyzed with the Dispersion Technology Sofware (Malvern).

CRYSTALLIZATION TESTS

Crystallization trials using commercial kits (Qiagen® and Molecular Dimensions) based on sparse matrix, grid screen, and/or ionic sampling, were performed by the microbatch and vapour diffusion (with the sitting drop method) techniques, using the Oryx8 automatic system (Douglas Instrument).

CRYSTALLOGRAPHIC DATA COLLECTION AND STRUCTURE DETERMINATION

The native dataset of Chim1del (using 14 mg/ml protein solution and 0.09 M MES pH 6.5, 1.8 M ammonium sulfate, 4.5% (v/v) PEG400, 0.1% octyl-β-D-glucopyranoside) at 1.57 Å resolution was collected at the ESRF beamline ID14-1 (Grenoble, France). The single anomalous dispersion data set for the Se-Met derivative in the same condition of the native protein (1.60 Å resolution) was collected at the ESRF beamline ID23-2 (Grenoble, France). The datasets were measured at 100 K, using the precipitant solution including 20% glycerol as cryoprotectant. Crystals belong to space group $P3_121$ with unit cell parameters reported in table 10. Diffraction data were processed with MOSFLM (Leisle, 1991), reduced and merged with SCALA (Evans, 2006), which is included in the CCP4 suite. The selenium atom was localized by using SHELXD (Schneider *et al.*, 2002) and phases were calculated and refined by density modification with SHELXE (Sheldrick, 2002) and further optimized with DM (Cowtan, 1994). The first atomic model was built by automatic procedure, by using the software BUCCANEER (Cowtan, 2006); in particular, 126 amino acids were positioned with automatic model building, 6 amino acids were added manually and 11 residues are not visible in the map. The structure was refined alternating several cycles of automatic refinement with REFMAC (Murshudov *et al.*,

1997), and manual model building with COOT (Emsley & Cowtan, 2004). During refinement (with anisotropic atomic B-factors), water molecules were added to the model, both automatically and manually, and those with B factors higher than 50 were excluded. One molecule of octyl-β-D-glucopyranoside was also introduced and refined.

2.3 RESULTS AND DISCUSSION

EXPRESSION, CLONING AND PURIFICATION

The location of the STAS domain, as reported in proteins and domains databases, is predicted on the basis of multiple sequence alignments with bacterial ASAs (Aravind & Koonin, 2000). However, the low sequence conservation between the mammalian STAS domain and the bacterial ASA proteins (identity between 10-15%), the presence of the variable loop and of long extensions both at the C- and N-termini make difficult to establish the exact boundaries of the transporters STAS domain. For these reasons, in the attempt to identify the protein with the correct ends for a structural characterization, we designed and studied different variants of prestin STAS domains and a construct of C-terminal of Sultr1.2 from *Arabidopsis thaliana*. In particular, we designed five chimera constructs without the variable loop that is predicted mostly disordered.

All the selected constructs were cloned successfully. The cloning of chimera prestin variant required the introduction of a BamHI restriction site, which encodes for the amino acids GS.

Two expression systems were chosen to clone the selected sequences: the Champion™ pET Directional TOPO® Expression Kits and Champion™ pET SUMO Protein Expression System by Invitrogen. Both the systems allow to insert the selected PCR DNA sequence directly in the expression vector with high efficiency. Moreover, the SUMO expression system offers various advantages: increase of expression and solubility of recombinant fusion proteins and generation of native protein using SUMO. The tertiary structure of the SUMO protein is recognized by a cysteine protease, SUMO Protease, which specifically cleaves conjugated SUMO from target proteins (Li & Hochstrasser, 1999). Cleavage of SUMO by SUMO Protease results in production of native protein with no extra amino acids added between the cleavage site and the start of the desired protein. The last point is very important especially for the study of chimera prestin constructs which differ by N-terminal boundaries.

The results of purification of STAS constructs are summarized in table 5.

Table 5: Survey of the STAS domains cloned and expressed in *E. coli*

Construct	Sequence	AA	MW (kDa)	Vector	Expression level	Solubility level
Prestin from *Rattus norvegicus*						
$STAS_L$	[583-727]	145	15.9	pET151	High	Medium
$STAS_S$	[623-727]	105	11.7	pET151	High	Low
Chim1	[505-563]GS[637-727]	152	15.7	pET SUMO	High	High
Chim2	[522-563]GS[637-727]	135	14.9	pET SUMO	High	High
Chim3	S[529-563]GS[637-727]	129	14.2	pET SUMO	High	High
Chim1del	[505-563]GS[637-718]	143	15.7	pET SUMO	High	High
Chim3del	S[529-563]GS[637-718]	120	13.1	pET SUMO	High	Medium
Sultr1.2 from *Arabidopsis thaliana*						
	[517-653]	137	15.6	pET SUMO	High	High

Numeration is relative to the entire sequence of prestin and Sultr1.2. In red the amino acids introduced during the cloning. The prefix Chim indicates the prestin chimera STAS variants devoid of the variable loop.

Among the STAS variants, only the shorter prestin STAS variant, $STAS_S$, showed low solubility level (figure 17 A). Both $STAS_L$ and $STAS_S$ had a strong tendency to aggregate, as shown by gel filtration elution profiles reported in figure 18. This unspecific aggregation was probably also the cause of the failure of tag-cut with TEV protease. The amount and the quality of purified proteins were not sufficient for the characterization of both constructs.

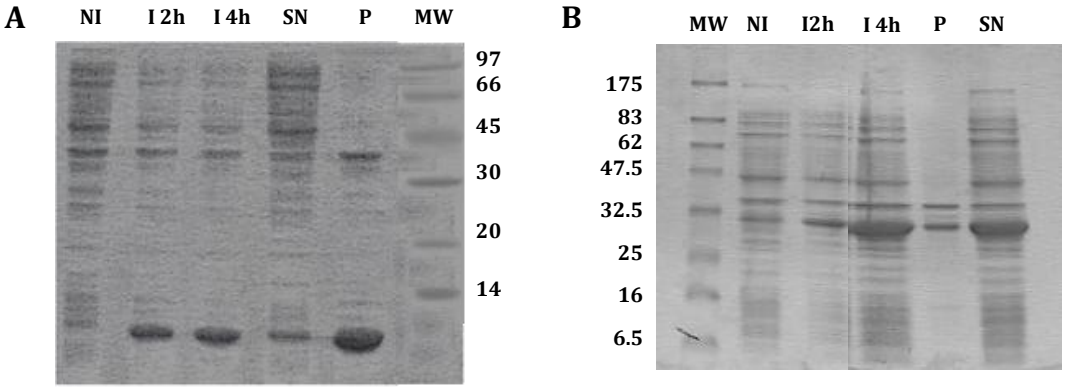

Figure 17: Coomassie-stained SDS–PAGE of protein expression in BL21(DE3) of His_6-$STAS_S$ (**A**) and of His_6SUMO-Chim1 (**B**). NI: control, not induced bacterial cells. I2h I4h: IPTG induced cells after 2 and 4 hours. SN: soluble portion of bacterial lysate. P: insoluble fraction of bacterial lysate. MW: protein markers.

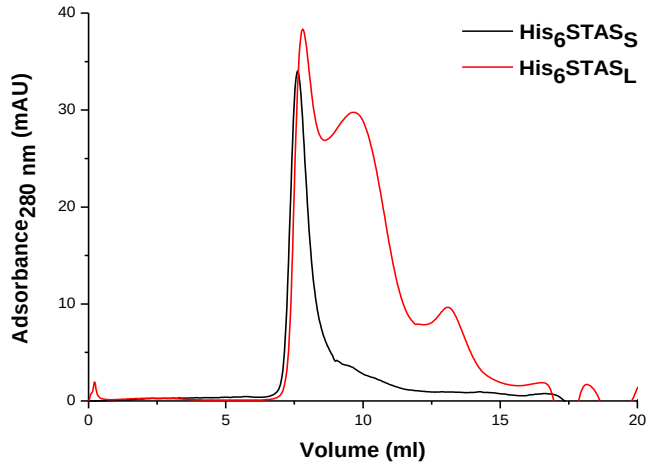

Figure 18: Gel permeation elution profile of $STAS_L$ and $STAS_S$, using a Superose 12 10/300 GL column (GE Healthcare) equilibrated with 20 mM TRIS, 150 mM NaCl, 5 mM DTT, pH 7.5.

The deletion of the variable loop and the use of the vector pET SUMO increased noticeably the expression and the solubility of the fusion proteins, as shown in figure 17 B for the chim1 construct (similar results were obtained with the other constructs). In the optimized protocol the total yield of the crude products was estimated around 30 mg for 1 L of culture medium.

The soluble fractions of the $(His)_6$-SUMO fusion proteins were purified by an IMAC affinity step using a phosphate buffer (50 mM Na_2HPO_4, 300 mM NaCl, 10 mM β-mercaptoethanol, pH 8), followed by the proteolytic cleavage of the $(His)_6$-SUMO-tag. After an incubation at 4 °C overnight, the cleavage with SUMO protease was very efficient (~95% SUMO-protein was cleaved) as shown in figure 19 A for the Chim1del construct.

A small amount of fusion protein is still present after the proteolytic reaction of Chim2 variant. This is because not all junctions between SUMO and protein are processed with equal velocity by SUMO protease. SUMO-protein fusions in which the C-terminal of SUMO protein is followed by large negatively charged (DIDA are the initial N-terminal residues of Chim2) are processed up to five times slower (Malakhov *et al.*, 2004). For this reason, the temperature of incubation with SUMO protease was increased at 16 °C.

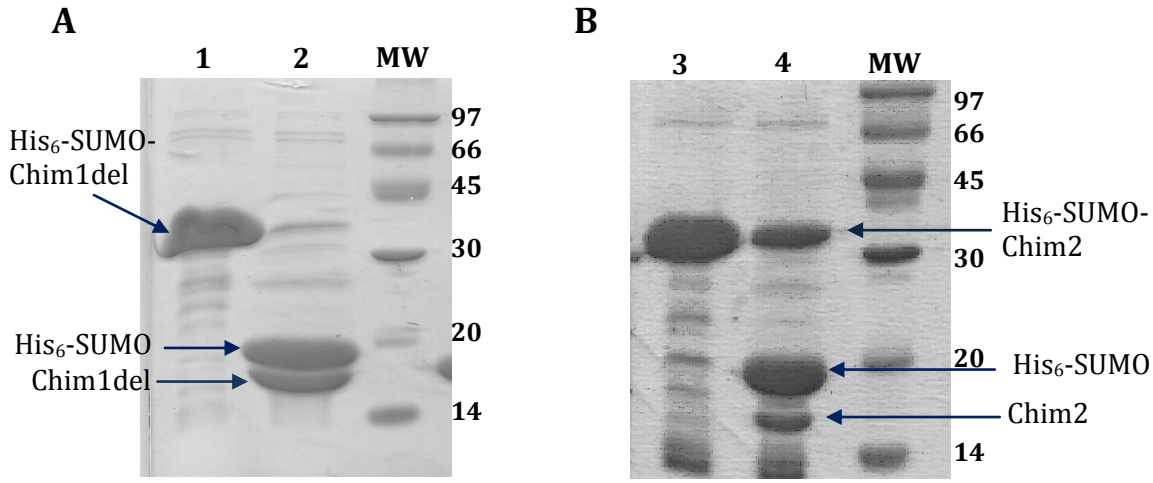

Figure 19: Coomassie-stained SDS–PAGE of the proteolytic cleavage of the $(His)_6$-SUMO tag from Chim1 (**A**) and Chim2 (**B**). Lanes 1 and 3: fusion proteins eluted from the IMAC column. Lanes 2 and 4 samples after the proteolytic cleavage by the SUMO protease. MW: protein markers.

After the proteolytic cleavage of His_6-SUMO tag and during the concentration step, Chim3del precipitated partially and this reduced the final yield of protein (only 1 mg for 1 L of culture).

The proteolytic products were further purified with a gel permeation step. The elution profiles and final results of the proteins concentration are shown in figures 20-23.

With the exception of Chim3 construct, no high molecular weight aggregates were present in solution, as pointed out by the gel permeation elution profile. The final yield of purified proteins were around 3 mg for 1 L of culture medium for Chim1, Chim2 and Chim3; 6 mg for 1 L for STAS Sultr1.2 and 8 mg for l L for Chim1del.

Fractions corresponding to the proteins peaks were collected and concentrated in 20 mM TRIS, 150 mM NaCl, 5 mM DTT, pH 7.5 for the following characterization.

Besides by SDS-PAGE, the quality of final products was checked by reverse phase chromatography, which revealed a purity greater than 95%. ESI-TOF mass analysis confirmed the correct molecular weight for the final cleaved samples (table 6).

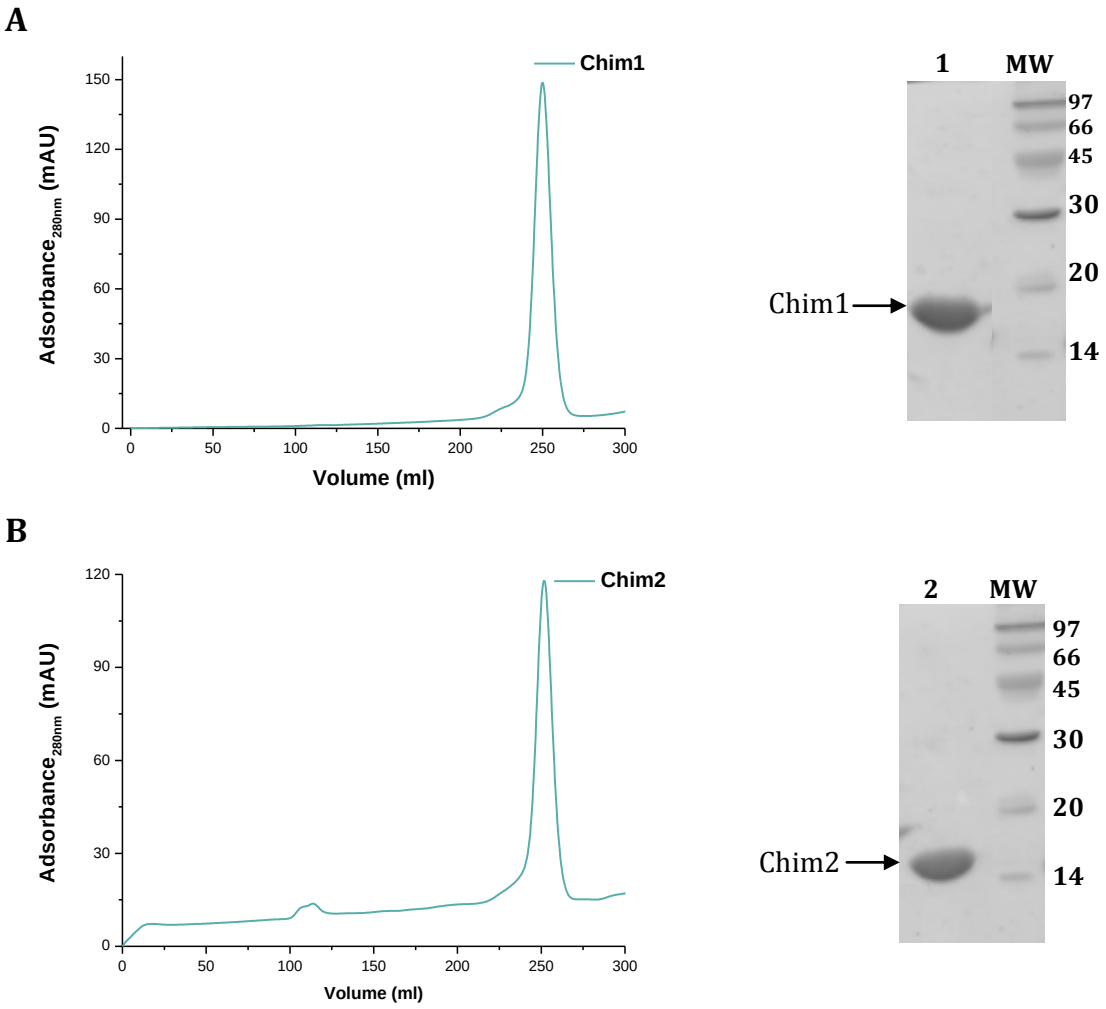

Figure 20: Gel permeation elution profile and Coomassie-stained SDS–PAGE after gel permeation chromatography of Chim1 (**A**) and Chim2 (**B**). Column: HiLoad 26/60 Superdex 200 (GE Healthcare) equilibrated with 20 mM TRIS, 150 mM NaCl, 5 mM DTT, pH 7.5. Lanes 1 and 2: purified proteins. MW: protein markers.

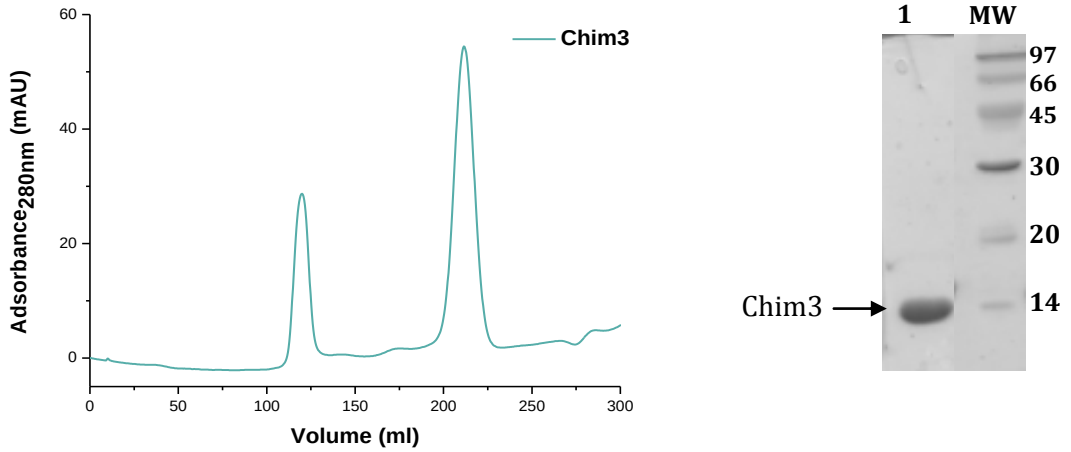

Figure 21: Gel permeation elution profile and Coomassie-stained SDS–PAGE after gel permeation chromatography of Chim3. Column: HiLoad 26/60 Superdex 75 (GE Healthcare) equilibrated with 20 mM TRIS, 150 mM NaCl, 5 mM DTT, pH 7.5. Lanes 1: purified protein. MW: protein markers.

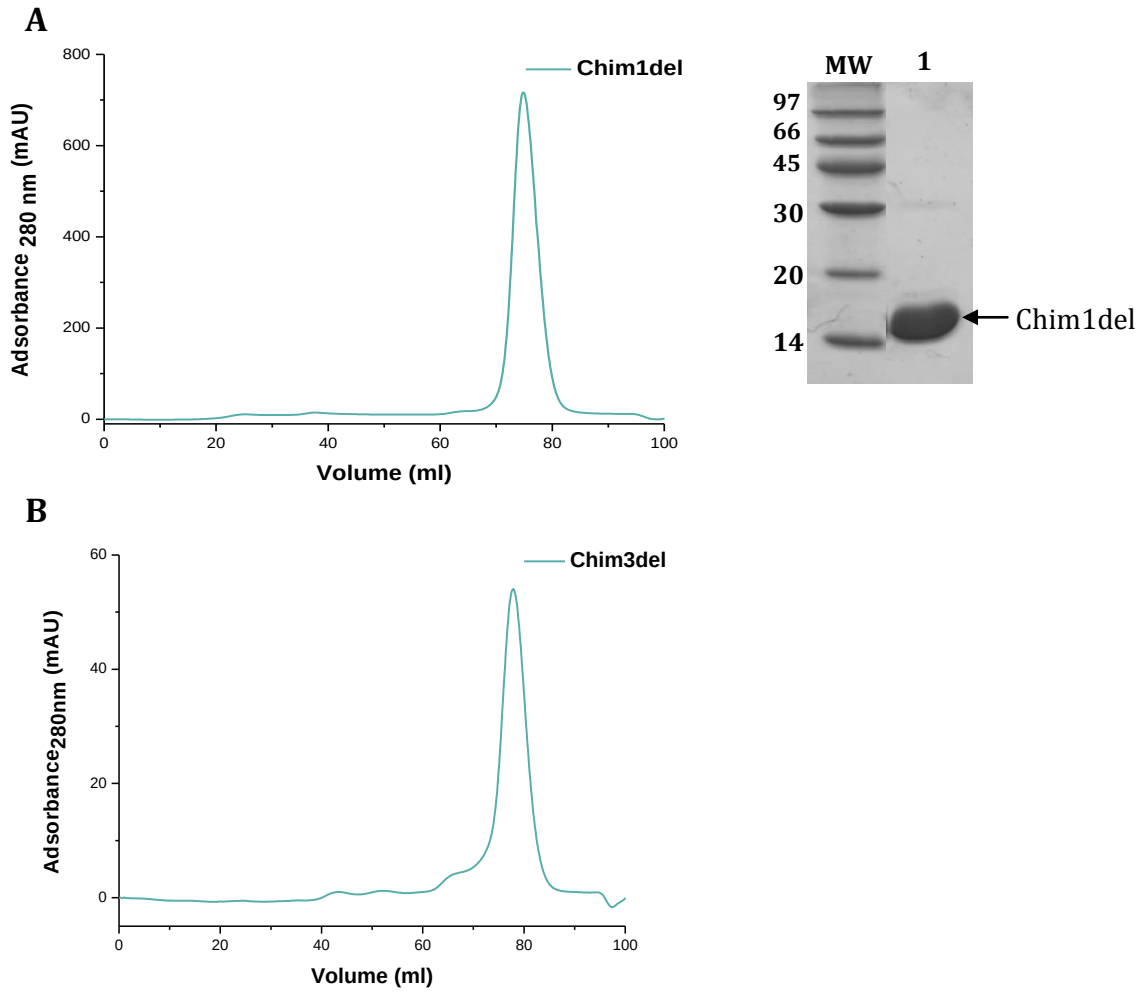

Figure 22: Gel permeation elution profiles and Coomassie-stained SDS–PAGE after gel permeation chromatography of Chim1del (**A**) and Chim3del (**B**). Column: HiLoad 16/60 Superdex 75 (GE Healthcare) equilibrated with 20 mM TRIS, 150 mM NaCl, 5 mM DTT, pH 7.5 Lane 1: purified protein. MW: protein markers.

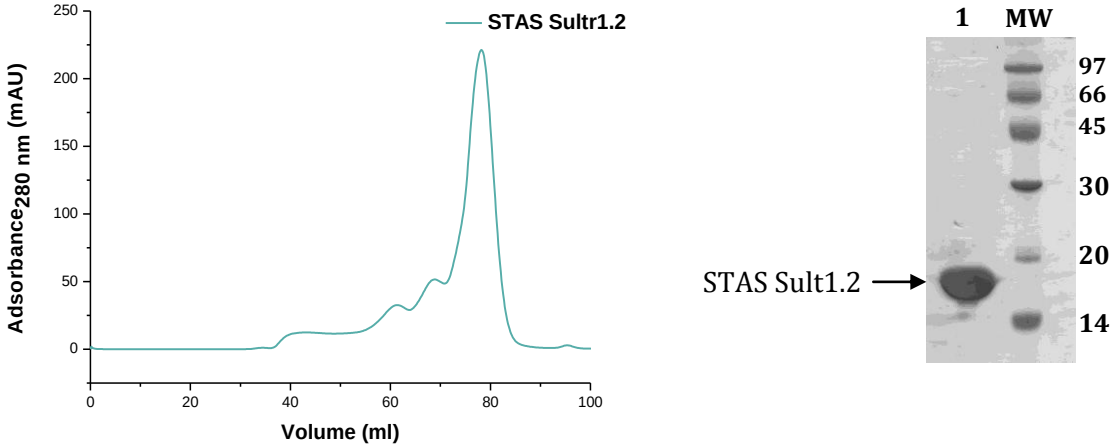

Figure 23: Gel permeation elution profile and Coomassie-stained SDS–PAGE after gel permeation chromatography of STAS OF Sultr1.2. Column: HiLoad 16/60 Superdex 75 (GE Healthcare) equilibrated with 20 mM TRIS, 300 mM NaCl, pH 7.5. Lane 1: purified protein. MW: protein markers.

Table 6: Survey of the results of ESI-TOF mass analysis of studied constructs

Construct	AA	MW	
		Theoretical	Experimental
Chim1	152	16756.9	16755.5
Chim2	135	14906.8	14905.6
Chim3	129	14158.1	14158.3
Chim1del	143	15753.7	15754.6
$STAS_{Sultr1.2}$	137	15553.8	15553.8

Abbreviations: AA: number of amino acids. MW: Molecular weight. Experimental: MW ensued from ESI-TOF mass analysis.

CIRCULAR DICHROISM (CD) SPECTROSCOPY

To verify whether the recombinant form of STAS domain constructs have defined secondary structure, the purified samples were characterized by circular dichroism spectroscopy in the far-UV region. CD spectra of all chimera constructs have a similar shape (figure 24). The two negative bands around 208 and 222 nm denote the presence of a considerable amount of helical secondary structure. The overall shape of the spectra is consistent also with the presence of β-structure (relative elipticity around 215 nm, crossing of the horizontal axis at around 202 nm).

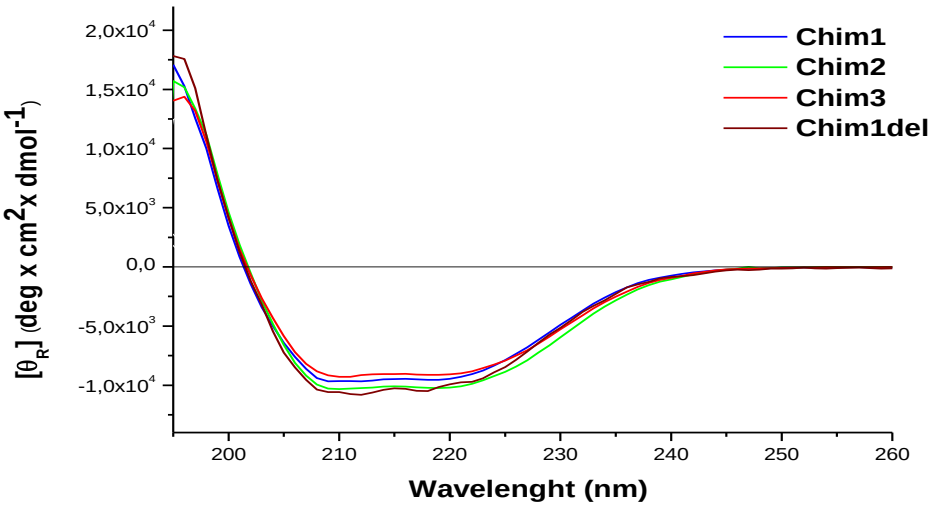

Figure 24: Far-UV circular dichroism spectra of prestin chimera STAS domain variants.

From the comparison between one of the chimera spectra (red line in figure 25) and the spectrum of a prestin variant with the variable loop (magenta line in figure 25), it is clearly evident that the chimera construct has a higher percentage of secondary structure in solution. The difference between the two compared prestin C-terminal variants is the presence or not of the variable loop. According to the secondary structure prediction, the obtained results confirm that the variable loop (70 amino acids long in prestin) is mostly unstructured.

It is very interesting the comparison between the C-terminus, including the STAS domain, of three SulP transporters: prestin, Sultr1.2 and Rv1739c from *Mycobacterium tuberculosis* (figure 25). The deletion of the variable loop makes the CD prestin chimera spectrum similar to the spectra of the other SulP transporters STAS domain, with no or very short loops. For all three SulP transporters, the STAS domain is a mixed α/β protein, consistent with the predicted structure of the STAS domain and the 3D structure of ASA proteins.

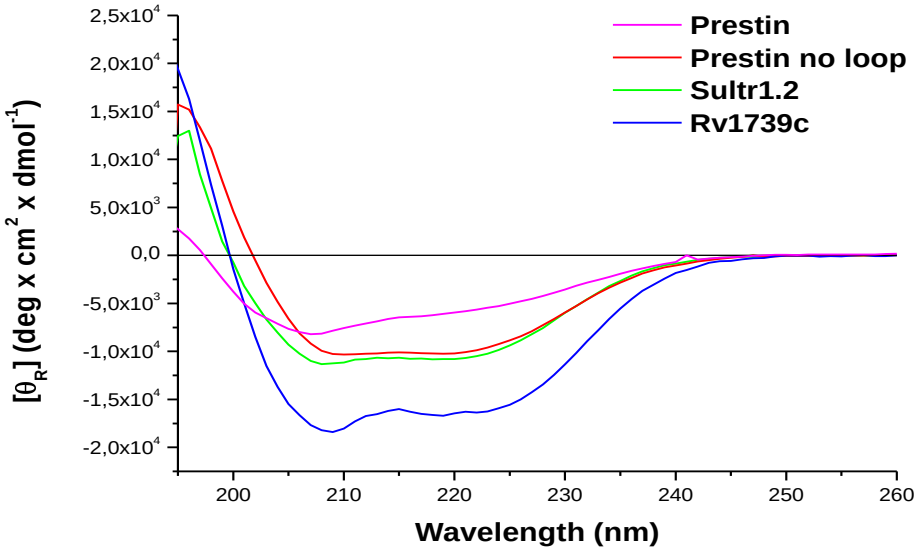

Figure 25: Far-UV circular dichroism spectra of the prestin C-terminal construct [529-720] (magenta), prestin Chim3 (red), Sultr1.2 C-terminus (green) and Rv1739c [349-560] (blue).

THERMOFLUOR ASSAY

Chim1, Chim1del, Chim2 and STAS variant of Sultr1.2 were characterized by Thermofluor analysis. Different buffers, salts, or small organic compounds were tested.

The difference in thermal stability (T_m) is particularly relevant for proteins with or without the variable loop (table 7). There is a difference of at least 14 Celsius degrees in melting temperature. The deletion of an unstructured and flexible region makes more stable the chimera variants.

Table 7: Melting Temperatures of selected constructs

Construct	T_m (°C)
Prestin [529-744]	39.5
Chim1	56
Chim1del	54.5
Chim2	53.5
$STAS_{Sultr1.2}$	52.3

The T_m (melting Temperature) values are the mean of three measurements. Proteins concentration: 0.5 mg/ml in 20 mM Tris, 7.5 mM NaCl, 5 mM DTT, pH 7.5.

Prestin constructs were tested in presence of different salts. As example, in table 8 the melting temperature value of Chim2 are reported (similar results were obtained with the other chimera).

In the C-terminal of prestin there are two clusters of charged amino acids (figure 13) which may play an important role in controlling the operating voltage range through the interaction with anions via allosteric interactions (Bai *et al.*, 2006). In the chimera constructs the cut of the variable loop results in the loss of the region of positive residues (residues 571-580) which are in the N-terminal end of the variable loop. The longer chimera constructs (Chim1, Chim1del and partially Chim2) keeps only the region of negative amino acids (516-531 residues). This is probably the reason of the different behavior of chimera and prestin constructs with the loop in response to the addition of different salts (table 8).

In particular, $CaCl_2$ lowers only the T_m of chimera variant of 8 °C. By DLS measurements we found that the addiction of calcium ions in solution induces aspecific aggregation but it does not have effect on secondary structure (data not shown).

The role of [Ca^{2+}] in the function and in the aggregation state of prestin is not well understood. There is no evidence of a direct relationship between prestin activity and intracellular [Ca^{2+}] in OHC. A recent study revealed that the elevation of intracellular calcium level inhibits specifically the activity of SLC26A3 and that this involves its interaction with PDZ adapter protein (Lamprecht *et al*, 2009).

In particular $CaCl_2$ lowers only the T_m of chimera variant of 8 °C. By DLS measurements we found that the addiction of calcium in solution induces aspecific aggregation but it does not have effect on secondary structure (data not shown).

The role of $[Ca^{2+}]$ in the function and in the aggregation state of prestin is not well understood. There is no evidence of a direct relationship between prestin activity and intracellular $[Ca^{2+}]$ in OHC. A recent study revealed that the elevation of intracellular calcium level inhibits specifically the activity of SLC26A3 and that this involves its interaction with PDZ adapter protein (Lamprecht *et al*, 2009).

Table 8: Results of thermal denaturation of prestin constructs with and without variable loop

Additive	T_m (°C)	T_m (°C)
	Prestin with loop	Prestin without loop
NaCl 7.5 mM	39.5	53.5
NaCl 100 mM	39.5	51
NaFl 100 mM	32	50.5
NaI 100 mM	41	52
NaBr 100 mM	40	51
Na_2SO_4 100 mM	39.5	52
$CaCl_2$ 100 mM	39	45.5

The T_m values are the mean of three measurements. Proteins concentration: 0.5mg/ml in 20 mM TRIS, 5 mM DTT, pH 7.5.

OLIGOMERIZATION PROPERTIES

It was reported that full-length prestin aggregates in living cells at the level of the plasma membrane, forming stable dimers or tetramers that are supposed to be essential for the physiological function of the protein (Detro-Dassen *et al.*, 2008; Mio *et al.*, 2008; Zheng *et al.*, 2006). In this study, the aggregation propensity in solution of chimera prestin variants was investigated by gel filtration chromatography and dynamic light scattering.

The analytical gel permeation profiles show that for the prestin chimera constructs high-molecular weight aggregates are essentially absent in solution (the exclusion volume of the column is 1.1 ml, MW $\geq$ 600 kDa) and that proteins elute with a retention volume

corresponding to a hydrodynamic volume between that of a monomer and a dimer (figure 26).

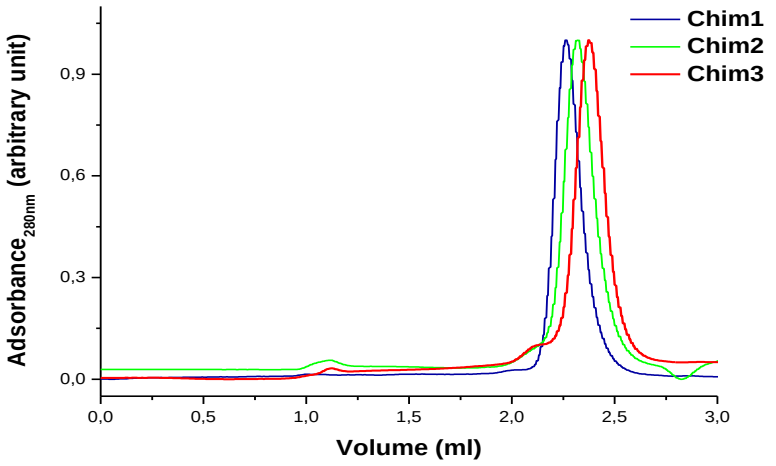

Figure 26: Gel permeation elution profiles of Chim1, Chim2 and Chim3 using a Superdex 200 5/150 column (GE Healthcare) equilibrated with 20 mM TRIS, 150 mM NaCl, 5 mM DTT, pH 7.5.

The aggregation state of the proteins were further characterized by DLS measurements. The particles size distributions by intensity and the results of DLS analysis of selected constructs are showed in figures 27 and 28

For the STAS variant of Sultr1.2 (figure 27) the main form in solution is the monomeric one but the presence of some high-molecular weight aggregates is also evident.

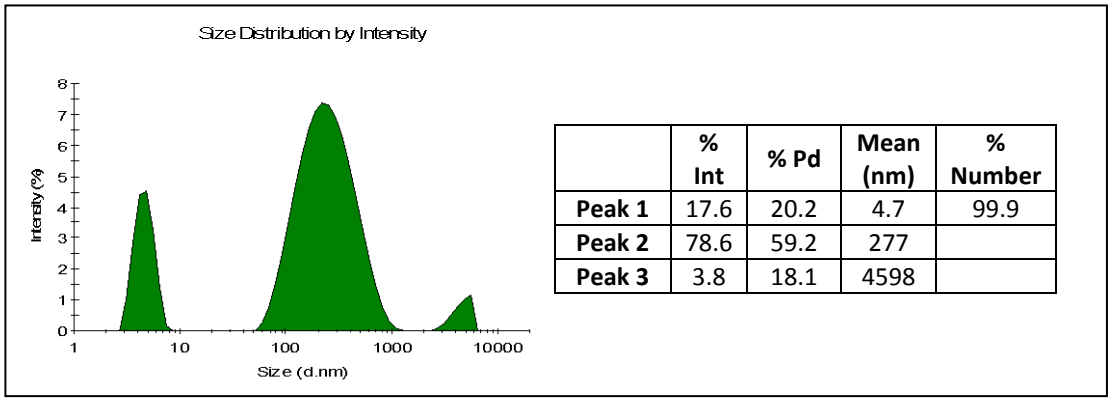

	% Int	% Pd	Mean (nm)	% Number
Peak 1	17.6	20.2	4.7	99.9
Peak 2	78.6	59.2	277	
Peak 3	3.8	18.1	4598	

Figure 27: Particles size distribution by intensity and summarizing table of $STAS_{Sultr1.2}$. Every measurement is the result of at least 15 accumulations. The protein are concentrated 5mg/ml (1mg/ml chim3 del) in 20 mM TRIS, 300 mM NaCl, 5mM DTT, pH 7.5. Int: intensity. Pd: polydispersion.

Also for the prestin variants Chim1, Chim1del, Chim2 and Chim3 (figure 28) the main form in solution is the monomeric. High-molecular weight aggregates is evident for Chim3del (probably the cause of the protein precipitation during the purification steps) and for the prestin STAS with the variable loop (figure 29), confirming the hypothesis that the presence of the variable induces aspecific aggregation.

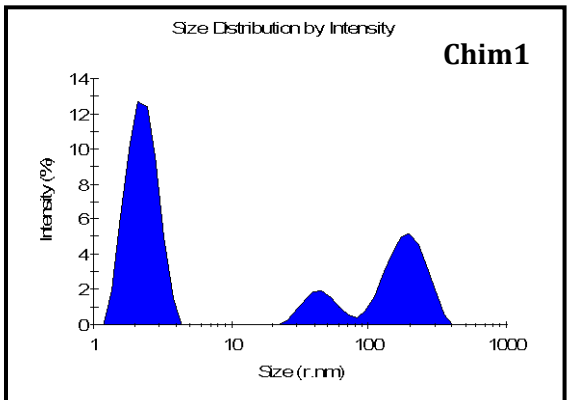

	% Int	% PD	Mean (nm)	% Number
Peak 1	58.6	24.3	4.58	100
Peak 2	9.6	28.6	93.36	
Peak 3	30	31.2	385.2	

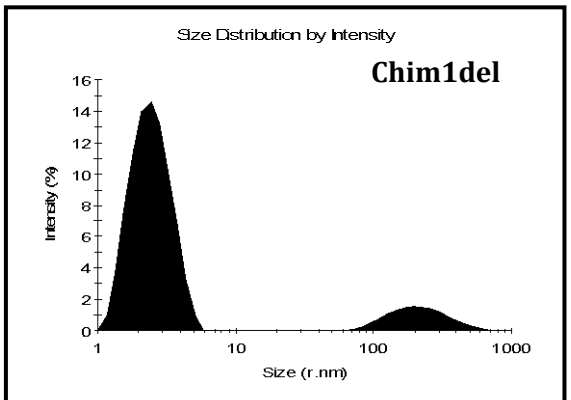

	% Int	% Pd	Mean (nm)	% Number
Peak 1	86.9	32.2	5.04	100
Peak 2	13.1	47.3	459.6	

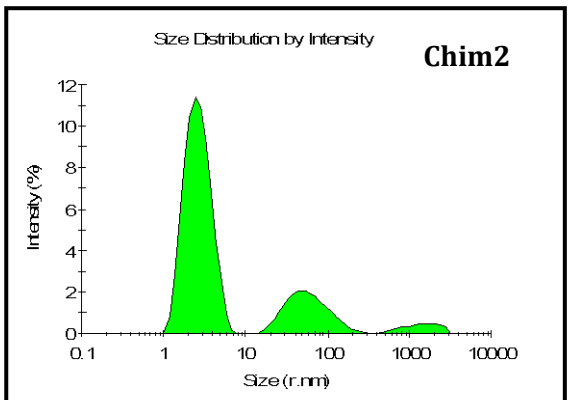

	% Int	% Pd	Mean (nm)	% Number
Peak 1	74.8	36.3	5.456	100
Peak 2	21	61.4	129.7	
Peak 3	4.2	42.9	3580	

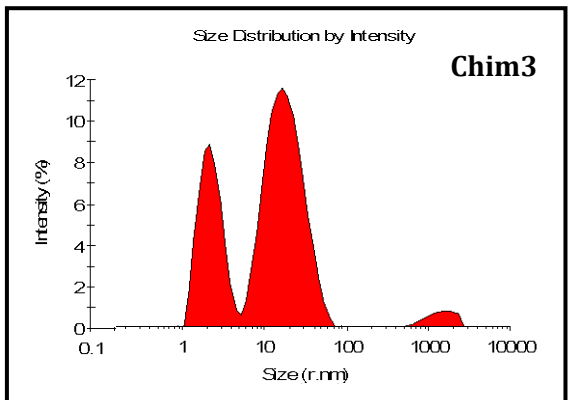

	% Int	% Pd	Mean (nm)	% Number
Peak 1	31.2	34.3	5.2	99.3
Peak 2	65	53.9	44.90	0.7
Peak 3	3.8	37	3400	

Figure 28: Particles size distribution by intensity and summarizing table of prestin chimera constructs Chim1 (blue), Chim1del (black), Chim2 (green) and Chim3 (red). Every measurement is the result of at least 15 accumulations. The proteins are concentrated 5mg/ml in 20 mM TRIS, 150 mM NaCl, 5mM DTT, pH 7.5. Int: intensity. Pd: polydispersion.

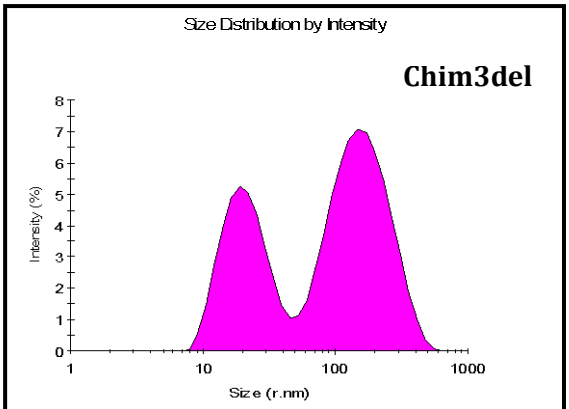

	% Int	% Pd	Mean (nm)	% Number
Peak 1	36.2	38.9	21.73	92.7
Peak 2	63.8	50.5	168.6	7.3

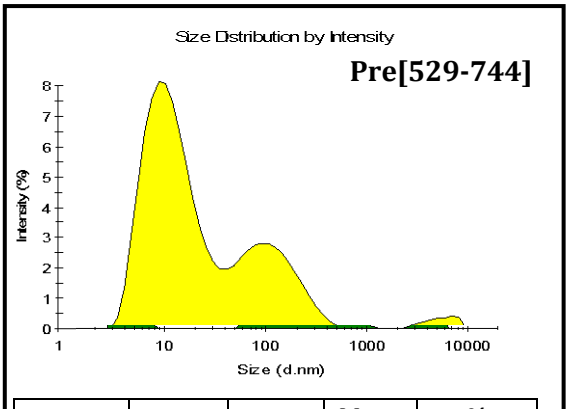

	% Int	% Pd	Mean (nm)	% Number
Peak 1	69.5	60	12.86	100
Peak 2	28.2	60.9	107.6	
Peak 3	2.3	31.1	3757	

Figure 29: Particles size distribution by intensity and summarizing table of prestin chimera Chim3del (magenta) and prestin [529-744] (yellow). Every measurement is the result of at least 15 accumulations. The proteins are concentrated 1mg/ml chim3 del and 5mg/ml pre[529-744] in 20 mM TRIS, 150 mM NaCl, 5mM DTT, pH 7.5. Int: intensity. Pd: polydispersion.

Looking at the results of the characterization of the prestin constructs, we can affirm that the chimera constructs (especially the longer variants) are good candidates for the crystallographic studies. They have a secondary structure similar to the C-terminal domain of the other SulP transporters (figure 25), and its higher amount and the higher T_m values compared to the forms with the presence of the variable loop are indicative of more structured and stable proteins. Further, the aggregation propensities of the chimeras are clearly lower than those in the presence of the variable loop. This loop, essentially unstructured as seen by difference CD analysis, seems to modulate the aggregation state of prestin STAS.

CRYSTALLIZATION TESTS

Several standard screens were tested (Qiagen and Molecular Dimension Ltd.) on the constructs reported in table 9. Many small crystals were obtained and were subjected to diffraction analysis to ELETTRA synchrotron (Trieste, Italy) or ESRF synchrotron

(Grenoble, France) but the images had few and very intense spots, typically generated by the diffraction of salts.

Table 9: selected constructs for crystallization test and their concentration

Construct	Concentration
Chim1	15 mg/ml
Chim2	10 mg/ml
Chim3	8 mg/ml
Chim1del	14 mg/ml

Proteins buffer: 20 mM TRIS, 150 mM NaCl, 5 mM DTT, pH 7.5.

Small needle-like crystals for Chim1del (figure 30A) were obtained at 20 °C, using the following precipitant solution: 0.1 M MES pH 6.5, 2 M ammonium sulfate, 5% (v/v) PEG400. After an optimization screening, bigger crystals (figure 30B) were obtained using a 14 mg/ml protein stock solution and 0.09 M MES pH 6.5, 1.8 M ammonium sulfate, 4.5% (v/v) PEG400, 0.1% octyl-β-D-glucopyranoside. The same conditions were used for the crystallization of the Se-Met derivative.

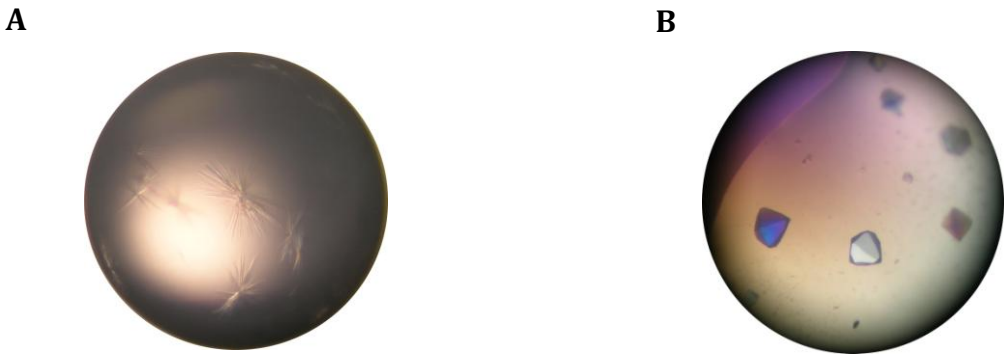

Figure 30: Chim1del crystals before (**A**) and after (**B**) addition of 0.1% octyl-β-D-glucopyranoside.

Attempts to solve the structure by molecular replacement using the ASA protein 3D structures failed and hence a Se-Met derivative was produced and the structure solved by SAD (Single Anomalous Dispersion). Statistics on data collections and refinement are reported in table 10. Proteins crystallizes in space group $P3_121$. There is a monomer in the asymmetric unit, corresponding to a V_M of 2.23 $Å^3$/Da and a solvent content of around 47% of the crystal volume. The eleven amino acids preceding the position of the variable loop (from residue 556) are not visible in the electron density because disordered and were

not included in the final model. The final model has a crystallographic R-factor of 15.7% (R_{free} = 19.8%). 97.4%, 2.6%, 0% and 0% of the amino acids in the final atomic model reside in the most favorable, additional allowed, generously allowed and disallowed regions of the Ramachandran plot, respectively.

Table 10: Data collection, phasing and refinement statistics for SAD (SeMet) structures

	Prestin STAS - Native	Prestin STAS – Seleno-methionine derivative
Data collection statistics	ESRF beamline ID 14-1, λ = 0.93	ESRF beamline ID 23-2, λ = 0.87 Å
Space group	P 3_1 2 1	P 3_1 2 1
Cell dimensions *a, b, c* **(Å)** α, β, γ **(°)**	61.59, 61.59, 67.13 90.0, 90.0, 120.0	61.94, 61.94, 67.25 90.0, 90.0, 120.0
Total number of observations	235045 (29737)	660833 (94427)
Total number unique	20860 (2931)	20184 (2912)
Resolution (Å)	28.41 – 1.57 (1.65)	41.94 – 1.60 (1.69)
R_{sym} (%)	5.5 (49.6)	6.6 (51.3)
R_{meas} (%)	5.8 (52.1)	6.8 (52.9)
I/σ(I)	8.5 (1.6)	6.5 (1.5)
Completeness (%)	99.3 (97.6)	100 (100)
Multiplicity	11.3 (10.1)	32.7 (32.4)
Bwilson (Å)	21.4	19.5
Solvent content (%)	47	47
Refinement statistics		
Resolution (Å)	28.41 – 1.57	
N° reflections	20831 (1062)	
R_{crys}/R_{free}(%)	15.4 /19.5	
N° atoms (Average B-value (Å^2))		
All atoms	1161 (25.15)	
Protein	1048 (24.24)	
Ligands	10 (32.01)	
Water	103 (36.17)	
Root mean square deviations from ideality		
Bond lengths (Å)	0.027	
Bond Angles (°)	2.108	
Ramachandran plot statistic (%) (excl Gly, Pro)		
Most favoured regions	97.4	
Additionally allowed regiios	2.6	
Generously allowed regions	0	
Disallowed region	0	

The values in brackets are referred to the highest resolution shell.

STRUCTURE DESCRIPTION OF PRESTIN STAS DOMAIN

The core of the prestin STAS domain is composed by a β-sheet of 6 β-strands, named β_0, β_1, β_2, β_3, β_4 and β_5 (figure 31). The four C-terminal strands (β_2-β_5) are surrounded by five α-helices (α_1 to α_5). (We have adopted this nomenclature to simplify the comparison between SLC26 and ASAs STAS domain). The structure is stabilized by two extensive networks of hydrophobic residues connecting each side of the β-sheet with the nearby helices.

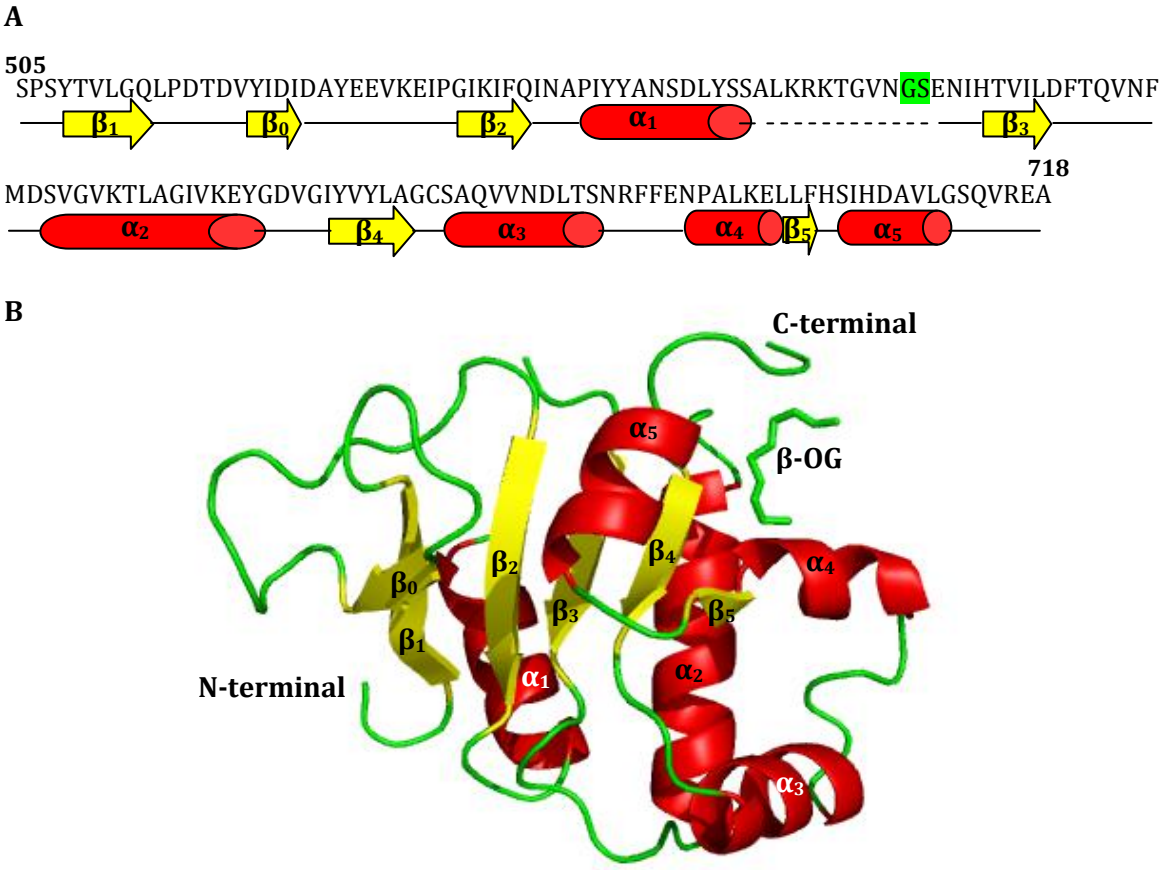

Figure 31: Representation of the secondary structure elements (**A**) and crystal structure of the prestin STAS domain (**B**). α-helices and β-strands are numbered sequentially from N-terminus to C-terminus. The dotted lines indicate the amino acids not visible in the structure. The amino acids introduced during the cloning are highlighted in green. β-OG: octyl-β-D-glucopyranoside.

The C-terminal part of this prestin domain (from β_3 to α_5 and β_2) is structurally and topologically similar to bacterial ASAs (figure 32), justifying also from a structural point of view the notion of STAS (Sulphate Transporters and Anti-Sigma factor antagonists) domain (Aravind & Koonin, 2000).

At the N-terminal end, two long rigid loops, connecting β_1 to β_0 and β_0 to β_2, comprise a series of β-turns linked by short amino acids sequences. This is the most relevant characteristic of the prestin STAS domain that substantially differentiates it from the bacterial ASAs, where the long insertion between β_1 and β_2 (of around 19 residues) is missed, substituted by a short turn (figure 32).

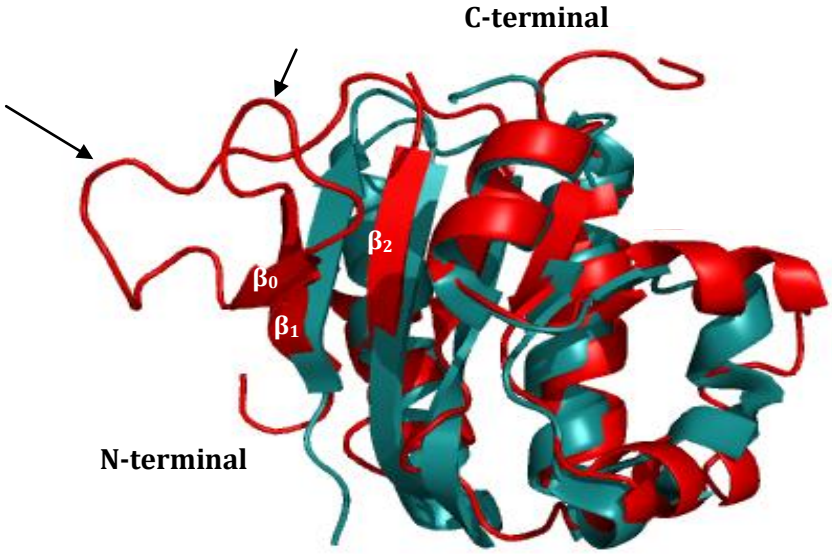

Figure 32: Superimposition between the prestin STAS domain (in red) and the spoIIAA from *Bacillus stearothermophilus* (cyan) (PDB: 1TID). Arrows indicate the loop between β_1 to β_0 and β_0 to β_2.

The N-terminal region is made quite rigid by an extensive network of hydrogen bonds mainly between amide and carbonyl groups of the backbone. Notably, this part of the molecule interacts directly with the extreme C-terminal end, in particular with helix α_5, through an hydrogen bond between the side chains of Tyr520 and His707 and an hydrophobic core made by Leu511, Tyr520 and Ile532 from the N-terminus and Ile706 and Val710 from the C-terminus (figure 33). These hydrophobic residues are fully part of one of the two hydrophobic cores that surround the central β-sheet, indicating that this portion, absent in the ASA proteins, is not simply an appendix of a smaller domain connected to the rest of the molecule.

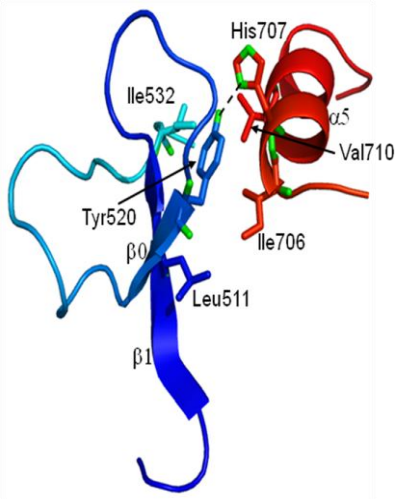

Figure 33: Interaction between the N- and C-terminus of prestin STAS domain. The side chain of amino acids involved in this interaction are shown.

The other prestin constructs starting at position

522 or 529 (Chim2 or Chim3), instead of 505, do not crystallize. They have CD spectra similar to Chim1del (figure 24) but show a slightly higher propensity to aggregate (figure 28). This indicates that the main contribution to the stability of the STAS construct comes from the core region between β_2 and α_5. The N-terminal extension seems to have a role mainly in modulating both intra- and inter-molecular interactions, in a functional important way.

Another important difference from the bacterial ASAs is the direction of helix α_1. In prestin STAS domain it is bended in such a way that its C-terminal end is distant from the beginning of α_2 (figure 34). In this respect, an important role is played by Tyr667 at the beginning of α_2, that points towards α_1 pushing it away from α_2. The parallel arrangement of α_1 and α_2 seen in the ASA proteins is not possible in this case for the steric hindrance caused by Tyr667.

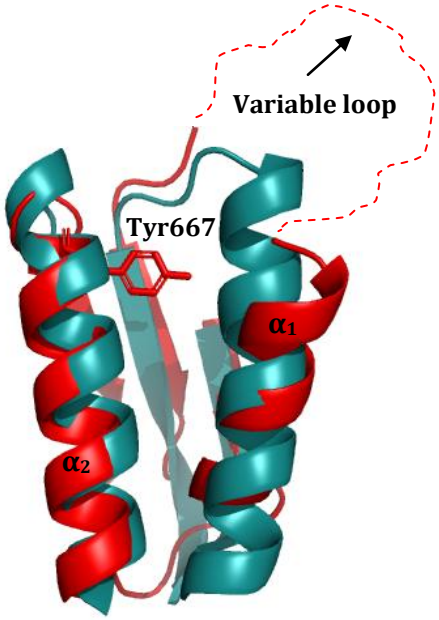

Figure 34: Superimposition between the helix α_1 and the helix α_2 of prestin STAS domain (in red) and the corresponding helix of spoIIAA from *Bacillus stearothermophilus* (cyan). The location of the variable loop and the side chain of prestin Tyr 667 are shown.

This bending of α_1 is necessary to create the space required to accommodate the insertion of the long variable loop, not present in bacterial ASAs. The importance of position 667 is highlighted by the conservation of an aromatic residue (a tyrosine but also a phenylalanine) in this position in transporters (with the exception of SLC26A7 and A10, the more distant in the evolutionary tree), while it is substituted by amino acids with shorter side chains (Ile/Leu/Ala) in bacterial ASAs (figure 35). It is interesting to note that, despite the variant was designed on the basis of the structure of ASA proteins, in particular as far as the connection between helix α_1 and strand β_3 is concerned, in this region our structure deviates from the bacterial proteins, indicating a strong stability of the new fold. The flexibility of the eleven residues starting from position 556 is most probably a consequence of the deletion of the variable loop.

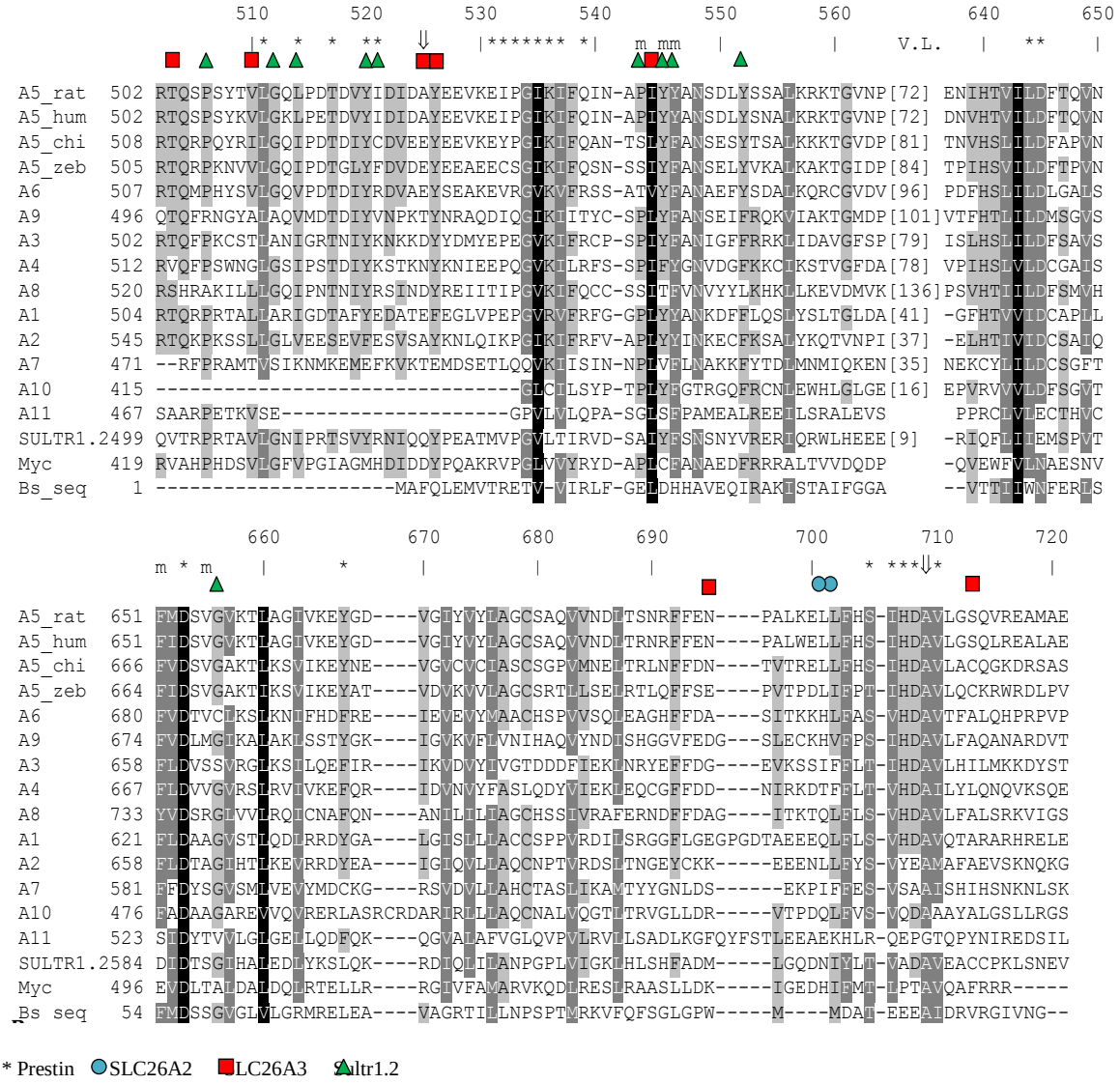

Figure 35: Multiple sequence alignment of the eleven SLC26 transporters, Sultr1.2 from *A. thaliana*, bacterial transporter Rv1739c from *M. tuberculosis* (Myc) and spoIIAA from *B. sphaericus* (Bs_seq). For prestin (A5), the sequences from *Rattus norvegicus* (rat), human (hum), chicken (chi) and zebrafish (zeb) are reported. V. L. = variable loop. Vertical arrows indicate the boundaries of the STAS domain according to Aravind and Koonin. Asterisks, circles, squares, triangles indicate important residues discussed in the text of, respectively: prestin, SLC26A2, SLC26A3 and Sultr1.2. m = residues facing the membrane.

STAS ORIENTATION WITH RESPECT TO THE MEMBRANE

As the prestin STAS domain is located in the cytosolic portion of a membrane protein, in close proximity to the lipid bilayer, we have tried to identify which is the part of the molecule facing the membrane surface. Recently, it has been proposed a

computational approach (PPM) for positioning of integral and peripheral membrane proteins with respect to the lipid bilayer on the basis of their 3D structures (Lomize *et al.*, 2006). The submission of our 3D structure to the program PPM revealed the existence of a non-polar surface region, composed by residues Pro543, Tyr545, Tyr546, Phe651 and Val655, that shows a possibility of weak association with a lipid bilayer (figure 35). Interestingly, with this hydrophobic spot facing the membrane, the N-terminal end of the molecule, only few residues after the last transmembrane domain, is oriented just toward the membrane, as one would expect. With this orientation (figure 35), the C-terminal end places toward the cytosol, in agreement with the hypothesis that the extreme C-terminal tail (from residue 719 to 744) is involved in intermolecular protein-protein interactions. For instance, in this part a PDZ-binding motif has been detected. Interestingly, residues Pro543, Tyr545, Tyr546, Phe651 and Val655 are well conserved within the SLC26 family (or changed with residues with similar properties) (figure 34), while in bacterial spoIIAA the corresponding residues are more variable and generally much less hydrophobic.

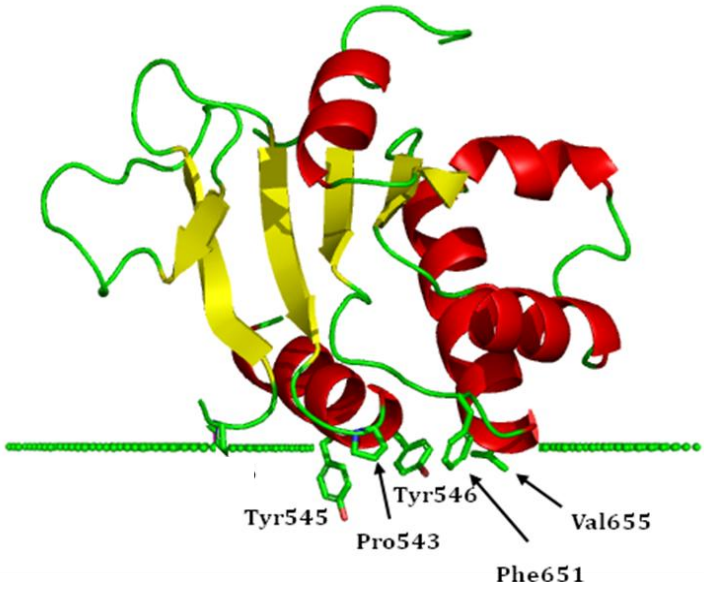

Figure 35: Proposed orientation of prestin STAS with respect to the membrane (small green spheres). The side chain of the amino acids which have been detected interacting the lipid bilayer by the program PPM are shown.

BINDING SITE

A linear ligand was found bound to the STAS domain between helices α2 and α4, near the C-terminal end of the protein (figure 31**)**. The electron density was interpreted as

the hydrophobic tail of the detergent octyl-β-D-glucopyranoside (β-OG) that was fundamental in getting well-diffracting hexagonal crystals from poorly diffracting needle-like ones (figure 30), showing the ability to change the crystal morphology modulating the protein crystal packing The position of this β-OG is similar to one of the two β-OG found in the crystal structure of the *Saccharomyces cerevisiae* phosphatidylinositol transfer protein Sec14p (Sha *et al.*, 1998), the prototype of the lipid-binding SEC14 domain (named CRAL-TRIO in mammalian proteins) (Saito *et al.*, 2007), which share the same structural fold with the STAS domain (Aravind & Koonin, 2000). This suggests that the long hollow hosting the β-OG could represent a genuine ligand binding site for small molecule or proteins that could modulate prestin function.

PRESTIN STAS DOMAIN MODEL AND PRESTIN FUNCTIONAL DATA

Our model of the prestin STAS domain, identified between residues 505 and 718, is well in accordance with the available functional data. For instance, it has been demonstrated that the deletion of the extreme C-terminal tail, from residue 719 on, does not compromise the prestin localization and function (characterized by the presence of nonlinear capacitance, NLC), while the mutant deleted from residue 709 or 710, where helix α5 is almost completely omitted, lacks NLC (Zheng *et al.*, 2005; He *et al.*, 2006). Given the cytosolic localization of Del709, it has been proposed that the region from 709 and 719 is essential for proper plasma membrane targeting. Our structure indicates that the STAS domain of the Del709 mutant is strongly destabilized by the lack of helix α5. In the same study it was found that the double mutation Y520A/Y526A produces a variant that lacks NLC and that is intracellularly accumulated. As indicated above, this region is not crucial for the stability of the tertiary structure, so it is probable that the double mutation Y520A/Y526A does not directly cause the misfolding of the STAS domain but rather hampers in some way the appropriate functional assembly of the transporter.

PRESTIN STAS DOMAIN AS TEMPLATE FOR SLC26/SulP STAS

PRESTIN STAS DOMAIN AS MODEL FOR SLC26 STAS

As summarized in figure 34, many residues structurally important in prestin STAS are conserved among SLC26 transporters, with the exception of members A7, A10 and A11, the most distant in the evolutionary tree (Dorwart *et al.*, 2008b). This suggests that the structure of the prestin STAS domain can be a valuable model at least for the 8 more conserved SLC26 proteins A1, A2, A3, A4, A5, A6, A8 and A9. This hypothesis is corroborated by the fact that secondary structure predictions on the cytosolic portion of these transporters, starting from residues corresponding to prestin Ser505, are in agreement with the elements found in the 3D structure of prestin STAS.

Of particular relevance the fact that this is true also as far as the N-terminal end, hypothesis comes from the fact that for some SLC26 such as A1 and A3, for which functional data are available, the structure of prestin STAS domain is able to nicely explain why mutations or deletions of certain amino acids affect the protein localization and function.

In SLC26A1 (sat-1) the removal of the last three residues, on the basis of our structure beyond the C-terminal boundary of the STAS domain (figure 34), had no effect on basolateral sorting and on sulfate transport. Instead, the removal of the last 30 residues, with the deletion of helices α4 and α5, led to an anomalous localization of the protein (Regeer & Markovich, 2004). Further, the double mutation L677A/L678A in rat sat-1 resulted in the loss of basolateral sorting. Sat-1 Leu 677 corresponds to prestin Leu701, at the end of helix α_4, part of a hydrophobic core that comprises residues also from helix α_2 and beta-strand β_4. L678 in sat-1 is in a conserved position in SLC26 transporters, indicating a common important function in the family. Clearly, the mutation of the two leucines with much less hydrophobic amino acids as alanine destabilizes the C-terminal portion of the STAS domain. In this case wrong localizations and loss of function can be attributed to misfolding.

Mutants of human SLC26A3 are linked to CLD and the STAS domain is responsible for the reciprocal regulatory interactions with the cystic fibrosis transmembrane conductance regulator CFTR . Dorwart and colleagues have investigated the possible boundaries of the STAS domain of SLC26A3 and four CLD-causing mutations localized

in the domain (Dorwart *et al.*, 2008b). Based on secondary structure and thermal stability data and on the ability to bind to the CFTR R-domain, authors hypothesis that the DRA STAS domain extend from somewhere between amino acids 510 and 525 until a position between 720 and 741. On the basis of our model, we predict that the DRA STAS domain boundaries are around residues 505 and 726. This seems to indicate that the DRA STAS N-teminal region, absent in the studied constructs, is not involved in the interaction with the CFTR R domain. The three STAS variants with different N-termini (503, 510 and 525) but all ending at position 720 (corresponding to prestin Ser 713) were insoluble in *E. coli*. Based on our model, the variants are structurally unstable because of the destabilization of helix α_5. And the destabilization of the C-terminal region and the resulting misfolding is also the result of the G702Tins mutations (G702T + GFEVKIQNF insertion).

According to CD, NMR and thermal denaturation data, the other two mutations, ΔY526/7 and I544N, do not alter significantly the structure of the domain, especially the first one, and this is in accordance with our model. Mutations ΔY526/7 maps in the long loop connecting β_0 to β_2 at the periphery of the domain, with side chains pointing toward the solvent, indicating that this is the less dangerous for the 3D domain structure. Mutation I544N maps to a position invariably occupied by an hydrophobic residue (Ile or Val) in SLC26, at the beginning of helix α_1, with the side chain pointing to the hydrophobic interior of the domain. All this is in accordance with the hypothesis of Dorwart and *colleagues* that variations ΔY526/7 and I544N, that can be somehow structurally accommodated, produce only subtle perturbations of the structure, if any. These mutations, however, could be able to disrupt critical intra- or inter-molecular protein-protein interactions, as suggested by their surface localization, again suggesting that the STAS domain can have a key role in the proper assembly of the oligomeric state of these transporters (Dorwart *et al.*, 2008a).

OTHER STRUCTURALLY IMPORTANT RESIDUES

The analysis of the 3D structure allowed the identification of other structurally important residues conserved among the SLC26 transporters and that, therefore, seem to play an important role in the STAS domain of this family. These residues were not

previously recognized as important in prestin STAS structure and function. The most relevant are: Thr517, Gly534, Asp645, Asp653, Ser705 and Asp708.

The Thr517 hydroxyl makes two hydrogen bonds with the backbone carbonyl and amide of Leu514 and Val519, respectively, stabilizing and stiffening the loop between β_1 and β_0 (figure 33).

Gly534 is in the position i+2 of a type II β-turn, a position in which a glycine is largely preferred for this type of turn, that is further stabilized by Pro533 in position i+1. This stable turn has the important function to bend the main chain for the correct positioning of the following β_2 strand, starting with I535.

The side chain of Asp645 at the end of β_3 interacts with the side chains of Gln539, at the end of β_2, and of Thr647, via two hydrogen bonds, stabilizing the beginning of the so-called "conserved loop".

At the extreme C-end of the conserved loop, just preceding the start of helix α_2, Asp653 contribute in the stabilization of α_2 in two ways: with the negative side chain interacts with the positive dipole of the N-terminal end of the α-helix; with the carboxyl side chain establishes two hydrogen bonds with the backbone amide of Gly656 and the side chain of Tyr545, at the beginning of α_1. To note that in this zone, at position 654, there is a serine that is phosphorylated in bacterial ASAs.

It is highly conceivable that mutations in these key structural residues can cause severe alteration in prestin structure and function.

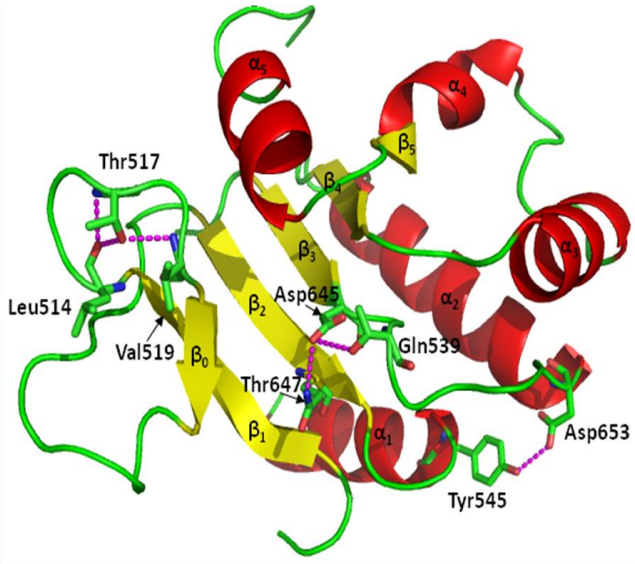

Figure 36: Crystal structure of prestin STAS. The magenta dashes indicate the hydrogen bonds between the side chain of some residues, important for the structure stabilization of the STAS domain.

PRESTIN C-TERMINAL DOMAIN AS POSSIBLE GENERAL TEMPLATE FOR SulP TRANSPORTERS

Because of the sequence homology between SLC26 and SulP transporters, one could raise the question whether this 3D STAS structure can be a reliable model also for the whole family of transporters, not only for the SLC26 subfamily. Data on the STAS domain of the SulP transporter Sultr1.2 suggests a positive answer (Rouached *et al.*, 2005, Shibagaki & Grossman, 2006) (figure 8). For instance, Shibagaki & Grossman found that mutations in five amino acids in the "linking region", between Sultr1.2 residues 503-518, (figure 34) abolish the capacity of efficiently transport sulfate into cells, while causing only little changes in protein abundance or plasmamembrane localization. In our model these residues belong to the well-structured N-terminal end of the domain, previously not recognized as part of the STAS domain, validating the hypothesis that this region is important not only for the (stability) global folding of the STAS domain, but also that it is involved in intra- and/or inter-molecular interactions.

In fact, our Sultr1.2 STAS construct, designed on the basis of the sequence alignment reported by Shibagaki & Grossman starting from residue 517, excludes the linking region and shows a strong tendency on the aggregation (figure 27).

Another interesting observation was that other mutations, again affecting function but not accumulation and localization, correspond to prestin Pro543, Tyr545, Tyr546 and Val656 that were identified by the PPM program as putative membrane interacting residues.

MAPPING OF NON-FUNCTIONAL MUTATIONS ON THE STAS SURFACE

As seen above, on the basis of a structure-function analysis, mutations that negatively affect the function of transporters carrying a STAS domain can be divided into two classes: those that cause a general large misfolding of the domain and those that do not substantially alter its 3D structure but that most probably affect its ability to properly interact with specific partners. It is noteworthy that mutations of the last class, mapping on the surface of the STAS structure, are found mainly in two regions: in the one we have supposed facing the plasma membrane and in the N-terminal portion of the domain,

previously considered a linker region (figure 37). This allows suggesting that the first region is probably involved in functionally important interactions with the membrane portion of the transporters and/or the lipid bilayer and that the second one is involved in some important protein-protein interactions. The last one could also be intramolecular interactions regulating the oligomerization state of prestin, for instance with the N-terminal cytosolic portion that was seen important for the formation of multimers (Navaratman *et al.*, 2005). Mutations in these two surface regions result in mistrafficking, as seen for SLC26A3 (mutants ΔY526/7 and I544N) and prestin (double mutation Y520A/Y526A) or loss of function while retaining the correct localization, as seen for Sultr1.2. The hypothesis of the involvement of the N-terminal region in functionally important protein-protein interactions was also suggested on the basis of the observation that when its acidic cluster is *en-block* mutated in lysines, reversing the charge, the amount of functional transporter decreases with no variation in the protein localization (Bai *et al.*, 2006). This was interpreted as an interference with the interaction properties of the prestin C-terminal domain, in accordance with our model.

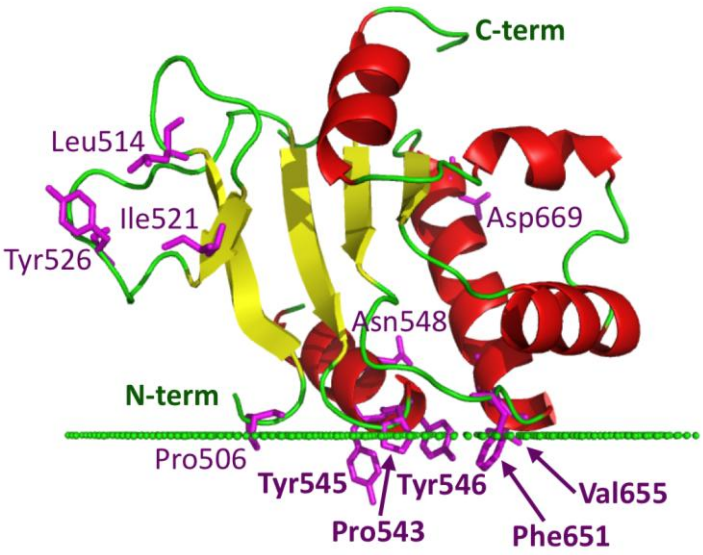

Figure 37: Proposed orientation of prestin STAS with respect to the membrane (small green spheres) and mapping of mutations that affect function (residues in magenta) discussed in the text. In bold, residues that have been detected interacting with the membrane by the program PPM.

3

CONCLUSIONS

The structure of prestin STAS presented here is the first 3D structural characterization of a STAS domain of SLC26/SulP anion transporters. To identify the localization of the STAS in the C-terminal of prestin, we cloned successfully various constructs, with and without the variable loop, which is the main difference with the ASA proteins. The obtained data confirm the hypothesis that this loop is unstructured and the its presence induces unspecific aggregation.

Subsequently the comparison of our 3D structure of prestin STAS and the bacterial ASA proteins revealed that there is another important difference: the N-terminal region from residue 505 to residue 525 (prestin numbering), previously considered merely a generic linker region between the last transmembrane region and the STAS domain, is indeed fully part of the STAS domain from a structural point of view. So, our STAS structure allows to redefine the STAS boundaries not only for prestin but also for more conserved SLC26 members and, possibly, for many SulP transporters.

The structure-function analysis indicates that the STAS domain can be implicated in molecular interactions involving different types of possible partners: the lipid bilayer; the transmembrane domain of the same protein; other intracellular portions of the transporter for the correct assembly of the oligomeric state; small molecules that can regulate protein function (as suggested by the presence of a long hollow on the STAS surface occupied by the β-OG tail).

Given the sequence homology between the SLC26/SulP family, the structure presented here can help in guiding functional studies aimed at deciphering the transport mechanism not only of prestin.

Another important consideration emerge from the mapping of the known SulP mutations on the surface of the our structure. disease-associated or functionally harmful mutations on the STAS model indicates that they can be divided into two categories: those causing a significant misfolding of the domain and those altering its interaction properties. These findings could have important consequences also for the planning of therapeutic-potential intervention.

References

Albert J.T., Winter H., Schaechinger T.J., Weber T., Wang X., He D.Z.Z., Hendrich O., Geisler H.-S., Zimmermann U., Oelmann K., Knipper M., Gopfert M.C., Oliver D. (2007). Voltage-sensitive prestin orthologue expressed in zebrafish hair cells. *J. Physiol.* **580**: 451-461.

Alper S., Duncan L., Losick R. (1994). An adenosine nucleotide switch controlling the activity of a cell type-specific transcription factor in *B. subtilis*. *Cell* **77**: 195-205.

Alvarez B.V., Vilas G.L., Casey J.R. (2005). Metabolon disruption: a mechanism that regulates bicarbonate transport. *EMBO J.* **24**: 2499-2511.

Aravind L., Koonin E.V. (2000). The STAS domain - a link between anion transporters and antisigma-factor antagonists *Curr. Biol*. **10**: 53-55.

Ashmore J.F. (1990). Forward and reverse transduction in the mammalian cochlea. *Neurosci. Res. Suppl.* **12**: 39-50.

Bai J.P., Navaratnam D., Samaranayake H., Santos-Sacchi J. (2006). En block C-terminal charge cluster reversals in prestin (SLC26A5): effects on voltage-dependent electromechanical activity. *Neurosci. Lett.* **404**: 270-275.

Blons H., Feldmann D., Duval V., Messaz O., Denoyelle F., Loundon N., Sergout-Allaoui A., Houang M., Duriez F., Lacombe D., Delobel B., Leman J., Catros H., Journel H., Drouin-Garraud V., Obstoy M.F., Toutain A., Oden S., Toublanc J.E., Couderc R., Petit C., Garabédian E.N., Marlin S. (2004). Screening of SLC26A4 (PDS) gene in Pendred's syndrome: a large spectrum of mutations in France and phenotypic heterogeneity. *Clin. Genet*. **66**: 333-340.

Brownell W.E., Bader C.R., Bertrand D., de Ribaupierre Y. (1985). Evoked mechanical responses of isolated cochlear outer hair cells. *Science* **227**: 194-196.

Campbell C., Cucci R.A., Prasad S., Green G.E., Edeal J.B., Galer C.E., Karniski L.P., Sheffield V.C., Smith R.J. (2001). Pendred syndrome, DFNB4, and PDS/SLC26A4

identification of eight novel mutations and possible genotype–phenotype correlations. *Hum. Mutat.* **17**: 403-411.

Campbell E.A., Masuda S., Sun J.L., Muzzin O., Olson C.A., Wang S., Darst S.A. (2002). Crystal structure of the Bacillus stearothermophilus anti-sigma factor SpoIIAB with the sporulation sigma factor sigmaF. *Cell* **108**: 795-807.

Chang M.H., Plata C., Sindic A., Ranatunga W.K., Chen A.P., Zandi-Nejad K., Chan K.W., Thompson J., Mount D.B., Romero M.F. (2009a). Slc26a9 is inhibited by the R-region of the cystic fibrosis transmembrane conductance regulator via the STAS domain. *J. Biol. Chem.* **284**: 28306-28318.

Chang M.H., Plata C., Zandi-Nejad K., Sindić A., Sussman C.R., Mercado A., Broumand V., Raghuram. V, Mount D.B., Romero M.F. (2009b). Slc26a9-anion exchanger, channel and Na^+ transporter. *J. Membr. Biol.* **228**: 125-140.

Cheatham M.A., Huynh K.H., Gao J., Zuo J., Dallos P. (2004). Cochlear function in Prestin knockout mice. *J. Physiol*. **560**: 821-830.

Cherest H., Davidian J.C., Thomas D., Benes V., Ansorge W., Surdin-Kerjan Y. (1997). Molecular characterization of two high affinity sulfate transporters in *Saccharomyces cerevisiae*. *Genetics* **145**: 627-635.

Chernova M.N., Jiang L., Shmukler B.E., Schweinfest C.W., Blanco P., Freedman S.D., Stewart A.K., Alper S.L. (2003). Acute regulation of the SLC26A3 congenital chloride diarrhoea anion exchanger (DRA) expressed in Xenopus oocytes. *J. Physiol*. **549**: 3-19.

Choi J.Y., Muallem D., Kiselyov K., Lee M.G., Thomas P.J., Muallem S. (2001). Aberrant CFTR-dependent HCO_3^- transport in mutations associated with cystic fibrosis. *Nature* **410**: 94-97.

Cowtan K. (1994). dm: An automated procedure for phase improvement by density modification. *Joint CCP4 and ESF-EACBM Newsletter on Protein Crystallography* **31**: 34-38

Cowtan K. (2006). The Buccaneer software for automated model building. 1. Tracing protein chains. *Acta Crystallogr. D Biol. Crystallogr.* **62**: 1002-1011.

Dallos P. (1992). The active cochlea. *J. Neurosci.* **12**: 4575-4585.

Dallos P., Fakler B. (2002). Prestin, a new type of motor protein. *Nat. Rev. Mol. Cell Biol.* **3**: 104-111.

Dallos P., Zheng J., Cheatham M.A. (2006). Prestin and the cochlear amplifier. *J. Physiol.* **76**: 37-42.

Dawson P.A., Marchovich D. (2005). Pathogenetics of the human SLC26 transporters. *Curr. Medicinal Chem.* **12**: 385-396.

Deak L., Zheng J., Orem A., Du G.G., Aguinaga S., Matsuda K., Dallos P. (2005). Effects of cyclic nucleotides on the function of prestin. *J. Physiol.* **563**: 483-496.

Detro-Dassen S., Schänzler M., Lauks H., Martin I., zu Berstenhorst S.M., Nothmann D., Torres-Salazar D., Hidalgo P., Schmalzing G., Fahlke C. (2008). Conserved dimeric subunit stoichiometry of SLC26 multifunctional anion exchangers. *J. Biol Chem.* **283**: 4177-4188.

Dong X.X., Iwasa K.H. (2004). Tension sensitivity of prestin: comparison with the membrane motor in outer hair cells. *Biophys. J.* **86**:1201-1208.

Dong X.X., Ospeck M., Iwasa K.H. (2002). Piezoelectric reciprocal relationship of the membrane motor in the cochlear outer hair cell. *Biophys. J.* **82:** 1254-1259.

Dorwart M.R., Shcheynikov N., Baker J.M., Forman-Kay J.D., Muallem S., Thomas P.J. (2008a). Congenital chloride-losing diarrhea causing mutations in the STAS domain result in misfolding and mistrafficking of SLC26A3. *J. Biol. Chem.* **283**: 8711-8722.

Dorwart M.R., Shcheynikov N., Yang D., Muallem S. (2008b). The solute carrier 26 family of proteins in epithelial ion transport. *Physiology* **23**:104-114.

Dossena S., Rodighiero S., Vezzoli V., Nofziger C., Salvioni E., Boccazzi M., Grabmayer E., Bottà G., Meyer G., Fugazzola L., Beck-Peccoz P., Paulmichl M. (2009). Functional characterization of wild-type and mutated pendrin (SLC26A4), the anion transporter involved in Pendred syndrome. *J. Mol. Endocrinol*. **43**: 93-103.

Emsley P., Cowtan K. (2004). Coot: model-building tools for molecular graphics. *Acta Crystallogr. D Biol. Crystallogr*. **60**: 2126-2132.

Errington J. (1996). Determination of cell fate in Bacillus subtilis. *Trends Genet.* **12**: 31-34.

Etezady-Esfarjani T., Placzek W.J., Herrmann T., Wüthrich K. (2006). Solution structures of the putative anti-sigma-factor antagonist TM1442 from *Thermotoga maritima* in the free and phosphorylated states. *Magn. Reson. Chem.* **44**: 61-70.

Evans P. (2006). Scaling and assessment of data quality. *Acta Crystallogr. D Biol. Crystallogr*. **62**: 72-82.

Everett L.A. and Green E.D. (1999). A family of mammalian anion transporters and their involvement in human genetic diseases. *Hum. Mol. Genet.* **8**: 1883-1891.

Felce J., Saier M.H. (2004). Carbonic anhydrases fused to anion transporters of the SulP family: evidence for a novel type of bicarbonate transporter. *J. Mol. Microbiol. Biotechnol*. **8**: 169-176.

Feucht A., Magnin T., Yudkin M.D., Errington J. (1996). Bifunctional protein required for asymmetric cell division and cell-specific transcription in Bacillus subtilis. *Genes Dev*. **10**: 794-803.

Forge A. (1991). Structural features of the lateral walls in mammalian cochlear outer hair cells. *Cell Tissue Res*. **265**: 473-483.

Frank G., Hemmert W., Gummer A.W. (1999). Limiting dynamics of high-frequency electromechanical transduction of outer hair cells. *Proc. Natl. Acad. Sci. USA* **96**: 4420-4425.

Greeson J.N., Organ L.E., Pereira F.A., Raphael R.M. (2006). Assessment of prestin self-association using fluorescence resonance energy transfer. *Brain Res.* **1091**: 140-150.

Hastbacka J., de la Chapelle A., Mahtani M.M., Clines G., Reeve-Daly M.P., Daly M., Hamilton B.A., Kusumi K., Trivedi B., Weaver A, Coloma A., Lovett M., Buckler A., Kaitila I., Lander E.S. (1994). The diastrophic dysplasia gene encodes a novel sulphate transporter: positional cloning by fine-structure linkage disequilibrium mapping. *Cell* **78**: 1073-1087.

Hästbacka J., Superti-Furga A., Wilcox W.R., Rimoin D.L., Cohn D.H., Lander E.S. (1996). Atelosteogenesis type II is caused by mutations in the diastrophic dysplasia

sulfate-transporter gene (DTDST): evidence for a phenotypic series involving three chondrodysplasias. *Am. J. Hum. Genet.* **58**: 255-262.

Hawkesford M.J. (2003). Transporter gene families in plants: the sulphate transporter gene family-redundancy or specialization? *Physiol. Plant* **117**: 155-163.

He D.Z., Zheng J., Kalinec F., Kakehata S., Santos-Sacchi J. (2006). Tuning in to the amazing outer hair cell: membrane wizardry with a twist and shout *J. Membr. Biol.* **209**: 119-134.

Kalinec F., Holley M.C., Iwasa K.H., Lim D.J., Kachar B. (1992). A membrane-based force generation mechanism in auditory sensory cells. *Proc. Natl. Acad. Sci. USA* **89**: 8671-8675.

Karniski L.P. (2004). Functional expression and cellular distribution of diastrophic dysplasia sulfate transporter (DTDST) gene mutations in HEK cells. *Hum. Mol. Genet*. **13**: 2165-2171.

Karniski L.P., Lötscher M., Fucentese M., Hilfiker H., Biber J., Murer H. (1998). Immunolocalization of sat-1 sulfate/oxalate/bicarbonate anion exchanger in the rat kidney. *Am. J. Physiol*. **275**: 79-87.

Keller P., Simons K. (1997). Post-Golgi biosynthetic trafficking. *J. Cell Sci.* **110**: 3001-3009.

Khurana O.K., Coupland L.A., Shelden M.C., Howitt S.M. (2000). Homologous mutations in two diverse sulphate transporters have similar effects. *FEBS Lett*. **477**: 118-122.

Ko S.B., Shcheynikov N., Choi J.Y., Luo X., Ishibashi K., Thomas P.J., Kim J.Y., Kim K.H., Lee M.G., Naruse S., Muallem S. (2002). A molecular mechanism for aberrant CFTR-dependent HCO_3^- transport in cystic fibrosis. *EMBO J.* **21**: 5662-5672.

Ko S.B.H., Zeng W., Dorwart M.R:, Luo X., Kim K.H., Millen L., Goto H., Naruse S., Soyombo A., Thomas P.J., Muallem S. (2004). Gating of CFTR by the STAS domain of the SLC26 transporters. *Nature Cell. Biology* **6**: 343-350.

Kovacs H., Comfort D., Lord M., Campbell I.D., Yudkin M.D. (1998) Solution structure of SpoIIAA, a phosphorylatable component of the system that regulates transcription factor sigmaF of *Bacillus subtilis*. *Proc. Natl. Acad. Sci. USA* **95**: 5067-5071.

Lamprecht G., Hsieh C.J., Lissner S., Nold L., Heil A., Gaco V., Schäfer J., Turner J.R., Gregor M. (2009). Intestinal anion exchanger down-regulated in adenoma (DRA) is inhibited by intracellular calcium. *J. Biol. Chem*. **284**:19744-19753.

Lee J.Y., Ahn H.J., Ha K.S., Suh S.W. (2004). Crystal structure of the TM1442 protein from *Thermotoga maritima*, a homolog of the *Bacillus subtilis* general stress response anti-anti-sigma factor RsbV. *Proteins* **56**: 176-179.

Leslie A.G.W. (1991). Crystallographic Computing V (Moras D., Podjarny A.D., Thierry J. P. eds), pp 27-38, Oxford University Press, Oxford.

Leves F.P., Tierney M.L., Howitt S.M. (2008). Polar residues in a conserved motif spanning helices 1 and 2 are functionally important in the SulP transporter family. *Int. J. Biochem. Cell Biol*. **40**: 2596-2605.

Li S.J., Hochstrasser M. (1999). A new protease required for cell-cycle progression in yeast. *Nature* **398**: 246-251.

Liberman M.C., Gao J., He D.Z., Wu X., Jia S., Zuo J. (2002). Prestin is required for electromotility of the outer hair cell and for the cochlear amplifier. *Nature* **419**:300-304.

Liu X.Z., Ouyang X.M., Xia X.J., Zheng J., Pandya A., Li F., Du L.L., Welch K.O., Petit C., Smith R.J., Webb B.T., Yan D., Arnos K.S., Corey D., Dallos P., Nance W.E., Chen Z.Y. (2003). Prestin, a cochlear motor protein, is defective in non-syndromic hearing loss. *Hum. Mol. Genet.* **12**:1155-1162.

Lohi H., Lamprecht G., Markovich D., Heil A., Kujala M., Seidler U., Kere J. (2003). Isoforms of SLC26A6 mediate anion transport and have functional PDZ interaction domains. *Am. J. Physiol. Cell Physiol.* **284**: 769-779.

Lomize M.A., Lomize A.L., Pogozheva I.D., Mosberg H.I. (2006). OPM: orientations of proteins in membranes database. *Bioinformatics* **22**: 623-635.

Loughlin P., Shelden M. C., Tierney M. L., Howitt S. M. (2002) Structure and function of a model member of the SulP transporter family. *Cell. Biochem. Biophys.* **36**: 183-190.

Ludwig J., Oliver D., Frank G., Klöcker N., Gummer A.W., Fakler B. (2001). Reciprocal electromechanical properties of rat prestin: The motor molecule from rat outer hair cells. *Proc. Natl. Acad. Sci. USA* **98**: 4178–4183.

Mammano F., Bortolozzi M., Ortolano S., Anselmi F. (2007). Ca^{2+} signaling in the inner ear. *Physiology* **22**: 131-144.

Masuda S., Murakami K.S., Wang S., Anders Olson C., Donigian J., Leon F., Darst S.A., Campbell E.A. (2004). Crystal structures of the ADP and ATP bound forms of the Bacillus anti-sigma factor SpoIIAB in complex with the anti-anti-sigma SpoIIAA. *J. Mol. Biol.* **340**: 941-956.

Matsuda K., Zheng J., Du G.G., Klöcker N., Madison L.D., Dallos P. (2004). N-linked glycosylation sites of the motor protein prestin: effects on membrane targeting and electrophysiological function. *J. Neurochem.* **89**: 928-938.

Meltzer J., Santos-Sacchi J. (2001). Temperature dependence of non-linear capacitance in human embryonic kidney cells transfected with prestin, the outer hair cell motor protein. *Neurosci. Lett.* **313**: 141-144.

Mio K., Kubo Y., Ogura T., Yamamoto T., Ariska F., Sato C. (2008). The motor protein prestin is a bullet-shaped molecule with inner cavities. *J. Biol. Chem.* **283**: 1137-1145.

Moseley R.H., Höglund P., Wu G.D., Silberg D.G., Haila S., de la Chapelle A. Holmberg C., Kere J. (1999). Downregulated in adenoma gene encodes a chloride transporter defective in congenital chloride diarrhea. *Am. J. Physiol*. **276**: 185-192.

Mount D.B., Romero M.F. (2004). The SLC26 gene family of multifunctional anion exchangers. *Pflugers. Arch*. **447**: 710-721.

Muallem D., Ashmore J. (2006). An anion antiporter model of prestin, the outer hair cell motor protein. *Biophys. J*. **90**: 4035-4045.

Murshudov G.N., Vagin A.A,. Dodson E.J. (1997). Refinement of macromolecular structures by the maximum-likelihood method. *Acta Crystallogr. D Biol. Crystallogr*. **53**: 240-255.

Najafi S.M., Harris D.A., Yudkin M.D. (1996). The SpoIIAA protein of Bacillus subtilis has GTP-binding properties. *J. Bacteriol*. **178**: 6632-6634.

Navaratnam D., Bai J.P., Samaranayake H., Santos-Sacchi J. (2005). N-terminal mediated homo-multimerization of prestin, the outer hair cell motor protein. *Biophys. J.* **89**: 3345-3352.

Okoruwa O.E., Weston M.D., Sanjeevi D.C., Millemon A.R., Fritzsch B., Hallworth R., Beisel K.W. (2008). Evolutionary insights into the unique electromotility motor of mammalian outer hair cells. *Evol. Dev.* **10**: 300-315.

Ohana E., Yang D., Shcheynikov N., Muallem S. (2009). Diverse transport modes by the solute carrier 26 family of anion transporters. *J. Physiol.* **587**: 2179-2185.

Oliver D., He D.Z., Klöcker N., Ludwig J., Schulte U., Waldegger S., Ruppersberg J.P., Dallos P., Fakler B. (2001). Intracellular anions as the voltage sensor of prestin, the outer hair cell motor protein *Science* **292**: 2340-2343.

Pasqualetto E., Seydel A., Pellini A., Battistutta R. (2008). Expression, purification and characterization of the C-terminal STAS domain of the SLC26 anion transporter prestin. *Protein Expr. Purif.* **58** :249-256.

Pendred V. (1896). Deaf-mutism and goiter. *Lancet* **148**: 532.

Price G., Woodger F., Badger M., Howitt S., Tucker L. (2004). Identification of a SulP type bicarbonate transporter in marine cyanobacteria. *Proc. Natl. Acad. Sci. USA* **101**: 18228-18233.

Rajagopalan L., Patel N., Madabushi S., Goddard J.A., Anjan V., Lin F., Shope C., Farrell B., Lichtarge O., Davidson A.L., Brownell W.E., Pereira F.A. (2006). Essential helix interactions in the anion transporter domain of prestin revealed by evolutionary trace analysis. *J. Neurosci.* **26**: 12727-12734.

Regeer R.R., Markovich D. (2004). A dileucine motif targets the sulfate anion transporter sat-1 to the basolateral membrane in renal cell lines. *Am. J. Physiol. Cell Physiol.* **287**: 365-372.

Rosenberg N.K., Lee R.W., Yancey, P.H. (2006). High contents of hypotaurine and thiotaurine in hydrothermal-vent gastropods without thiotrophic endosymbionts. *J. Exp. Zool. A Comp. Exp. Biol.* **305**: 655-662.

Rossi A., Bonaventure J., Delezoide A.L., Cetta G., Superti-Furga A. (1996). Undersulfation of proteoglycans synthesized by chondrocytes from a patient with achondrogenesis type 1B homozygous for an L483P substitution in the diastrophic dysplasia sulfate transporter *J. Biol. Chem.* **271**: 18456-18464.

Rossi A., Superti-Furga A. (2001). Mutations in the diastrophic dysplasia sulfate transporter (DTDST) gene (SLC26A2): 22 novel mutations, mutation review, associated skeletal phenotypes, and diagnostic relevance. *Hum. Mutat*. **17**: 159-171.

Rossmann H., Jacob P., Baisch S., Hassoun R., Meier J., Natour D., Yahya K., Yun C., Biber J., Lackner K.J., Fiehn W., Gregor M., Seidler U., Lamprecht G. (2005). The CFTR associated protein CAP70 interacts with the apical Cl^-/HCO_3^- exchanger DRA in rabbit small intestinal mucosa. *Biochemistry* **44**: 4477-4487.

Rotman-Pikielny P., Hirschberg K., Maruvada P., Suzuki K., Royaux I.E., Green E.D., Kohn L.D., Lippincott-Schwartz J., Yen P.M. (2002). Retention of pendrin in the endoplasmic reticulum is a major mechanism for Pendred syndrome. *Hum. Mol. Genet*. **11**: 2625-2633.

Rouached H., Berthomieu P., El Kassis E., Cathala N., Catherinot V., Labesse G., Davidian J.C., Fourcroy P. (2005). Structural and functional analysis of the C-terminal STAS (sulfate transporter and anti-sigma antagonist) domain of the Arabidopsis thaliana sulfate transporter SULTR1.2. *J. Biol. Chem.* **280**: 15976-15983.

Ryan A., Dallos P. (1975). Effect of absence of cochlear outer hair cells on behavioural auditory threshold. *Nature* **253**: 44-46.

Rybalchenko V., Santos-Sacchi J. (2003). Cl^- flux through a non-selective, stretch-sensitive conductance influences the outer hair cell motor of the guinea-pig. *J. Physiol.* **547**: 873-891.

Saier M.H. (1999). A functional–phylogenetic system for the classification of transport proteins. *J. Cell Biochem.* **33**: 84-94.

Saier M.H. Jr, Eng B.H., Fard S., Garg J., Haggerty D.A., Hutchinson W.J., Jack D.L., Lai E.C., Liu H.J., Nusinew D.P., Omar A.M., Pao S.S., Paulsen I.T., Quan J.A., Sliwinski M., Tseng T.T., Wachi S., Young G.B. (1999b). Phylogenetic characterization of novel

transport protein families revealed by genome analyses. *Biochim. Biophys. Acta* **1422**: 1-56.

Saito K., Tautz L., Mustelin T. (2007). The lipid-binding SEC14 domain. *Biochim. Biophys. Acta* 1771: 719-726.

Sandal N.N., Marcker K.A. (1994). Similarities between a soybean nodulin, *Neurospora crassa* sulphate permease II and a putative human tumour suppressor. *Trends Biochem. Sci.* **19**: 19

Santos-Sacchi J., Dilger J.P. (1988). Whole cell currents and mechanical responses of isolated outer hair cells. *Hear Res.* **35**: 143-150.

Santos-Sacchi J., Shen W., Zheng J., Dallos P. (2001). Effects of membrane potential and tension on prestin, the outer hair cell lateral membrane motor protein. *J. Physiol*. **531**: 661-666.

Santos-Sacchi J., Song L., Zheng J., Nuttall A.L. (2006). Control of mammalian cochlear amplification by chloride anions. *J. Neurosci.* **26**: 3992-3998.

Schaechinger T.J., Oliver D. (2007). Non mammalian orthologs of prestin (SLC26A5) are electrogenic divalent/chloride anion exchangers. *Proc. Natl. Acad. Sci. USA* **104**: 7693-7698.

Schneider T.R., Sheldrick G.M. (2002). Substructure solution with SHELXD. *Acta Crystallogr. D Biol. Crystallogr.* **58**: 1772-1779.

Schweinfest C.W., Henderson K.W., Suster S., Kondoh N., Papas T.S. (1993). Identification of a colon mucosa gene that is down-regulated in colon adenomas and adenocarcinomas. *Proc. Natl. Acad. Sci. USA* **90**: 4166-4170.

Scott D.A., Wang R., Kreman T.M., Andrews M., McDonald J.M., Bishop J.R., Smith R.J., Karniski L.P., Sheffield V.C. (2000). Functional differences of the PDS gene product are associated with phenotypic variation in patients with Pendred syndrome and non-syndromic hearing loss (DFNB4). *Hum. Mol. Genet.* **9**: 1709-1715.

Seavers P.R., Lewis R.J., Brannigan J.A., Verschueren K.H., Murshudov G.N., Wilkinson A.J. (2001). Structure of the Bacillus cell fate determinant SpoIIAA in phosphorylated and unphosphorylated forms. *Structure* **9**:605-614.

Sha B., Phillips S.E., Bankaitis V.A., Luo M. (1998). Crystal structure of the *Saccharomyces cerevisiae* phosphatidylinositol-transfer protein. *Nature* **391**:506-510.

Shcheynikov N., Wang Y., Park M., Ko S.B., Dorwart M., Naruse S., Thomas P.J., Muallem S. (2006). Coupling modes and stoichiometry of Cl^-/HCO_3^- exchange by slc26a3 and slc26a6. *J. Gen. Physiol.* **127**: 511-524.

Shcheynikov N., Yang D., Wang Y., Zeng W., Karniski L.P., So I., Wall S.M., Muallem S. (2008). The Slc26a4 transporter functions as an electroneutral $Cl^-/I^-/HCO3^-$ exchanger: role of Slc26a4 and Slc26a6 in I^- and $HCO3^-$ secretion and in regulation of CFTR in the parotid duct. *J. Physiol.* **586**: 3813-3824.

Shelden M.C., Loughlin P., Tierney M.L., Howitt S.M. (2001). Proline residues in two tightly coupled helices of the sulphate transporter, SHST1, are important for sulphate transport. *Biochem. J.* 356: 589-594.

Sheldrick G.M. (2002). Macromolecular phasing with SHELXE. *Z. Kristallogr*. **217**: 644-650.

Sheppard D.N., Welsh M.J. (1999). Structure and function of the CFTR chloride channel. *Physiol. Rev.* **79**: 23-45.

Shibagaki N., Grossman A.R. (2004). Probing the function of STAS domains of the Arabidopsis sulfate transporters. *J. Biol. Chem*. 279: 30791-30799.

Shibagaki N., Grossman A.R. (2006). The role of the STAS domain in the function and biogenesis of a sulfate transporter as probed by random mutagenesis. *J. Biol. Chem.* **281**: 22964-22973.

Smith F.W., Ealing P.M., Hawkesford M.J., Clarkson D.T. (1995). Plant members of a family of sulfate transporters reveal functional subtypes. *Proc. Natl. Acad. Sci. USA* **92**: 9373-9377.

Song L., Seeger A., Santos-Sacchi J. (2005). On membrane motor activity and chloride flux in the outer hair cell: lessons learned from the environmental toxin tributyltin. *Biophys. J.* **88**: 2350-2362.

Tang H.Y., Xia A., Oghalai J.S., Pereira F.A., Alford R.L. (2005). High frequency of the IVS2-2A>G DNA sequence variation in SLC26A5, encoding the cochlear motor protein prestin, precludes its involvement in hereditary hearing loss. *BMC Med. Genet.* **6**: 30.

Taylor J.P, Metcalfe R.A., Watson P.F., Weetman A.P., Trembath R.C. (2002). Mutations of the PDS gene, encoding pendrin, are associated with protein mislocalization and loss of iodide efflux: implications for thyroid dysfunction in Pendred syndrome. *J. Clin. Endocrinol. Metab.* **87**: 1778-1784.

Teek R., Oitmaa E., Kruustük K., Zordania R., Joost K., Raukas E., Tõnisson N., Gardner P., Schrijver I., Kull M., Ounap K. (2009). Splice variant IVS2-2A>G in the SLC26A5 (Prestin) gene in five Estonian families with hearing loss. *Int. J. Pediatr. Otorhinolaryngol.* **73**: 103-107.

Toth T., Deak L., Fazakas F., Zheng J., Muszbek L., Sziklai I. (2007). A new mutation in the human pres gene and its effect on prestin function. *Int. J. Mol. Med*. **20**: 545-550.

van de Kamp M., Pizzinini E., Vos A., van der Lende T.R., Schuurs T.A., Newbert R.W., Turner G., Konings W.N., Driessen A.J. (1999). Sulfate transport in Penicillium chrysogenum: cloning and characterization of the sutA and sutB genes. *J. Bacteriol*. **181**: 7228-7234.

Waterhouse A.M., Procter J.B., Martin D.M.A., Clamp M. Barton G. J. (2009) Jalview Version 2 - a multiple sequence alignment editor and analysis workbench. *Bioinformatics* **25**: 1189-1191.

Yoon J.S., Park H.J., Yoo S.Y., Namkung W., Jo M.J., Koo S.K., Park H.Y., Lee W.S., Kim K.H., Lee M.G. (2008). Heterogeneity in the processing defect of SLC26A4 mutants. *J Med Genet.* **45**: 411-419.

Zheng J., Du G.G., Anderson C.T., Keller J.P., Orem A., Dallos P., Cheatham M.A. (2006). Analysis of the oligomeric structure of the motor protein prestin. *J. Biol. Chem.* **281**: 19916-19924.

Zheng J., Du G.G., Matsuda K., Orem A., Aguinaga S., Levente D., Navarrete E., Madison L.D., Dallos P. (2005). The C-terminus of prestin influences nonlinear capacitance and plasma membrane targeting. *J. Cell Sci.* **118**: 2987-2996.

Zheng J., Long K.B., Shen W., Madison L.D., Dallos P. (2001). Prestin topology: localization of protein epitopes in relation to the plasma membrane. *Neuroreport*. **12**: 1929-1935.

Zheng J., Shen W., He D.Z., Long K.B., Madison L.D., Dallos P. (2000). Prestin is the motor protein of cochlear outer hair cells. *Nature* **405**:149-155.

Zolotarev A.S., Unnikrishnan M., Shmukler B.E., Clark J.S., Vandorpe D.H., Grigorieff N, Rubin E.J., Alper S.L. (2008). Increased sulfate uptake by *E. coli* overexpressing the SLC26–related SulP protein Rv1739c from *Mycobacterium tuberculosis*. *Comp. Biochem. Physiol. A Mol. Integr. Physiol.* **149**: 255-266.